R-05-28

Statistical model of fractures and deformation zones

Preliminary site description Simpevarp subarea – version 1.2

Paul R La Pointe, Golder Associates Inc

Jan Hermanson, Golder Associates AB

August 2006

Svensk Kärnbränslehantering AB
Swedish Nuclear Fuel
and Waste Management Co
Box 5864
SE-102 40 Stockholm Sweden
Tel 08-459 84 00
+46 8 459 84 00
Fax 08-661 57 19
+46 8 661 57 19

ISSN 1402-3091
SKB Rapport R-05-28

Statistical model of fractures and deformation zones

Preliminary site description Simpevarp subarea – version 1.2

Paul R La Pointe, Golder Associates Inc

Jan Hermanson, Golder Associates AB

August 2006

Preface

The current report constitutes the second (version 1.2) preliminary discrete fracture analysis for the Simpevarp subarea and is based on fracture data obtained before the Simpevarp 1.2 data freeze date of April 1, 2004. The publication of this report has been delayed until 2006; the report is published at this late date to document the development of the discrete fracture network modeling methodology in the Simpevarp and Laxemar area.

It should be noted that results contained in this report are superseded by new studies based on a wealth of newer data from both the Simpevarp and Laxemar subareas. The reader is therefore advised to use model results from the latest published model version which, at present (June, 2006) can be found in the Preliminary site description for the Laxemar subarea, version 1.2 /SKB 2006/ and background reports referred to therein.

Contents

1 Objectives and limitations

The purpose of this report is to document the data, software, experimental methods, assumptions, results and uncertainties for the evaluation of input parameters to discrete fracture network (DFN) models for the local site domain model SDM Simpevarp Version 1.2.

The parameters calculated for this model are presented so that they can be used for a variety of downstream models, including those pertaining to hydrological modelling and to mechanical modelling. Modelling assumptions are presented and discussed. Uncertainties related to both the conceptual model and to the data are presented, and recommendations for incorporating these uncertainties in downstream models are presented.

Chapter 2 describes the data used in the development of the DFN model.

Chapter 3 summarizes the software and the software modules used to carry out the analyses.

Chapter 4 lists assumptions.

Chapter 5 describes the experimental or analytical procedures used to analyze the data in order to calculate the fracture parameters needed for local site domain DFN modelling.

Chapter 6 describes the results of applying the experimental techniques described in Chapter 5 to the data listed in Chapter 2.

Chapter 7 describes the quantification of uncertainty and how it may be propagated to downstream models.

Chapter 8 summarizes the analysis and indicates where additional data, studies or other activities could benefit further development of the local site scale DFN model at Simpevarp.

This model is not intended to be a flow model or a mechanical model; as such, only the geometrical characterization is presented. The transmissivity properties of the fractures, or their mechanical properties are not within the scope of this report.

This model represents analyses carried out at particular data sets. If additional data are obtained, or values for existing data are changed or excluded, the conclusions reached in this report, and the parameter values calculated, may change as well.

2 Data sources

All of the data used for the development of this model are listed in this section. These data were obtained from SKB through SICADA data delivery 04_95 (2004-04-27), including correction delivery by mail (2004-05-27), and through GIS data as described below. Certain data were directly supplied from the development of the deformation zone and rock domain models. Each such input is also listed below.

2.1.1 Lineament data

The lineament data was not published in the SKB GIS database at the time of project execution and has been supplied from the GIS database at SKB /SDE 2004a/ to the geology team responsible for developing all geological models for Simpevarp SDM 1.2. The original geometry file was then reinterpreted by the geology team to enhance the structural pattern of possible lineaments, /SDE 2004b/.

The reinterpretation was reviewed by the geophysicists at both Geovista AB and SKB, and was used as the source of lineament information for both the deformation zone model and this analysis. The reinterpretation process is described in the Simpevarp 1.2 report /SKB 2005/. The reinterpreted lineament file /SDE 2004b/ used in this report, was later converted to AutoCad format, /SDE 2004c/, with identical geometries. In this analysis, all lineaments have been treated as potential deformation zones and hence the lineament map is interpreted as a two-dimensional trace map of deformation zones.

2.1.2 Outcrop data

Fracture outcrop data comes from the four detailed fracture maps of outcrops ASM000025, ASM000026, ASM000205 and ASM000206 /SDE 2004d/.

2.1.3 Borehole data

Fracture data available for this analysis was part of SICADA delivery 04_95 and the correction delivery by mail (2004-05-27) /SICADA 2004/. Fracture data from the following boreholes have been used in this analysis;

- KSH01A and KSH01B, KSH02, KSH03A and KSH03B, KAV01, KLX02, HSH01, HSH02 and HSH03.

For practical reasons, a number of key fracture parameters has been selected and cross-related to lithology and to single-hole interpretations from the SICADA delivered files /Golder 2004/; fract_core.xls (2004-05-04), rock.xls (2004-05-04) and from p_one_hole_interpret.xls (2004-05-24). This selection was made as part of this analysis and constitutes no “raw” data. However, this selection /Golder 2004/ has been distributed to other project members in the Simpevarp modeling team and has served as a common source of fracture data. Table 2-1 explains analyzed parameters and couplings between different data sets for boreholes.

Table 2-1. Analyzed parameters in borehole data.

Parameter	Data set	Comments
Orientation (strike/dip)	SICADA delivery 04_95	Fract_core.xls (2004-05-04)
Sec_up	SICADA delivery 04_95	Fract_core.xls (2004-05-04), Location of fracture
Type	SICADA delivery 04_95	Fract_core.xls (2004-05-04), Sealed, partly open, open
Confidence	SICADA delivery 04_95	Fract_core.xls (2004-05-04), Confidence in assigning type
Rock type	SICADA delivery 04_95	Rock.xls (2004-05-04), each fracture “marked” with rock type
Deformation zones	Single hole interpretations by /Mattson et al. 2004ab/	Each fracture “marked” as being in or outside of identified deformation zones
Rock domain	Rock domains /SKB 2005/	Each fracture “marked” with rock domain
Mineral coating	SICADA delivery 04_95	Fract_core.xls (2004-05-04), only the dominating mineral analysed (MIN1)
Roughness	SICADA delivery 04_95	Fract_core.xls (2004-05-04)
Alteration type	SICADA delivery 04_95	Fract_core.xls (2004-05-04)
Alteration	SICADA delivery 04_95	Fract_core.xls (2004-05-04)

3 Software used

Table 3-1 lists all of the software used to carry out the calculations in this report, including their name, version numbers, modules, address of vendor and what model parameters they were used for. Modules are listed in the case where there might be ambiguity as to which options were selected. This software has not been formally validated, but has been informally checked and verified that the results appear valid for its intended use. An exception is GeoFractal, which has been validated according to ISO 9001.

Table 3-1. List of software used for this report.

Software name	Version	Company	Modules used	Calculation performed
Excel 2002	(10.5815.4219) SP-2	Microsoft Corp. www.microsoft.com	General spreadsheet operations	Trace length scaling calculations; general data preparation for other programs
Analyse-It	Version 1.71 (Dec. 11, 2003)	Analyse-It Software, Ltd. PO Box 77, Leeds, LS12 5XA, England, UK. http://www.analyse-it.com/ telephone: +44 (0)113 229 5599	Excel add-in to perform non-parametric statistical tests and to summarize basic statistics for data	Summary tables for fracture intensity as a function of alteration zones and rock types; variation of fracture intensity with depth
SPSS for Windows	Version 11.0.0 (19 Sept. 2001)	SPSS Inc. Headquarters, 233 S. Wacker Drive, 11th floor Chicago, Illinois 60606 http://www.spss.com/	Tabs	Contingency table analyses
DIPS	Version 5.103 June 9, 2004	Rocscience Inc. 31 Balsam Avenue Toronto, Ontario M4E 3B5 Tel: (416) 698-8217 http://www.rocscience.com/		Orientation and display of fracture orientations; calculation of modal poles to fracture sets and Terzhagi corrections
Tecplot	Version 8.0-1-0 (Feb 16, 2000)	Tecplot, Inc. (formerly Amtec Engineering, Inc.) 13920 SE Eastgate Way Suite 220 Bellevue, WA 98005 Phone: 425.653.1200 http://www/tecplot.com		
GeoFractal	Version 1.2 (Build 3.21 Sept 20, 2002)	Golder Associates Inc. 18300 NE Union Hill Rd. Redmond, WA 98052 +1 425 883-0777 http://www.fracturedreservoirs.com		Mass dimension and display of fracture traces
FracMan DOS	Version 2.604	Golder Associates Inc. 18300 NE Union Hill Rd. Redmond, WA 98052 +1 425 883-0777 http://www.fracturedreservoirs.com		Analysis of fracture orientation statistics and size statistics for background sets.

4 Modelling assumptions and input from other disciplines

4.1 Deformation zone model

The DFN model described within this report utilized the same input data as the deformation zone model (lineaments) /SDE 2004bc/.

4.2 Stochastic DFN model

4.2.1 Assumptions

There are several assumptions that have been made in order to construct the stochastic DFN model for the Simpevarp site. Each assumption is described below, along with its impact on the model, a rationale for why the assumption is reasonable, and recommendations for future re-evaluation of the assumption.

Assumption 1: Lineaments represent fractures, or traces of deformation zones.

Discussion: Much care was taken to insure that the lineaments in the GIS file /SDE 2004b/ were structural features likely to be fractures (see /Triumf 2004/). However, this does not guarantee that each and every lineament trace is truly a mechanical fracture. Because of the care and protocols followed, however, it is likely that a very large proportion of the lineaments do represent mechanical fractures, and that the error that may arise from considering the few data that are not fractures in orientation and size statistics is likely to be small.

Assumption 2: The length of a linked lineament or a linked fracture in outcrop is an accurate and appropriate measure of a fracture's trace length for the purpose of building a stochastic DFN model.

Discussion: This assumption contains two parts: that the linked lineament is a sufficiently accurate measure of a fracture's length; and that it is the appropriate one for computing size statistics. One purpose of linking lineaments is to develop a DFN model that has fracture sizes and intensities that adequately reproduce flow and transport over large and small scales. It is not adequate to base the DFN model only on (unlinked) lineament segment lengths, because many of these segments cannot be proven to be truly unique rupture events, which could provide linked flow paths and failure surfaces, and thus are important for transport calculations and mechanical stability estimates. Moreover, the segments may also reflect effects of the geophysical acquisition and processing.

Although the size model depends on the lengths of the linked lineaments and the way outcrop segments are linked, the uncertainty can be bracketed and quantified. The potential uncertainties in trace lengths at the outcrop scale are manifested (along with other uncertainties) as the variance among area-normalized frequency values for the outcrops. It is likely that the variance due to outcrop differences is greater than the uncertainty produced by the linkage algorithm, and in any case, the uncertainty is quantified by calculating an envelope of parameters for the size of a specific fracture set.

Assumption 3: Fractures in outcrop may represent the smaller portion of a much larger population of fractures if the orientation of the sets in outcrop is similar to the orientation of linked lineaments (i.e. inferred two-dimensional deformation zone traces).

Discussion: The size calculation for lineament-related sets is based upon fitting a power law curve to lineament trace length values and outcrop trace length values. It is possible that most lineaments are actually faults, while most outcrop fractures are mostly joints. This could result in different orientations and size characteristics for outcrop fractures when compared to lineaments.

However, the fracturing in Simpevarp is likely to be very old and whatever the origin of the outcrop fracturing may have been, it is likely to have been re-activated many times. In this respect, large-scale deformation zones may have been more intensely re-activated because of higher stress or more focused deformation through time, and as such, share a common tectonic evolution as the outcrop fractures.

Assumption 4: Variations in fracture intensity as a function of rock type, alteration or other geological control can be estimated for unsampled rock units based on the inference of the controlling parameters for those units.

Discussion: Thus far, information on geological controls for fracture intensity variation suggests that lithology and alteration degree may be important controls. However, the four outcrops and limited number of boreholes have not provided data for all possible lithology/alteration degree combinations. In order to specify fracture intensity throughout the model region, it is necessary to infer the similarity of unsampled rock types to sampled ones, or to adjust sampled rock types to reflect unsampled rock type characteristics. It would be useful to validate this extrapolation to unsampled rock types by acquiring data in one of these unsampled units and comparing the observed values to predictions based on the geological model.

5 Strategy for the analysis of the data for calculating the parameters for local site scale DFN models for Simpevarp 1.2

The strategy for calculating the parameter values required for the DFN focuses on first defining fracture sets, and then to calculate properties for each set. Because each set may have its own distinct parameter values, the specification of the sets impacts the uncertainty in the parameter values. For example, if all fractures were combined into a single set, the variability in parameters such as size or orientation could be quite high. The separation of the fractures into multiple sets makes it possible to reduce the parameter variance associated with each group, thereby lowering the overall uncertainty in the DFN model. Also, the formation of a set or group of sets reflects a specific state of stress, at a specific time during which specific geochemical and hydraulic environs prevailed.

After sets have been specified, it is necessary to determine the stochastic geometrical description of each set. For each set, this geometry is composed of:

- Fracture orientations, expressed as the trend and plunge of the mean pole, with variability quantified by one or more of the following models and its associated parameters: Fisher, Bivariate Fisher, Bingham, Bivariate Normal, Bootstrap.
- Fracture sizes, expressed as a size-frequency distribution following one or more of the following distributions and their associated parameters: normal, lognormal, exponential, power law, uniform; and any minimum or maximum truncation values.
- Fracture shape
- Fracture intensity, specified as P_{32}, the amount of fracture surface area per unit volume of rock (m^2/m^3).
- Fracture spatial controls. These might be such models as Poissonian, fractal, geostatistical, or more complex combinations of these processes within specific geological domains.

Additional parameter values may be included depending upon the model's intended use, but for Simpevarp 1.2, no additional items have been identified.

The workflow for analyzing the individual borehole, outcrop and lineament data sets (Figure 5-1) is presented within its context for achieving the overall characterization objectives, which are to determine regional controls on fracture pattern geometry, in particular, to develop a predictive algorithm to specify fracture intensity, orientation and size throughout the spatial and depth extent of the Simpevarp local model domain. The workflow diagram begins with the analysis of data sets for each individual borehole, outcrop trace map or lineament data set. These individual data sets are described as "local" in the sense that it is not initially known whether the fracture controls and geometry determined for each individual set is found elsewhere; they may not have any regional consistency among boreholes or outcrops. The results from the analyses for each borehole or outcrop are assumed to initially only represent the fracturing in the rock in the immediate proximity of the outcrop or borehole, unless comparative analysis later demonstrates that fracture orientations, geological controls on intensity, etc exhibit a consistency over the whole local model domain. The term, local fracture set should not be confused with the DFN model of the local model domain. The local DFN model is independent of whether it is composed of local fracture sets where individual borehole or outcrop data sets show little spatial consistency, regional sets, which show great spatial consistency, or some combination of regional and local sets.

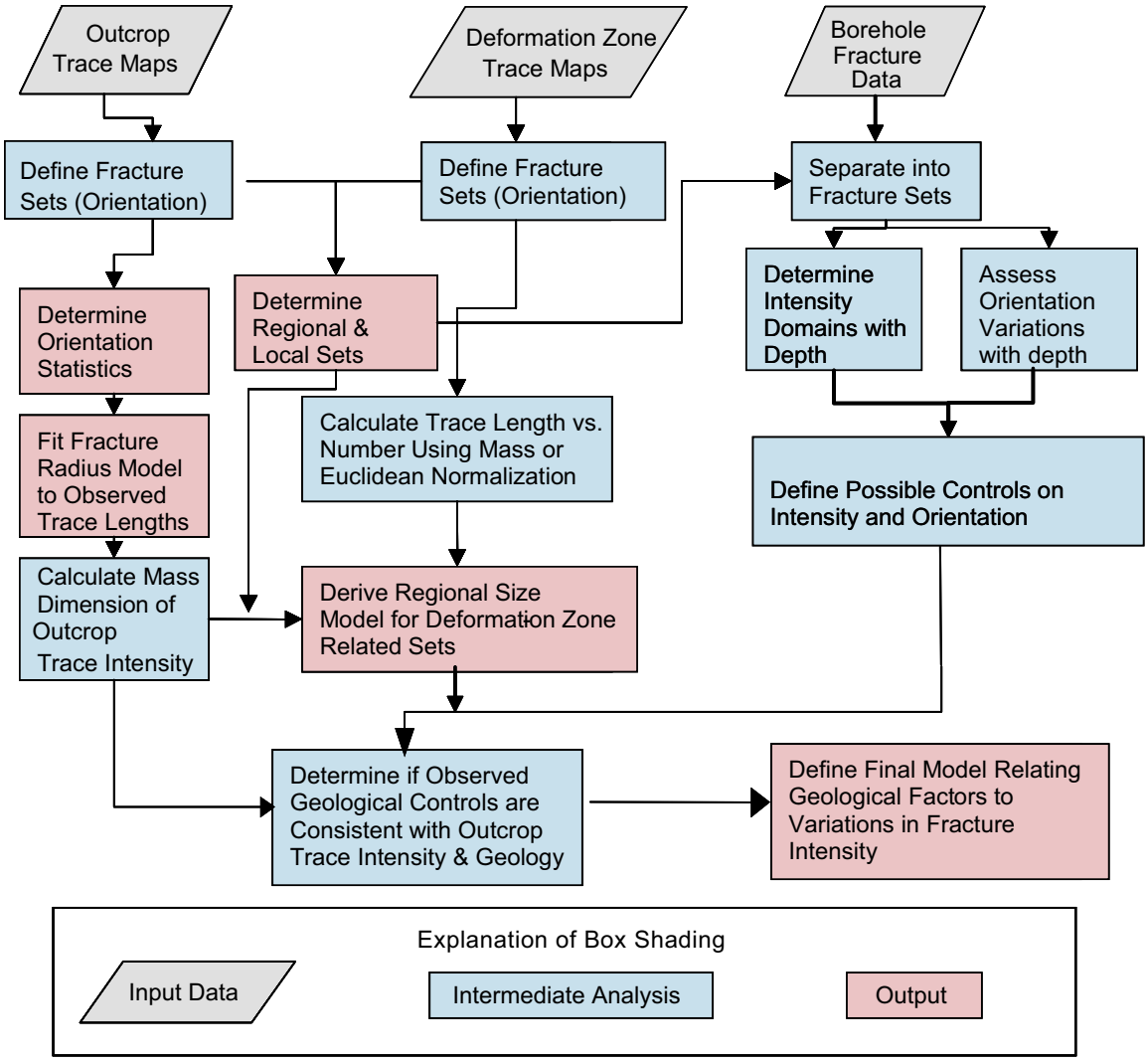

Figure 5-1. *Data analysis flow chart.*

The flowchart shows the components of the analysis of the local data sets. Any box that can be traced to an original input data source without connection to another data source is part of the local fracture data set analyses. For example, the chart shows that calculating the mass dimension of the trace intensity is part of the local data analysis for the outcrop trace data, but the derivation of the regional size model for lineament-related sets is not, as it relies upon the joint analysis of both the lineament and outcrop trace data sets, and whether the outcome of these analyses suggest that lineaments and smaller scale fracturing ought to be combined. In contrast, the stages in determining the possible regional controls on fracturing are based on the borehole data, as these data sets contain the most detailed geological information. Any controls identified in the borehole data set are then extended to the outcrop data to see if the controls appear to persist for these data sets as well. All of the analyses eventually flow towards the conceptual basis and parameters values for the local stochastic DFN model. This model consists of all of the pink-shaded output data sets and relations.

5.1 Set Identification and orientation statistics

5.1.1 Set determination

A fracture set is essentially a group of fractures whose orientations are either similar over a large spatial domain or whose orientations, intensities, and other properties can be closely related to geological factors in a statistically significant, predictable manner. It is not necessary that fracture orientations be invariant throughout the domain of interest; it is only necessary that they form according to the same geological factors. For example, dip parallel extension joints that form during the folding of rock will have different orientations based upon structural position, but may be treated as a single set despite the orientation variability, because they share a common geological origin that makes it possible to predict their orientation with a small degree of uncertainty. The fracture orientations are based on outcrop, borehole and lineament data. Fracture properties are measured in outcrop and borehole. The outcrop and lineament data are used for establishing the orientation statistics for the sub-vertical fracturing, since the orientation bias is minimal for these sets, while the borehole data is used for calculating orientation statistics for the sub-horizontal fractures for similar reasons. The borehole data is also used as a secondary validation of the outcrop data.

The first step, as shown in the chart (Figure 5-1) is to identify statistically homogeneous subpopulations for each of the four outcrops independently of any other outcrop, borehole or lineament data set. This analysis consists of plotting fracture orientations as stereoplots of the fracture data, expressed as poles to the fracture planes, and to identify visually distinct clusters of orientations. At the same time, plots of the trace pattern are visually evaluated to determine if there might be other, less prominent sets that were visually obscured in the stereoplots due to the greater number of fractures in some sets. Stereoplots were constructed using DIPS© (Table 3-1), while the trace plots were generated using GeoFractal©. An example of the analysis workflow follows.

Figure 5-2 shows the fracture traces measured for outcrop ASM000025, along with the stereoplot of fracture poles superimposed for reference in the lower right-hand corner. The stereoplot shows two dominant, nearly vertical fracture sets: one striking north-northeast and the other striking west-northwest. However, the fracture trace pattern is interpreted to contain more than two orientation sets.

For example, the north-northeast set in the stereoplot (Figure 5-3) looks to range in orientation from 340° to 60°, yet the traces in that same strike range appear to consist of at least two sets. The visual display of the fracture pattern suggested a further subdivision into a north-south set, ranging from 340° to 10°, a north-northeast set, ranging from 10° to 30°, and a northeast set ranging from 30° to 60°. When this subdivision is made, the resulting trace sets look geologically more reasonable (Figure 5-4).

The next step in the analysis of the outcrop trace data is to fit an orientation model to each identified set. This was done using the ISIS algorithm in FracMan.

The next step in the analysis is to determine, based on a qualitative analysis of several factors, whether the fracture sets identified in a single outcrop belong to a larger set of common fractures (‘regional’ fracture sets). The methodology for making this determination is detailed in Figure 5-5.

The primary observations to decide whether any sets identified in individual outcrops form part of a regional set are whether the orientations are similar AND the sets are in the same approximate chronological order; or if their orientations differ, do they still occupy about the same place in the chronological order AND can the difference in orientation be explained by changes in the lineament pattern geometry? The rationale for this decision tree is that similarity in orientation may be insufficient given the large number of sets in each outcrop.

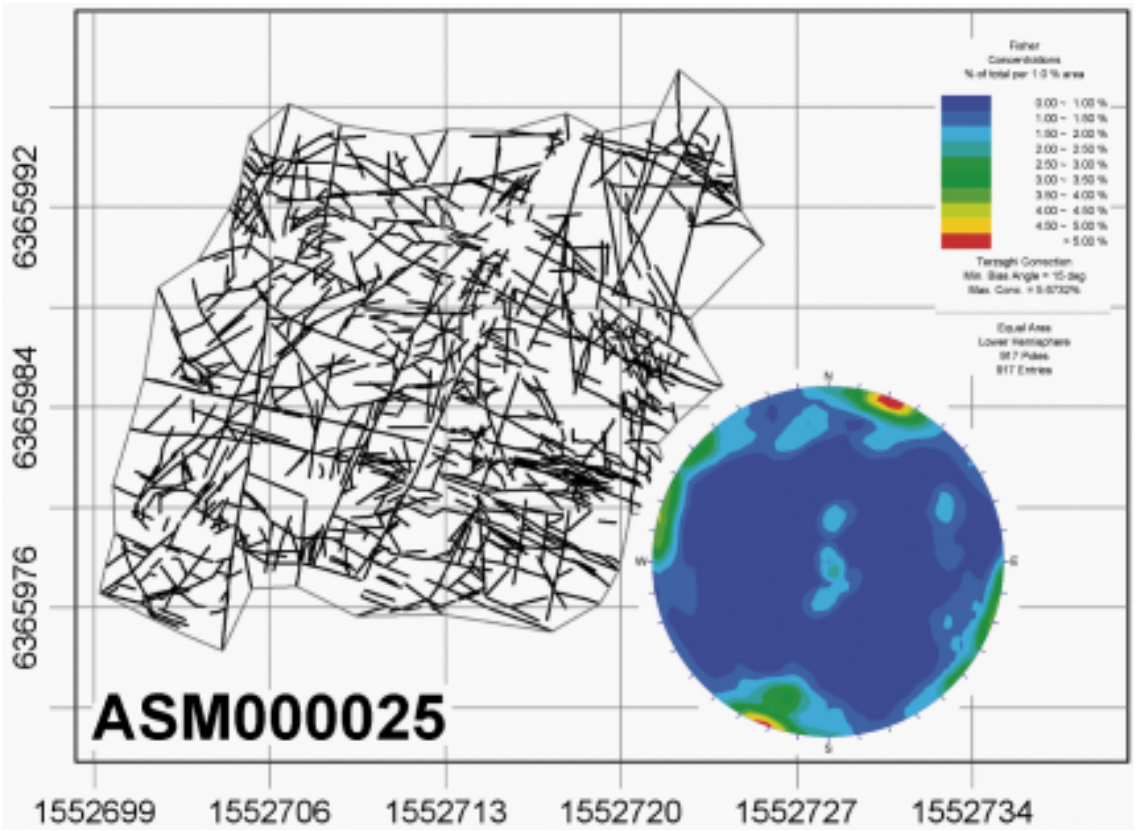

Figure 5-2. *Composite stereoplot of fracture poles and fracture traces for outcrop ASM000025.*

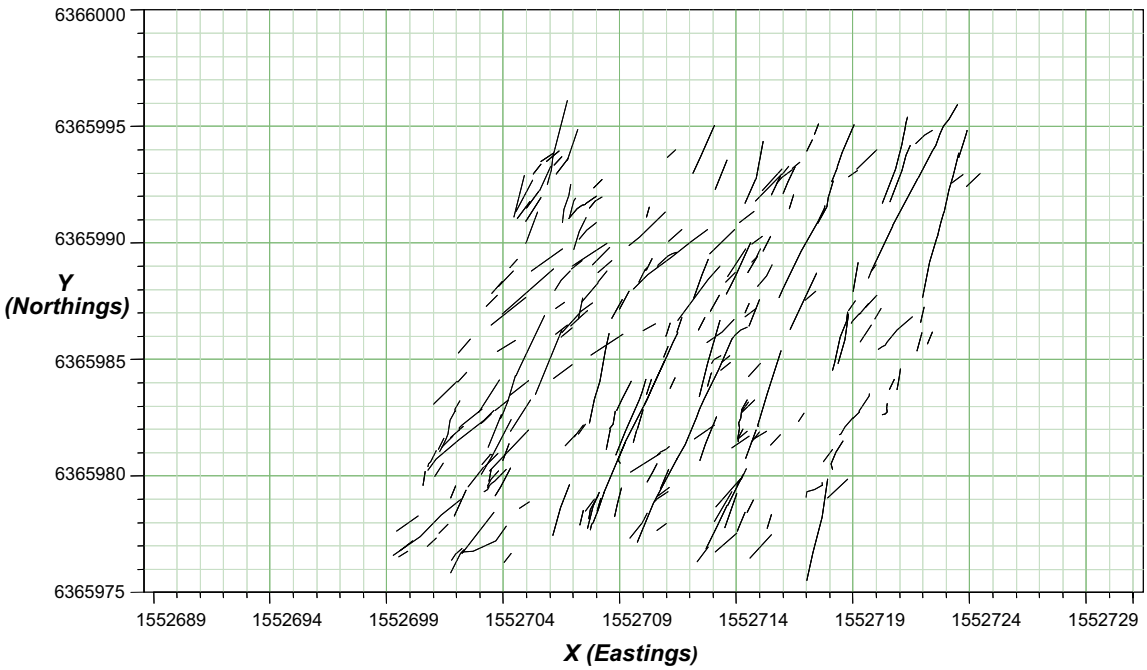

Figure 5-3. *North-northeast striking fracture set identified in stereoplot of outcrop ASM000025 fractures.*

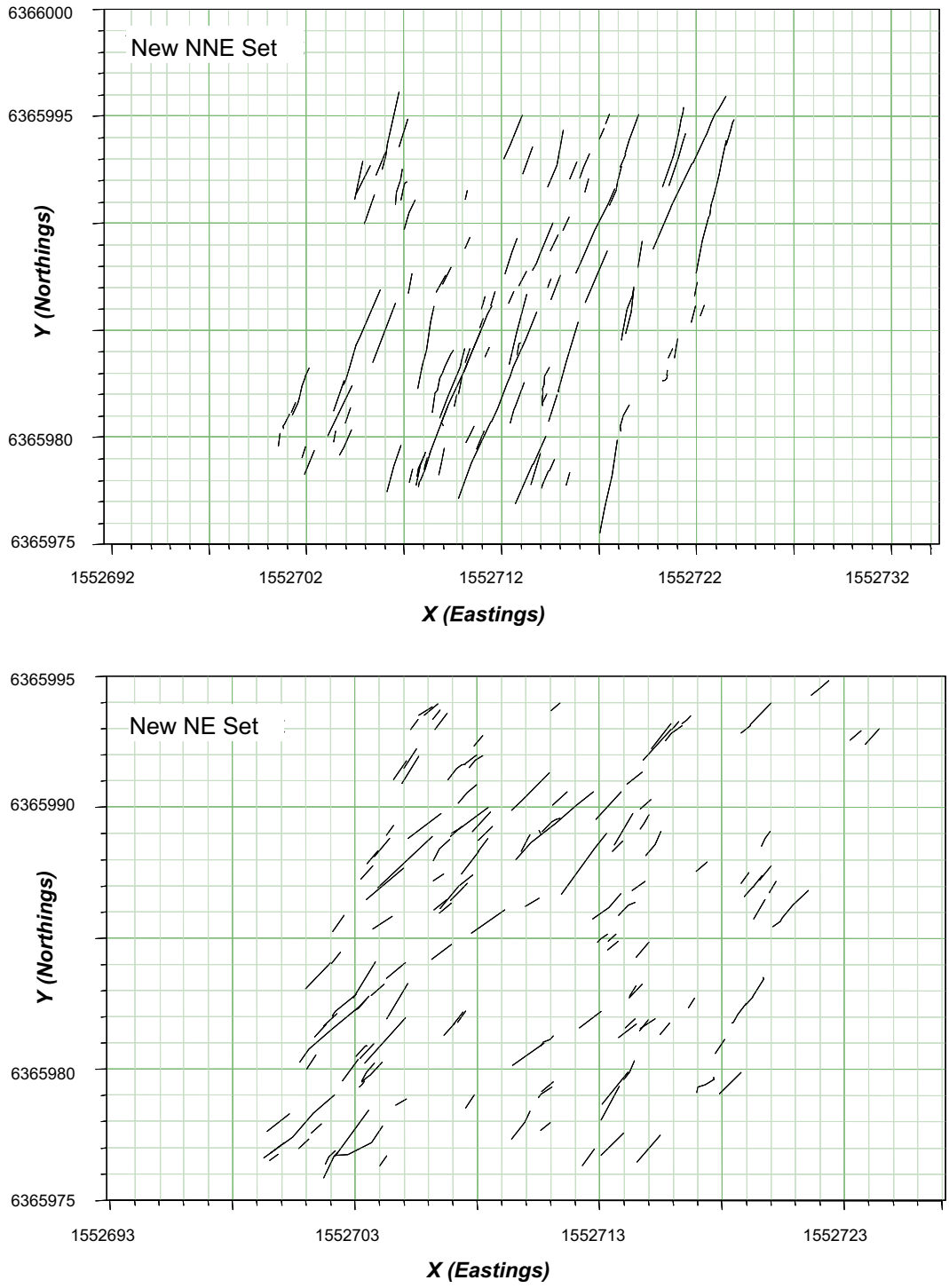

Figure 5-4. *Visual re-definition of north-northeast set initially defined in stereoplot into two local fracture sets (ASM000025).*

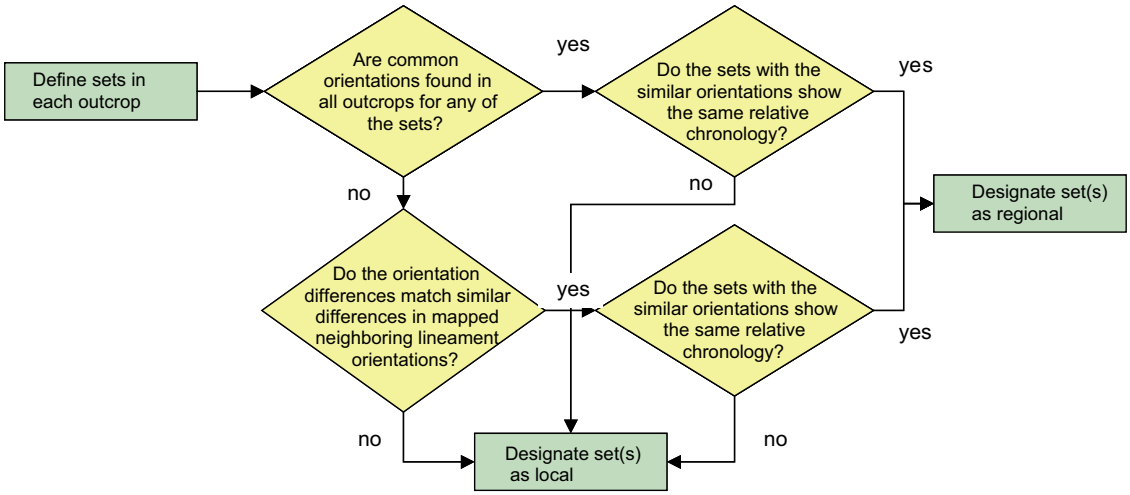

Figure 5-5. *Decision tree for identifying sets identified in separate outcrops as belonging to a regional fracture set.*

The addition of a second constraint that the fracture set order in the relative chronology should be approximately the same between outcrops helps to provide confidence that the sets in each outcrop are actually part of a regional set. On the other hand, it may be that the stress pattern has rotated slightly, so that the fracturing that was developing at a particular time actually has different orientations in different outcrops. If this were the case, then it would be expected that the relative set chronology would be very similar, and that the orientations would reflect the difference in the orientations of the lineament pattern near the outcrop.

5.1.2 Relation to lineaments

The lineament map presented in Chapter 6 (Figure 6-6) suggests that the trace pattern geometry may change spatially within the local model domain under study. If fractures found in outcrop were formed at the same time and in response to the same stress system that formed the lineaments (i.e. inferred deformation zone traces), then it would be expected that one or more outcrop regional sets would correspond to deformation zones. When fractures in outcrop show that they were among the earliest formed, and are possible old, as can be implied if they are filled with minerals possibly formed early in the history such as epidote /Munier 1989/, then it is likely that the regional outcrop set and the corresponding lineament set are samples from a single fracture population that spans a size range from at least as small as fracture seen in outcrop, to at least as large as the lineaments. These sets are termed lineament-related sets and are designated as Group 1 fractures.

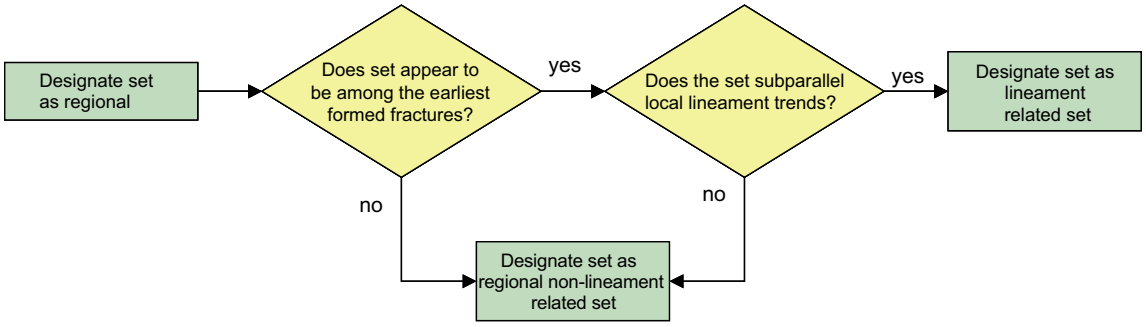

Figure 5-6. *Decision tree for identifying lineament-related sets.*

5.2 Size

5.2.1 Fracture sets not related to lineaments

Fracture size statistics are computed for each fracture set that varied according to whether the set was lineament-related or not. For any set identified in outcrop that is not related to a lineament set, a non-linear optimization process is used to calculate the parameters (e.g. mean, standard deviation) for a probability distribution model (e.g. lognormal) that best reproduces the observed trace length statistics. This is accomplished using the FracSize algorithm in FracMan™ Version 2.604, which is used to fit a fracture radius model to each of these sets using the orientation model derived from the ISIS analysis /Dershowitz et al. 1996/.

This first approach requires the specification of fracture shape and set orientation. For the purposes of the size analyses, fractures have been assumed to be circular planar discs, whose orientations conform to the orientation statistics found through the methods described in Section 5.1.

A probability distribution type, for example lognormal, is selected for the fracture radius probability density function. FracSize generates a stochastic radius value from the user-specified distribution, and then computes the probability that a fracture of that orientation and size (radius value) could intersect the user-specified trace plane. If the stochastic 'fracture' does intersect the trace plane, a random chord is then computed and placed, at random and truncated as necessary, within the simulation region. These series of intersection produce a set of trace lengths that can be compared with the measured trace lengths. Through a Simulated Annealing optimization routine /Press et al. 1992/, values of the mean and standard deviation are iterated until a statistically significant match is achieved. This process is repeated for several probability distribution functions, including lognormal, power law (Pareto), normal, exponential and uniform.

5.2.2 Fracture sets related to lineaments

The second method for computing a fracture size distribution, which was applied to lineament-related outcrop sets, was to calculate an area-normalized trace length frequency plot (Figure 5-7). This was done by combining trace lengths from outcrop and lineaments for the same set, and fitting a scaling function to them.

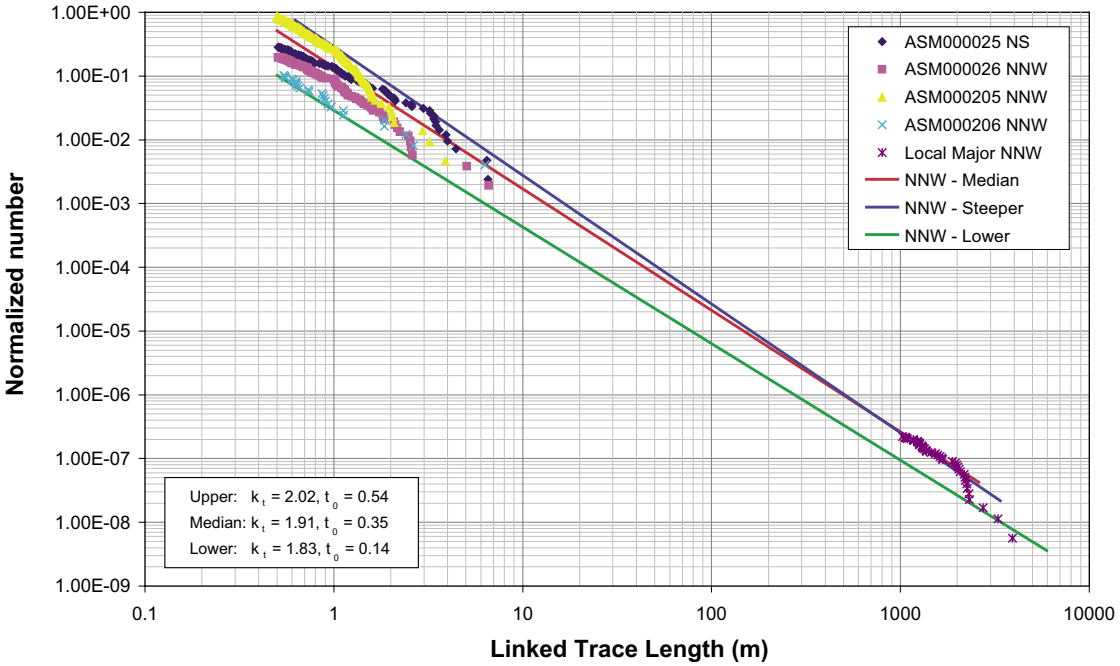

Figure 5-7. *Example of trace length model estimation plot resulting from fractal mass dimension normalization of fracture intensity with area.*

In the trace length scaling analysis, the number of fractures greater than or equal to a particular trace length is plotted as a function of trace length. Since the number of fractures relates to the size of the map area, the number needs to be normalized for this effect in order to plot data gathered from different sized exposures.

A simple way to compensate for different map areas among the data sets is to divide each data set by the map area (area normalization). This procedure assumes that the doubling of the area of the outcrop or map region would lead to a doubling of the number of fracture traces. This type of intensity scaling, in which the number of fractures is directly proportional to area, is Euclidean and is not fractal. The manner in which the fracture intensity scales with area can be quantified by the Mass Dimension of the fracture traces ($N(r) = \rho * r^{Dm}$ Equation 5-1). When the Mass Dimension of the traces has a value of 2.0, the intensity scales proportionately to area, and the spatial pattern of traces can be characterized by a Poissonian density function which inherently has no spatial correlation among the fractures.

It is possible that the intensity scaling of fractures is better described by a fractal model /La Pointe and others 2002/. In this type of model, intensity varies according to:

$$N(r) = \rho * r^{Dm} \qquad \text{Equation 5-1}$$

where ρ is a constant, termed the prefactor,

r is the radius of a circle

D_m is the Mass Fractal dimension, and

N(r) is the number of fracture traces (partial or entire) contained within the circle of radius r.

The computation of the mass dimension can take several distinct forms, such as the scaling properties of fracture center points or random points selected along the fracture trace, of the number of traces (P_{20}) themselves, or of the P_{21} (fracture trace length per unit area) measure of fracture intensity. All are useful for certain purposes. For size-scaling analysis, the desired parameter is how the number of fractures (P_{20}) changes with scale.

The procedure for calculating the mass dimension is illustrated in Figure 5-8. The value for D_m in Equation 5-1 is equal to the slope of the line when the data are plotted on doubly logarithmic axes. The value of the prefactor is equal to the ordinate value corresponding to a circle with radius = 1.0, and can be read directly from the graph It is important to make this calculation on individual sets rather than all of the traces at once, as each set may have different scaling properties.

The methodology for analyzing the size of lineament-related fracture sets has been presented in previous publications /La Pointe 2001/ and consists of a two-stage process. The first stage is to determine how fracture intensity for an individual fracture set scales with area. The second stage is to use this information to commensurate fracture trace data acquired over regions of different area.

The goal of this analysis is to relate the number of fractures of a given trace length measured over an area, A_i, to the number of fractures of the same size class measured over an area, A_j, of a different size. A simple way of resolving this issue is to assume that the number of fractures in a particular size class scales with area; if the area is doubled, the numbers of fractures are doubled. When the number scales linearly with area, as in this example, the scaling is termed Euclidean.

The calculation of the fractal mass dimension is used to determine whether Euclidean, Fractal or some other function best characterizes the scaling behavior of each individual lineament-related fracture set. The mass dimension exponent can vary from 2.0, which indicates Euclidean scaling, to lower values that imply that the traces scale in a fractal manner.

The procedure is to calculate and plot the cloud of mass dimension data points, as in Figure 5-8, and then compute a nonlinear least-square fit of Equation 5-1 to the locus of the mean and test for statistical significance. If the regression is found significant at the $\alpha = 0.05$ level, then the regression

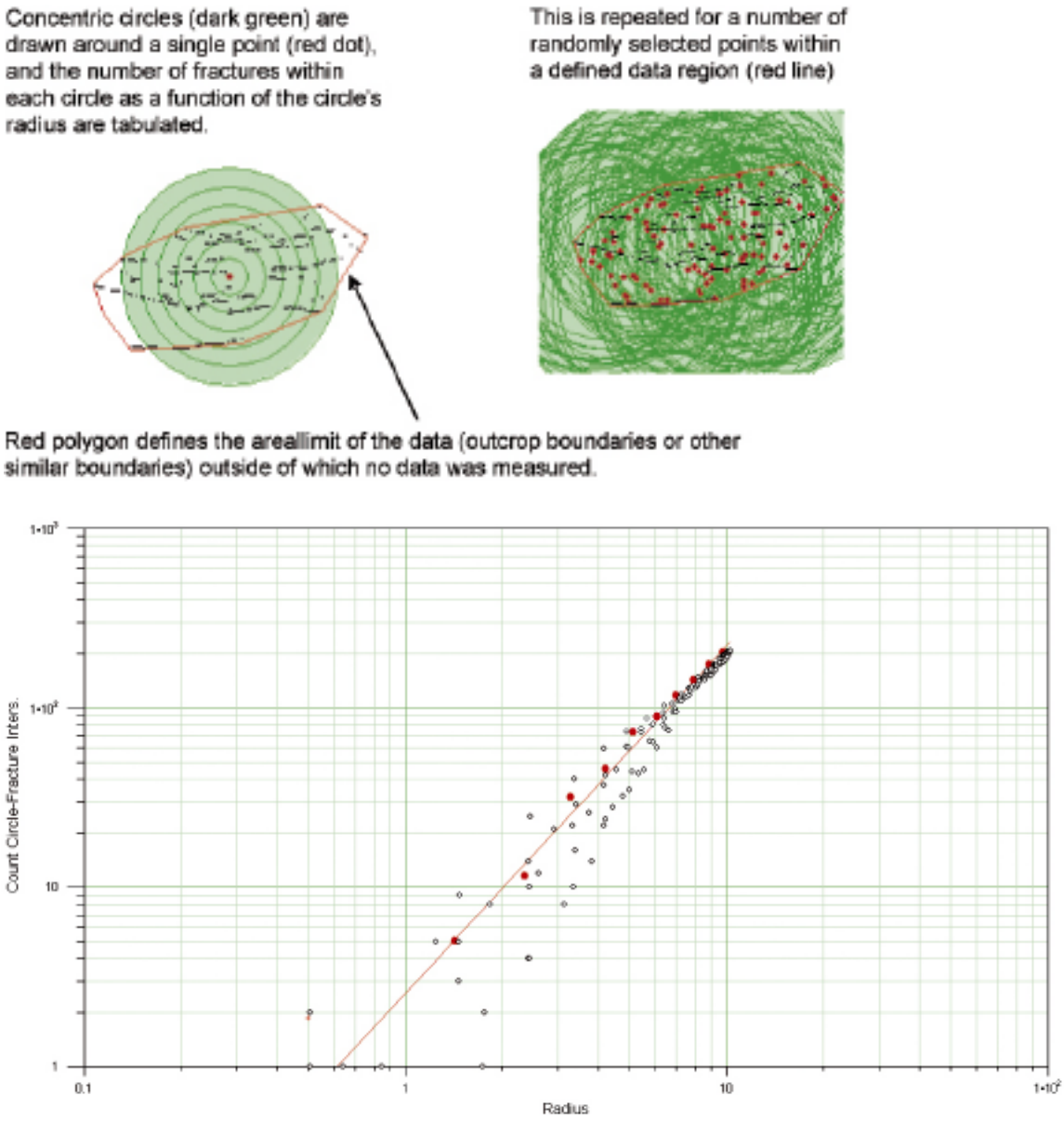

Figure 5-8. *Workflow for calculating the mass dimension from maps of fracture traces.*

is deemed significant and the scaling is treated as fractal. The calculations are always performed on the data set with the least censoring on the small trace end of the distribution, as censoring produces an underestimation of the number of fractures per unit area. For this reason, the mass dimensions were always calculated on the outcrop trace data rather than the lineament data.

The second stage is to use these results to combine data obtained over regions of very different area. The process is as follows:

Let the "o" subscript denote outcrop, and the "l" subscript denote lineament. Furthermore, let the variable "A" denote the area of the outcrop or lineament map, and "R" denote the radius of an imaginary circle that would have the same area as "A". Also, let "x" represent the trace length of a fracture. Then, from Equation 5-1, it is possible to calculate the number of fracture

traces that would be expected in the lineament map area based on what was measured in the outcrop area, or:

$$A_l = \pi R_l^2$$

$$So\ R_l = \sqrt{\frac{A_l}{\pi}} \qquad \text{Equation 5-2}$$

$$and\ N(R_l) = \rho R_l^{D_m}$$

Equation 5-3 makes it possible to compensate for the difference in area by computing a normalization factor NF that is the ratio of the number of fracture traces measured in outcrop to the number estimated in Equation 5-2:

$$NF = N(R_o) / N(R_l) \qquad \text{Equation 5-3}$$

This equation also describes how many fractures would be expected in an area of any size, for example, a reference area of 1 square meter.

It is easiest when comparing multiple data sets to reference all of them to an easily converted reference scale like the number of fractures per square meter. In this case, Equation 5-3 becomes:

$$NF_i = N(R_i) / N(\sqrt{\frac{1}{\pi}}) \qquad \text{Equation 5-4}$$

where

NF_i is the correction factor for converting the number of fractures actually measured in a domain, *I*, to the reference domain

$N(R_i)$ is the number of fracture traces measured in domain *i*, and

$N(1/\pi)$ is the number of fractures estimated from Equation 5-2.

To construct the plot, the trace lengths actually measured in the domain are ordered from shortest to longest. Each trace is numbered according to its cumulative frequency. If there were 50 traces, then the shortest trace would be assigned the number *50*, indicating that there are 50 traces greater than or equal to the length of this shortest trace. The second shortest trace would be assigned the number 49, and so on through the longest trace in the data set, which would have a complimentary cumulative frequency of 1. More generally, if k_i fracture traces were measured in domain *I*, then the shortest trace has the cumulative frequency value of k_i, and the next longest has the value of $k_i - 1$, and so on such that the longest trace measured has the value of *1*. Next, these cumulative frequency numbers are each divided by NF_i. The values are plotted with the normalized cumulative frequency value on the ordinate (Y-axis), and the trace length value on the abscissa (X-axis) as shown in Figure 5-7.

In order to distinguish between the parameters for the various power law distributions used in this report, the following nomenclature is adopted, (Table 5-1):

Table 5-1. Nomenclature used to describe power law relations in this report.

Distribution name	Parameter 1	Parameter 2
Mass Dimension	ρ (prefactor)	D_m (mass dimension)
Cumulative number of trace lengths	t_{0n} (coefficient)	k_t (trace length exponent)
Trace length CCDF	t_0 (coefficient)	k_t (trace length exponent)
Radius CCDF	r_0 (coefficient)	k_r (radius exponent)

Note that Parameter 2 for both the cumulative number of trace lengths *and* the trace length CCDF are identical.

This graph shows the results of normalization of 5 outcrop sets, the lineament set, and a model fitted to the composite data.

The equation of the black line shown on the figure conforms to a power law. The complementary cumulative number (CCN) plot shown in Figure 5-7 represents the number of traces, per unit area, greater than or equal to a specific trace length:

$$Number/area(x \geq t_{0n}) = \left(\frac{t_{0n}}{x} \right)^{k_t} \qquad \text{Equation 5-5}$$

The value of t_{0n} corresponds to a trace length of which it is expected that there is only one of them per unit area of this length or longer. Note that the relation depicted in Figure 5-7 and does not describe a probability distribution, but rather a cumulative number distribution. The parameter k_t is the slope of the black line on Figure 5-7, and the parameter t_{0n} is the abscissa value that corresponds to the ordinate value of 1.0.

It is possible to calculate a probability distribution from the cumulative number distribution, but this requires fixing the value of t_0 or r_0. *This* probability density (CCDF) function for trace lengths, which is quantified by this line, has the functional form:

$$\text{Prob}(t \geq t_0) = \left(\frac{t_0}{t} \right)^{k_t} \qquad \text{Equation 5-6}$$

where

t_0 is the minimum trace length;

t is any trace length greater than or equal to t_0 ;

k_t is the Trace Length Dimension, and

Prob($t \geq t_0$) is the probability that x is greater than or equal to t_0.

The value of t_0 is not the same as t_{0n}. t_0 corresponds to a minimum trace length, and is not calculated from t_{0n}. r_0 and t_0 are related, however, as are k_r and k_t /La Pointe 2002/, according to Equation 5-7:

$$k_r = k_t + 1.0$$
$$r_0 = t_0 * \frac{2}{\pi} \qquad \text{Equation 5-7}$$

This equation implies that the exponent describing the radius CCDF can be calculated from the slope of the cumulative number plot by simply adding 1.0 to the slope. The values of r_0 or t_0 are not calculated from the cumulative number plot, but are based either on the minimum fracture trace or radius required in the simulation. The methods for calculating P_{32} for a specific combination of fracture minimum size and radius distribution exponent, as well as re-adjusting the P_{32} for different minimum sizes, is described in Section 5.3.

Note also that the shape parameter of the parent radius distribution is sometimes specified by a parameter, b, often termed the Pareto Exponent. This exponent is related to the trace dimension in Equation 5-8 as:

$$k_r = b - 1 \qquad \text{Equation 5-8}$$

Those using results from these analyses should be aware of which convention is being used in the specification of the radius distribution model parameters in their particular application.

Also note that the parameter k_t is not the same as the mass fractal dimension, D_m! They are, in fact, independent parameters.

5.3 Intensity

Fracture intensity can be quantified by several measures, including the number of fractures per unit length (P_{10}), the number of fractures per unit area (P_{20}), the amount of trace length per unit area (P_{21}), and the amount of fracture surface area per unit volume of rock (P_{32}). The parameter P_{32} is often the most useful way to describe fracture intensity in a stochastic DFN model, as it is independent of model scale and direction. However, P_{32} is not measured in the field; usually only values of P_{10} from boreholes or P_{21} from outcrop maps are available.

Fortunately, it is possible to estimate P_{32} from either P_{10} or P_{21} through simulation. Thus, the procedure to calculate fracture intensity involves first determining geological controls on P_{10} and/or P_{21}, and then converting these values to values of P_{32}.

5.3.1 Determination of geological controls on fracture intensity

The determination of geological controls on fracture intensity relies upon comparing fracture intensity from boreholes with borehole geology, and subsequent evaluation of possible controls with intensity variations in outcrop. The boreholes form the primary source of data since:

1) They provide a record of fracturing from the surface or near-surface to beyond the depth of the proposed repository.
2) There are large volumes of fracture data from the boreholes, leading to better statistical power for hypothesis testing.
3) The data encounter a wider variety of geological settings than do the outcrops.

Outcrop fracture data is much more limited. However, borehole data may be biased towards sub-horizontal fracturing and hence be better suited for investigating controls on sub-horizontal fracture intensity. Possible biases towards sub-horizontal fracturing in boreholes was investigated by separating fractures into sub-horizontal and sub-vertical sets, to see if there were any significant differences.

Borehole fracture intensity was measured in two ways: by plotting the average intensity over borehole intervals of fixed length; and through Cumulative Fracture Intensity (CFI) plots (Figure 5-9).

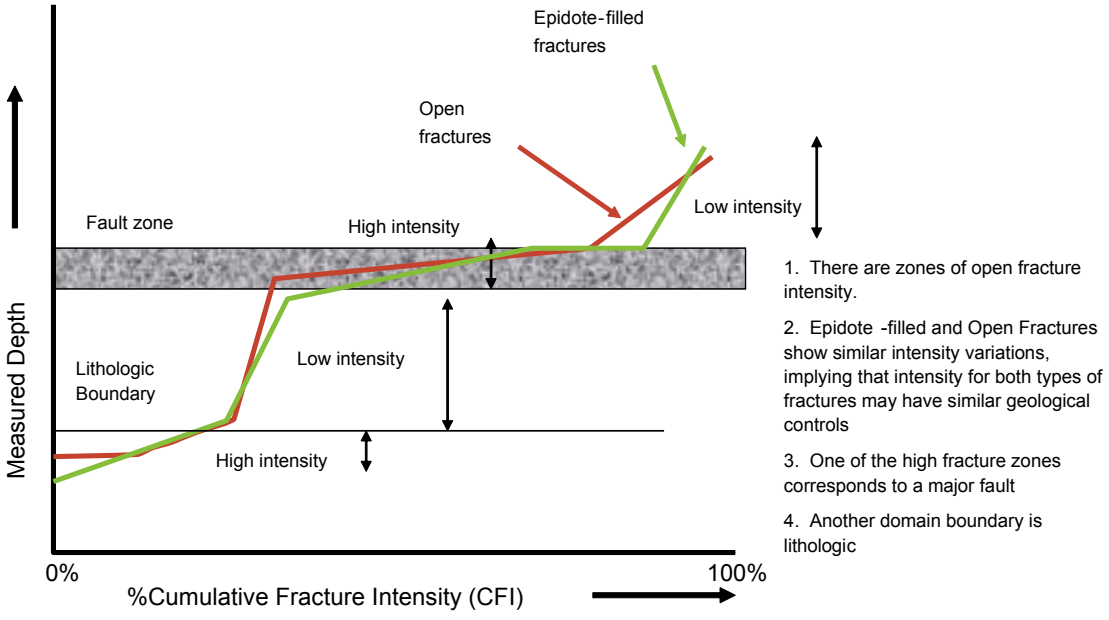

Figure 5-9. *Hypothetical Cumulative Fracture Intensity (CFI) plot.*

The first option consists of specifying the fixed interval length, and then dividing the number of fractures by the interval length. This method can be very sensitive to the interval length selected, and there are no simple procedures to ascertain what the most useful length might be.

The CFI plots do not have this particular limitation. These plots are constructed by sorting the fracture data by measured depth, starting either at the top or the bottom of the borehole. The depth value is the ordinate in the CFI plot. Next, the fractures are numbered from 1 to n, where n is the total number of fractures that are to be plotted. These numbers are divided by n, such that the 1st fracture has the abscissa value of 1/n, the 2nd fracture has the value 2/n, continuing to the last fracture, which has the value of n/n or 1.

In the CFI plot, portions of the line that have constant slope indicate where the fracture intensity has a constant value. Shallow slopes indicate higher intensity, while steeper slopes indicate lower intensity. The range of depth values over which the line maintains constant slope indicates domains of constant fracture intensity. As an example, surface stress-relief effects (resulting in localized higher fracture intensities) would manifest themselves as a domain extending down from the surface possibly a few tens of meters, with a slope much shallower than found below in rock of similar geological character.

The intensity domains can also be compared to mapped geological factors such as lithology, alteration, mineral infilling and other variables to see if zones of consistently higher or lower intensity correspond to specific geological characteristics.

The fracture frequency analysis was carried out in two steps: superimposition of the CFI plots on graphical displays of geological variables to formulate testable hypotheses regarding possible geological controls; and statistical testing and analysis to refute or buttress the hypotheses. The statistical tests employed standard parametric and non-parametric tests of confidence intervals about the mean and median, tests to examine the similarities of means and medians among groups, and linear regression. CFI plots were constructed using Excel2000©./Microsoft Corporation 2000/ Statistical analyses were carried out using the Excel Add-In Analyse-It© Version 1.71 /Analyse-It Software Ltd 2003/.

Additional analyses involved the construction of depth vs orientation plots to see if orientations and intensities remained constant throughout, or whether are zones with distinct orientations, such as the absence of a set or the addition of a new set, that also corresponded to the presence or absence of a particular fracture set. Depth vs orientations plots were constructed using Excel2000©.

5.4 Assessment of regional geological controls on fracturing and specification of the regional site model

As previously described, the development of the Simpevarp site model is built upon the analyses of individual local data sets from boreholes and outcrops together with regional lineament patterns. A critical question is how consistent the results are among the local data sets, for example, are the controls on fracture intensity identified in one borehole consistent with the controls identified in other boreholes and in outcrop? Do the fracture sets defined in each outcrop appear in all other outcrops, or do some outcrops have unique sets? Are any of these sets found in outcrops related to the sets identified in the lineament data? If so, is there further evidence that the outcrop and lineament data sets are size-limited subsets of single parent fracture populations whose sizes span the range from outcrop to lineament?

Once these and related questions are satisfactorily resolved, it is possible to aggregate the local data in ways that are consistent with the resolution, and summarize or re-analyze these aggregated groups of data to derive the regional site-scale fracture model parameters.

The regional consistency of geological controls is evaluated by testing the observations made in the boreholes against the observed open fracture intensity variations in the outcrops. If the same relations are found, then the confidence that the geological controls on fracture intensity are regional is increased.

5.4.1 Assessment of chronology of sets using terminations

The chronology of fracture sets is based upon three semi-quantitative parameters:

- Whether one set consistently terminates against another set.
- Whether a set that appears to be earlier based on terminations has long traces, or a set that appears to be younger has short traces.
- Whether a set that appears to be earlier based on terminations has more uniformly or periodically distributed traces, or a set that appears to be younger exhibits spatially restricted traces.

These three observational criteria are used to classify fracture sets as early or late (or somewhere in between) in their relative formation chronology (Figure 5-10 and Figure 5-11).

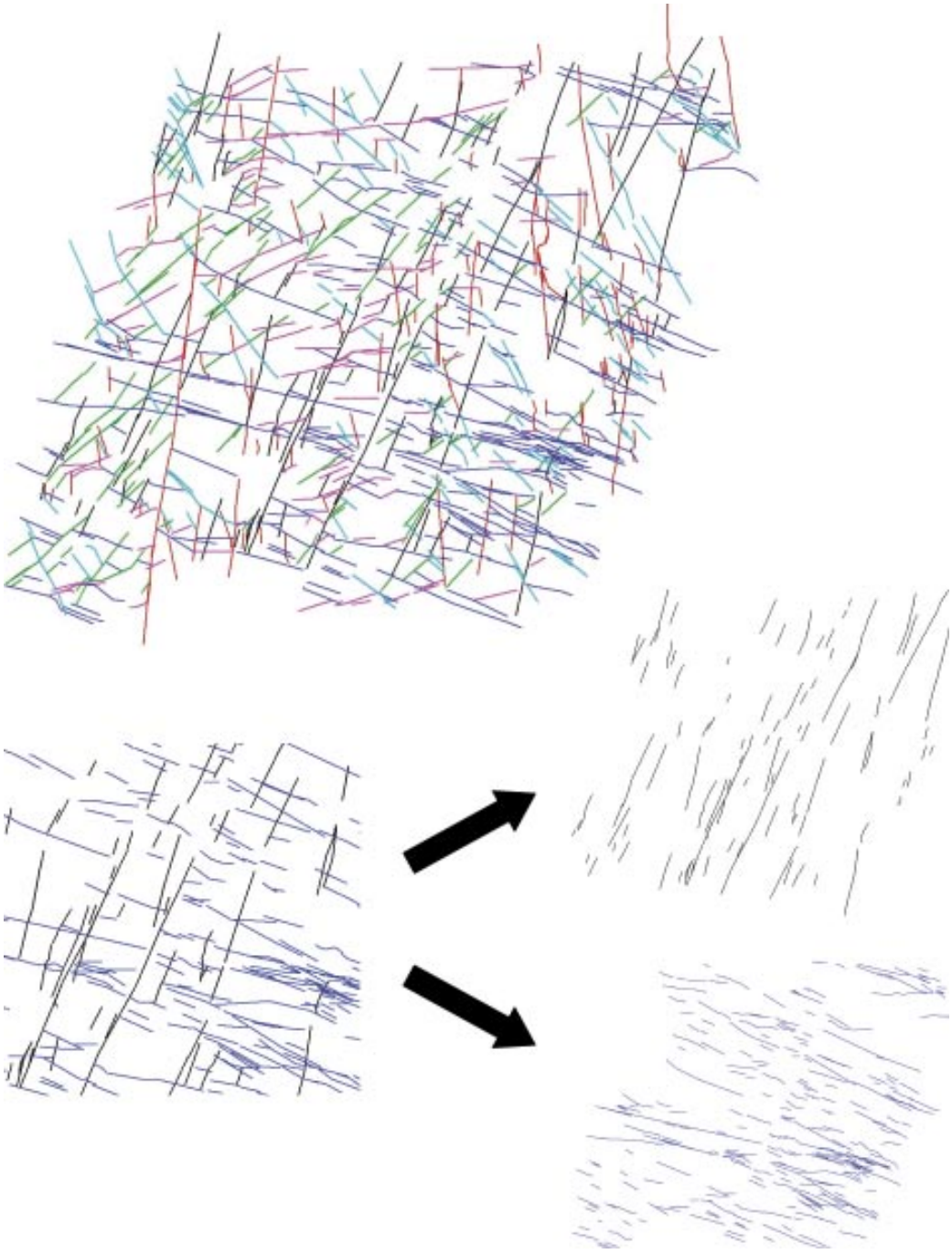

Figure 5-10. *Methodology for assigning chronology to identified outcrop fracture sets (outcrop ASM000025).*

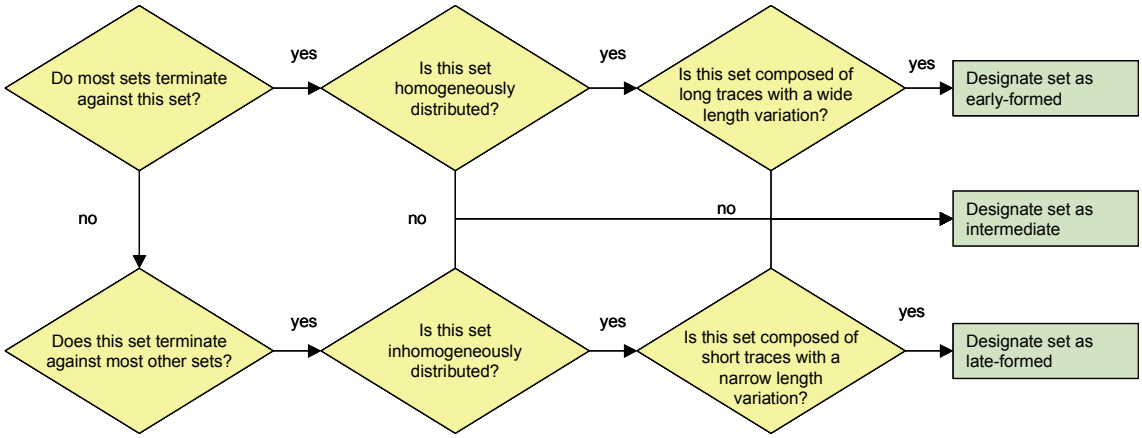

Figure 5-11. *Decision tree for identifying fracture set chronology.*

Figure 5-10 shows an interpretation for outcrop ASM000025. The oldest sets (shown as the leftmost diagram with blue and black traces) have long traces that are homogeneously scattered over the outcrop. The WNW set, however, shows some indications of banding caused by its terminations against the NNE set (a northeasterly trending band of WNW fractures is circled). The NNE set does not show this banding, and because of that and the terminations of blue fractures preferentially on black, the NNE set is interpreted to have earlier than the WNW set. In general, later-formed sets show higher percentages of terminations on older fractures; tend to develop bands of fractures; and have traces that are less spatially homogeneously distributed across the mapped area.

5.4.2 Consistency of site model with tectonic and geological history

Confidence is improved in the regional site model if the conclusions made are consistent with what is known concerning the tectonic and magmatic history of the Simpevarp region. For example, sets identified as regional lineament-related should show orientations that are as would be expected from the tectonic stresses that the rock has experienced in the past. Also, fracture sets identified as old should show mineral fillings indicative of a time when the rock was much hotter and under greater pressure. In this respect, epidote-filled fractures should be among the very oldest and /Munier 1989/, reports epidote being mobile not much later than about 1.4 bypb.

5.4.3 Estimation of P_{32} from P_{10} or P_{21}

The approach for calculating P_{32} from P_{10} or P_{21} requires simulation. The relation between P_{32} and the measurable fracture intensity quantity (P_{10} or P_{21}) is given by:

$$P_{32} = C_1 P_{10} \wedge P_{32} = C_2 P_{21} \qquad \text{Equation 5-9}$$

where the constants, C_1 and C_2 depend only upon the orientation and diameter of the borehole (C_1), or outcrop (C_2) and the orientation distribution of the fracture set. The goal of the simulations is to estimate C_1 if borehole data are being used and C_2 if outcrop data are used.

The first step is to create a DFN model with the same orientation statistics as the fracture set of interest. Next, a borehole or outcrop surface is inserted into the model with the same geometry as the borehole or outcrop for which actual data has been obtained (Figure 5-12). A guess for P_{32G} is made so that a statistically significant number of fractures in the simulation intersect the

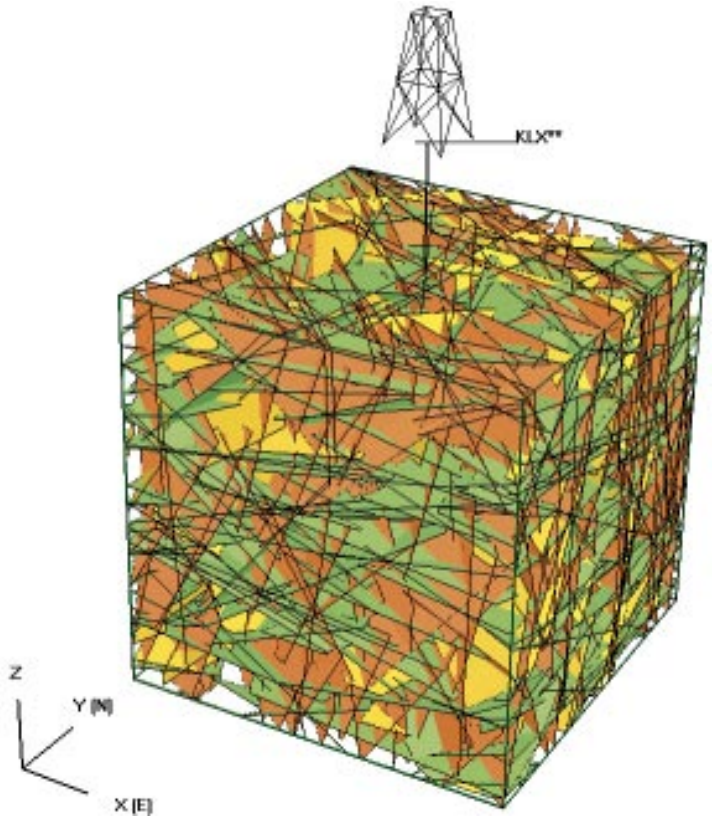

Figure 5-12. *DFN simulation to estimate the constant relating P_{10} to P_{32}.*

borehole. This results in a value of P_{10G} or P_{21G}. This computation for a specific P_{32G} is simulated as a Monte Carlo process for at least 25 realizations. The constant is estimated as:

$$E[C_1] = \frac{P_{32G}}{\langle P_{10G} \rangle} \quad \text{borehole}$$

$$E[C_2] = \frac{P_{32G}}{\langle P_{21G} \rangle} \quad \text{outcrop} \qquad \text{Equation 5-10}$$

where E[ ] denotes the expected value of the quantity in brackets, and ⟨ ⟩ represents the average value of the Monte Carlo realizations.

As previously mentioned, the value of P_{32} depends upon the specified minimum size and exponent for a power law CCDF, which is not normally the case. This is because the value of P_{32} is estimated from trace length data and traces shorter than a specified value have purposely not been measured. The P_{21} value for the outcrop represents only the trace length intensity for traces longer than the threshold, L_t. The complication arises because the amount of P_{21} that is removed by applying a threshold trace length size is sensitive to the distribution form (power law, lognormal, etc), and so the form of the distribution and its specific parameters become important. If there is no sampling truncation applied, then the form of the radius distribution is not important, and the specific parameter values of the distribution are also unimportant. It is important to note that L_t is not related to t_0 in the discussion that follows.

For any specified value of k_r, it is possible to find a combination of r_0 and P_{32} that will exactly match a value of P_{21} in which the measured and simulated traces have been excluded if they are shorter than L_t. In other words, the determination of P_{32} is not unique because there are two degrees of freedom, r_0 and P_{32}, and only one parameter to match, the truncated value of P_{21}.

However, it is possible to introduce a second constraint to make the solution unique. The second constraint is a value of P_{10} from boreholes in the same rock domain as the outcrop. A simultaneous match to the borehole P_{10} and the outcrop P_{21} does provide a unique set of values for r_0 and k_r. However, mainly due to time constraints this method has not been employed in this model version.

5.5 Spatial model

The spatial model is defined apart from the intensity model, though it is closely related to the intensity model. The location of the fractures is specified by a combination of the intensity and spatial models. For example, certain rock types have higher mean fracture intensities than others, but within each rock unit, the fractures are distributed according to the spatial model. Likewise, fractures related to lineaments may have a zone of higher intensity around mapped lineaments, but within this zone, they may be distributed according to a Poisson process. In this context, the spatial model describes how fractures vary *within* spatial domains of stationary intensity.

The spatial model is determined through the calculation of the mass dimension of the number of fractures per unit area for outcrop trace data, and the number of fractures per unit length for borehole data. The calculation of the mass dimension has previously been described in Section 5.2.2.

Outcrop trace data are used for calculating the spatial model for the sub-vertical fracture sets, as borehole data contain a bias that makes calculations for the sub-vertical sets in boreholes less reliable than the outcrop calculations. Conversely, the borehole data is used to determine the spatial model for the sub-horizontal sets in zones where intensity is stationary.

If the mass dimension has a value of 2.0 for trace data or 1.0 for borehole data, the fractures follow a Poisson distribution. Values less than 2.0 for trace data (less than 1.0 for borehole data) indicate a fractal process where there is some degree of spatial correlation among the locations of the fracturing. The failure of the data to approximate a straight line on the mass dimension plots indicates that the spatial model is something other than Poissonian or fractal, and needs to be further investigated using other types of calculations.

5.5.1 Estimating a different value of P_{32} for a different value of r_{min}

If a different value for the minimum modeled fracture radius (r_{min}) is needed for a particular application, it is relatively straightforward to calculate the adjusted value of P_{32} that corresponds to this new value. Note that r_{min} is a user-chosen size truncation, and is not the same thing as the minimum radius (r_0) of the Pareto probability distribution; the latter is a fixed statistical parameter that is not free to vary. If the new minimum radius size is denoted by r_{min}, a new maximum radius size by r_{max}, and the new adjusted value of intensity is denoted by P_{32adj}, then:

$$t(r) = \left(\frac{k_r r_0^{k_r}}{r^{k_r+1}} \right) * \pi r^2 \qquad \text{Equation 5-11}$$

$$T(r_{\min}, r_{\max}) = \int_{r_{\min}}^{r_{\max}} t(r) \partial r \qquad \text{Equation 5-12}$$

or

$$T(r_{\min}, r_{\max}) = \frac{\pi k_r r_0^{k_r}}{2 - k_r} \left[r^{2-k_r} \right]_{r_{\min}}^{x_{\max}} \qquad \text{Equation 5-13}$$

where

t(r) is the fracture area density function for a fracture of radius *x*;

T(r) is the total area of all of the fractures;

r_{min}, r_{max} are, respectively, any minimum and maximum radius values.

All other parameters are as previously explained.

Now these equations hold for any minimum and maximum fracture radius. Therefore, the original P_{32} for fractures with radii from r_0 to ∞ is:

$$T(r,\infty) = \frac{\pi k_r r_0^{k_r}}{2-k_r}\left[r^{2-k_r}\right]_r^{\infty} = -\frac{\pi k_r r_0^{2-k_r}}{k_r-2} \qquad \text{Equation 5-14}$$

and

$$T(r_{\min}, r_{\max}) = \frac{\pi k_r r_0^{k_r}}{2-k_r}\left[x^{2-k_r}\right]_{r_{\min}}^{r_{\max}} = \frac{\pi k_r\left[r_{\max}^{2-k_r} - r_{\min}^{2-k_r}\right]}{k_r-2} \qquad \text{Equation 5-15}$$

The adjustment of P_{32} is the ratio of $T(r_{min},r_{mx})$ to $T(r_0,\infty)$multiplied by the P_{32} corresponding to $T(r_0,\infty)$:

$$P_{32}(r_{\min}, r_{\max}) = \frac{\frac{\pi k_r\left[r_{\min}^{2-k_r} - r_{\max}^{2-k_r}\right]}{k_r-2}}{\frac{-\pi k_r r_0^{2-k_r}}{k_r-2}} * P_{32}(r_0,\infty) = \frac{\left[r_{\min}^{2-k_r} - r_{\max}^{2-k_r}\right]}{r_0^{2-k_r}} * P_{32}(r_0,\infty) \qquad \text{Equation 5-16}$$

Note that $k_r > 2.0$ for Equation 5-16 to be valid. For values of $k_r \leq 2.0$, the correction must be done empirically through DFN simulation.

6 Derivation of statistical model with properties

6.1 Set identification and orientation statistics

6.1.1 Sub-vertical sets

The sub-vertical sets were determined from the outcrop trace data and the lineament data. Figure 6-1 shows the outcrop trace patterns in which each identified set is shown by colours. The analysis of the sets suggested two alternative conceptual models for the fracturing: Alternative 1, in which vertical three sets were related to the lineaments, and three other vertical sets were not; and Alternative 2, in which all of the vertical sets were related to corresponding lineaments. In both alternatives, there was an additional sub-horizontal set.

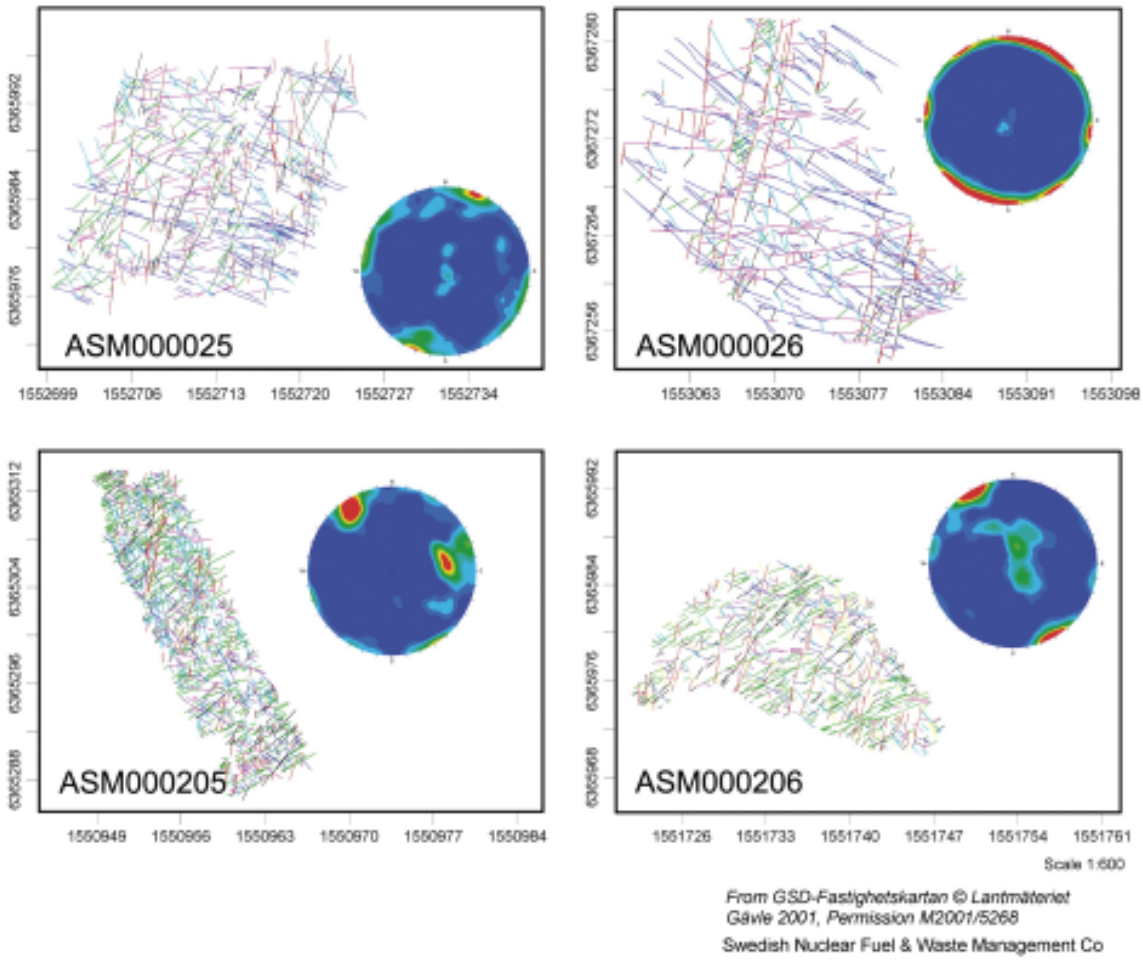

Figure 6-1. *Trace maps for outcrops ASM000025, ASM000026, ASM000205 and ASM000206. Colors represent different fracture sets.*

The traces belonging to each set can be seen in greater detail in Figure 6-2 through Figure 6-5. There were six sets found for each outcrop with the exception of seven for ASM000206, cf Table 6-1. Each set has been designated by a direction most closely reflecting the fracture set's strike. The relative chronology, based upon a visual assessment of abutting relations, is given in Table 6-2. Colors were selected to visually accentuate the differences of sets with similar azimuths, and this varied from outcrop to outcrop). This table and figure shows that there appear to be consistent, dominant older sets in each of the outcrops. The oldest set typically strikes northeast or north-northeast. There are also prominent, older sets striking west-northwest and northwest. However, there is enough variation in the set azimuths to conclude that the oldest sets do not have constant mean orientations for all four outcrops.

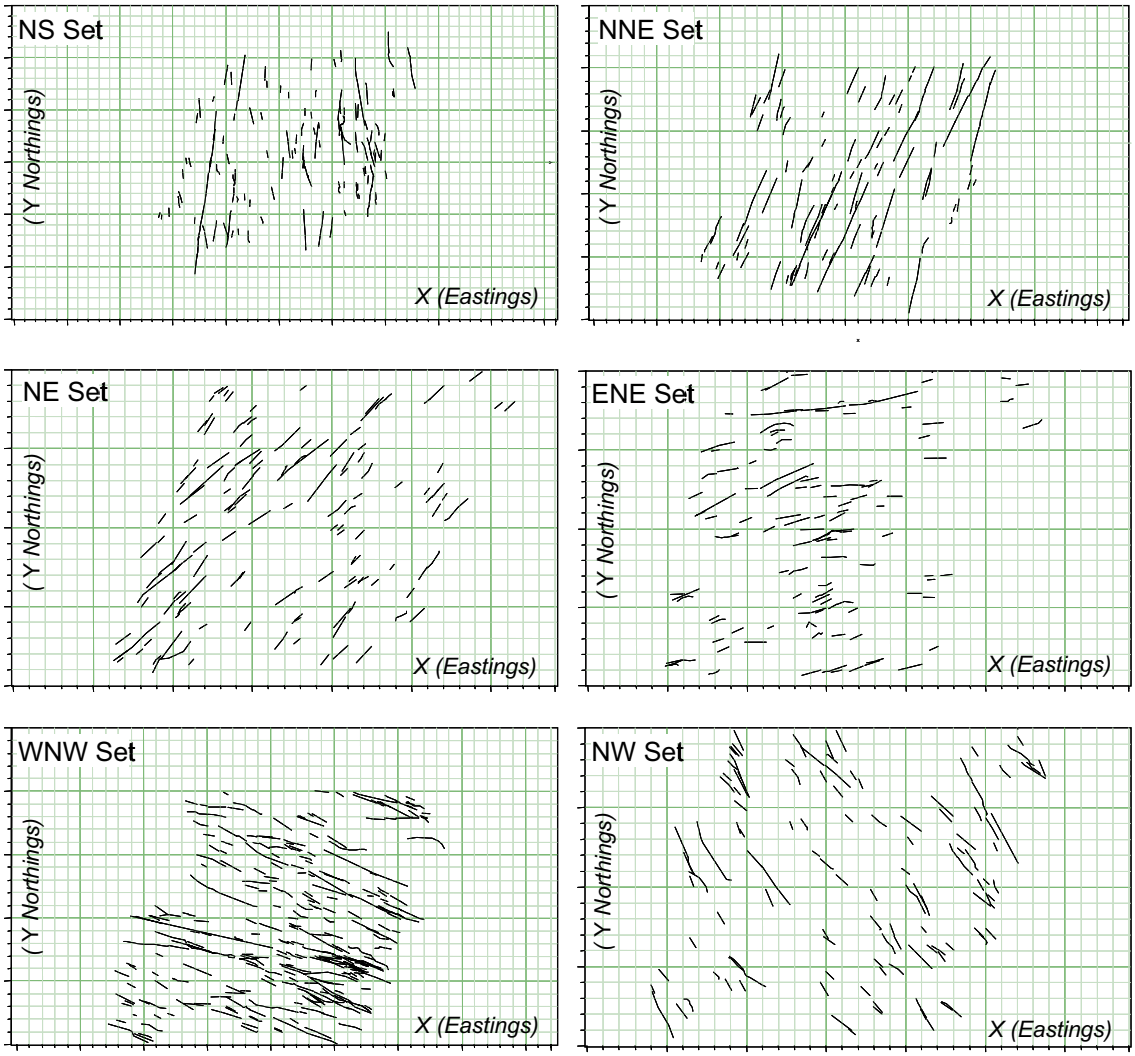

Figure 6-2. *Fracture sets identified in outcrop ASM000025.*

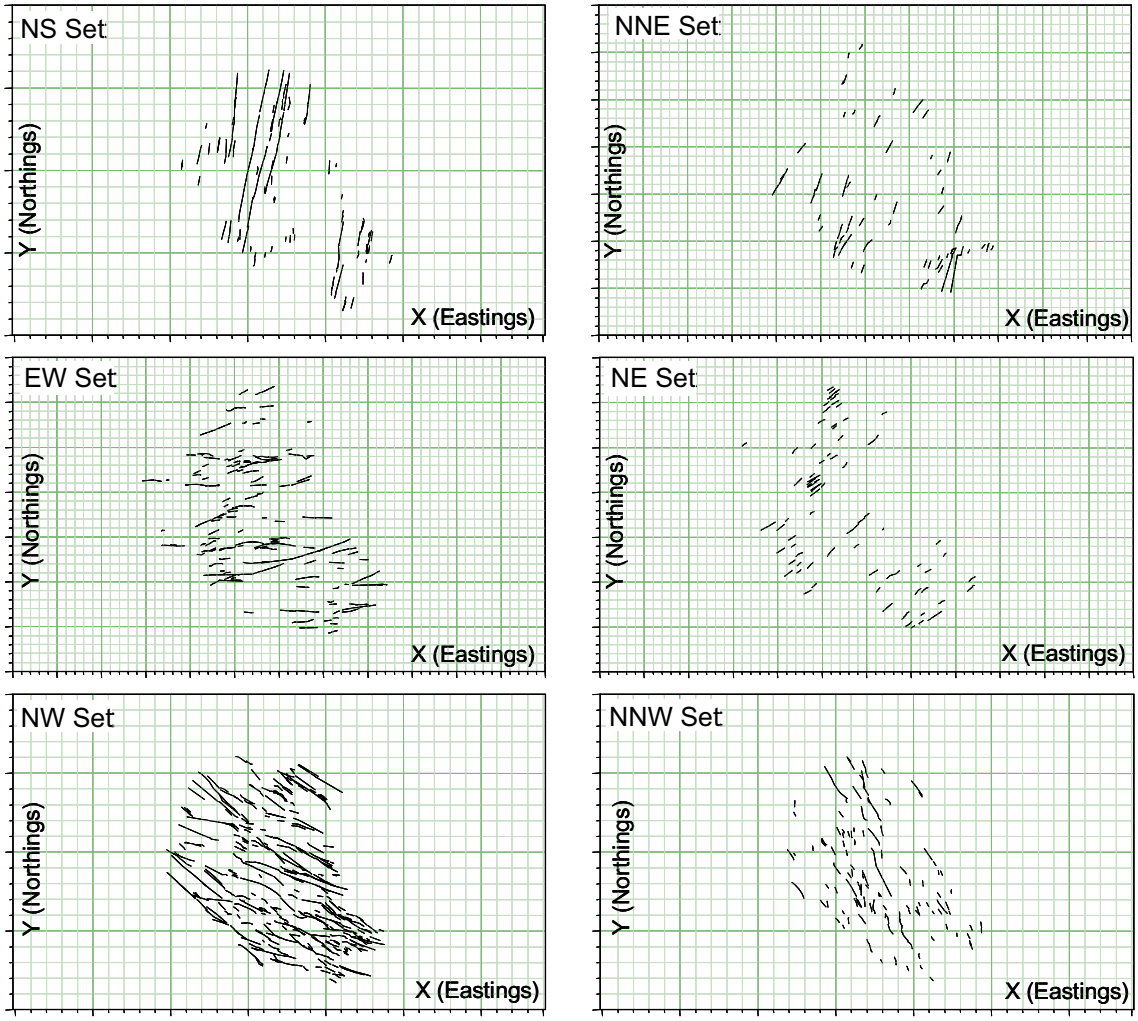

Figure 6-3. *Fracture sets identified in outcrop ASM000026.*

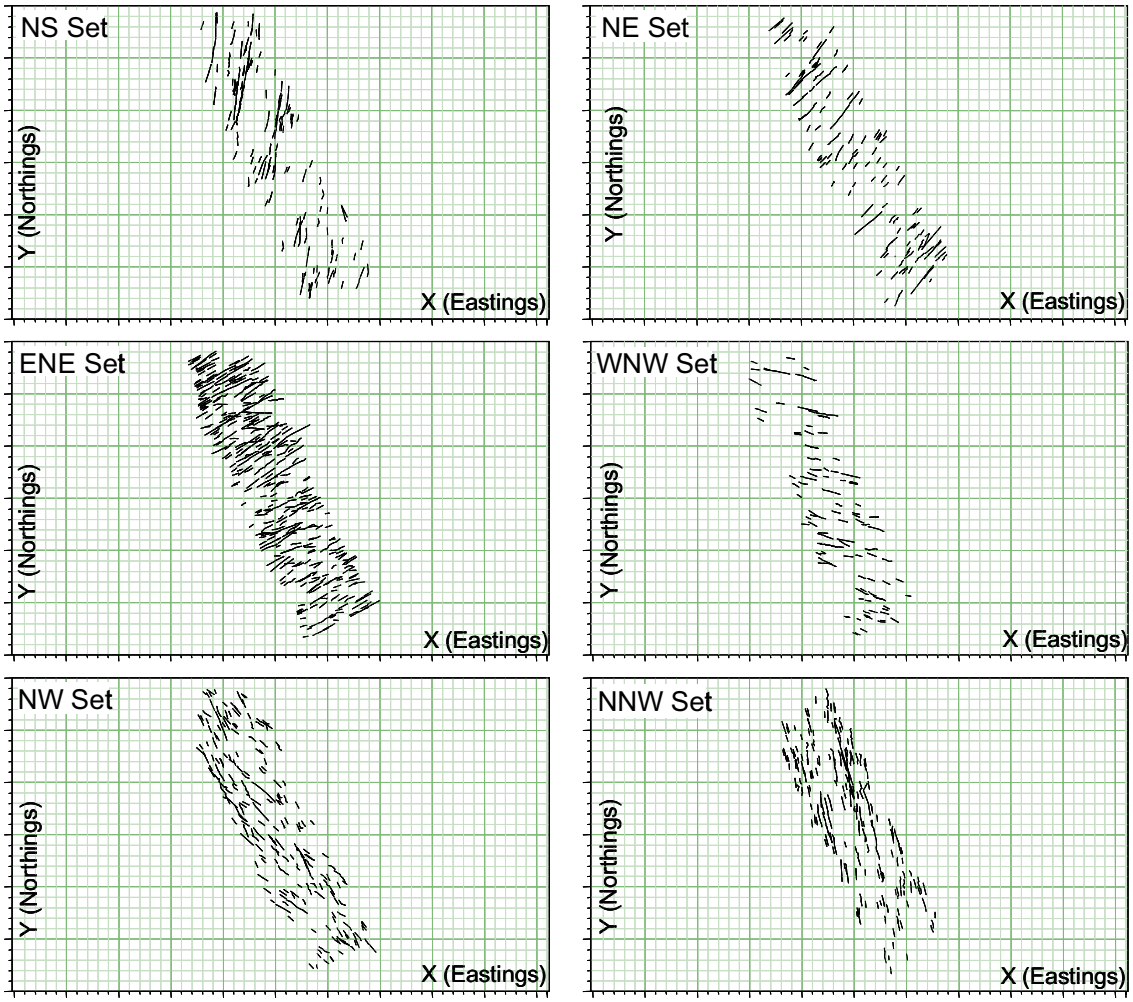

Figure 6-4. *Fracture sets identified in outcrop ASM000205.*

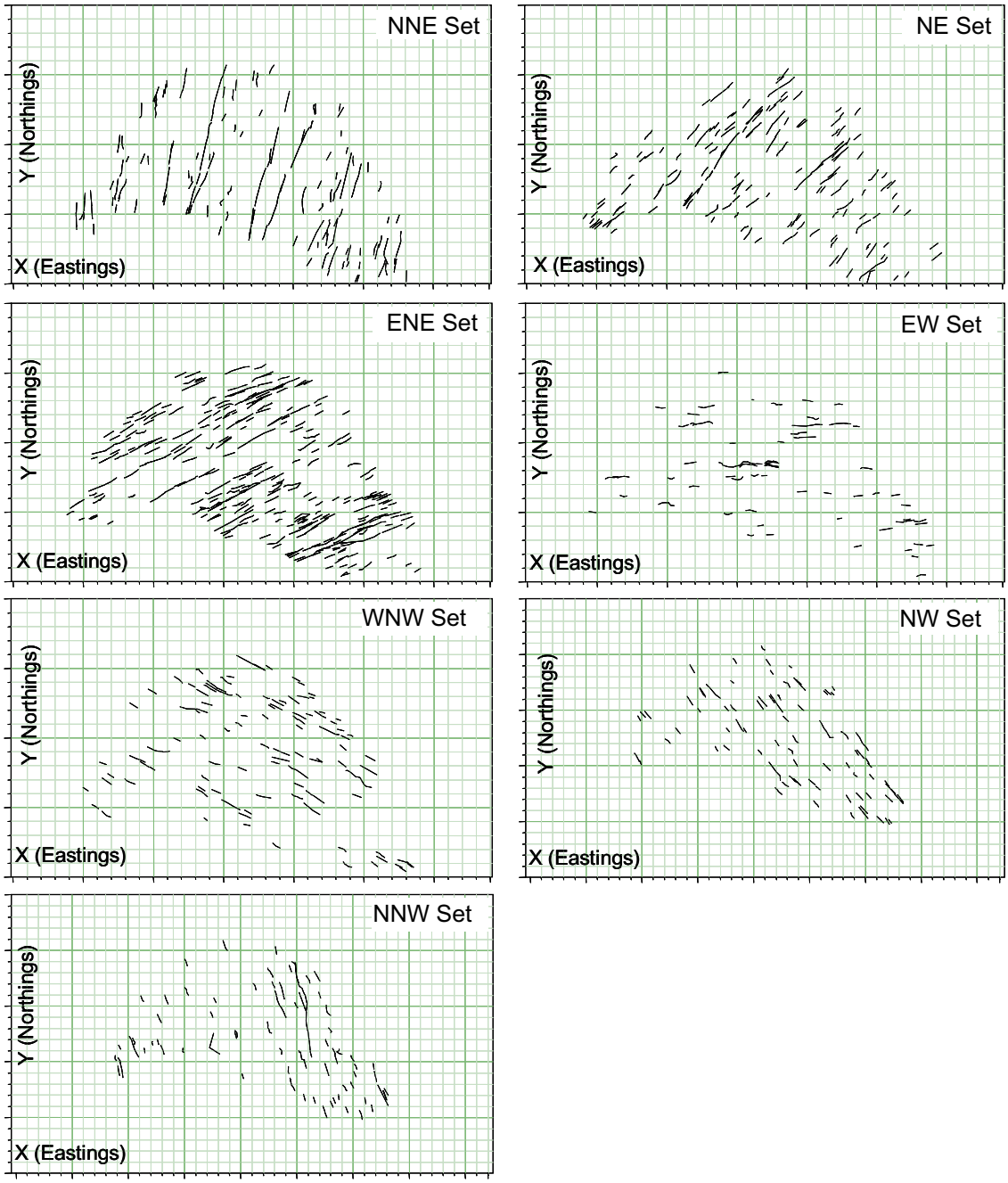

Figure 6-5. *Fracture sets identified in outcrop ASM000206.*

Table 6-1. Statistical parameters for fracture sets identified in outcrops.

Set name	Mean pole trend/ plunge/dispersion	Model	K-S
ASM000025NS	87.5/3.2/10.47	Fisher	Not significant
ASM000025NNE	110.0/3.7/19.31	Fisher	Not significant
ASM000025NE	135.5/3.0/12.78	Fisher	Not significant
ASM000025ENE	346.2/3.6/7.31	Fisher	Not significant
ASM000025WNW	199.0/0.04/10.7	Fisher	Not significant
ASM000025NW	51.5/5.2/8.73	Fisher	1.8%
ASM000026EW	186.3/1.2/32.15	Fisher	Not significant
ASM000026NE	334.5/0.4/30.34	Fisher	Not significant
ASM000026NNE	310.1/0.8/30.47	Fisher	Not significant
ASM000026NS	103.1/1.7/25.92	Fisher	Not significant
ASM000026NNW	67.5/0.2/19.36	Fisher	Not significant
ASM000026NW	214.3/0.8/25.71	Fisher	Not significant
ASM000205NS	101.5/12.3/12.21	Fisher	Not significant
ASM000205NE	128.6/3.3/10.97	Fisher	91.3%
ASM000205ENE	335.4/6.8/13.92	Fisher	Not significant
ASM000205WNW	16.0/1.0/11.11	Fisher	Not significant
ASM000205NW	50.7/3.1/8.86	Fisher	4.1%
ASM000205NNW	79.1/13.6/14.04	Fisher	Not significant
ASM000206NNE	103.5/0.4/7.43	Fisher	Not significant
ASM000206NE	314.8/4.2/6.7	Fisher	Not significant
ASM000206ENE	335.9/4.6/8.53	Fisher	Not significant
ASM000206EW	359.6/24.6/3.75	Fisher	27.8%
ASM000206WNW	27.2/26.9/3.79	Fisher	39.6%
ASM000206NW	50.5/10.9/6.42	Fisher	Not significant
ASM000206NNW	252.6/0.2/6.14	Fisher	Not significant

Table 6-2. Relative chronology of sets in outcrop inferred from abutting relations, length and spatial homogeneity (see also illustrations in Figure 6-1).

ASM000025	Black and Blue (NNE and WNW Sets; NNE older than WNW)
	Cyan and Red (NW and NS Sets; NW older than NS)
	Purple and Green (ENE and NE Sets)
ASM000026	Red (NS Set)
	Blue (NW Set)
	Purple (EW Set)
	Cyan (NNW Set)
	Black and Green (NNE and NE Sets)
ASM000205	Red (NS Set)
	Green and Black (ENE and NE Sets)
	Cyan and Blue (NNW and NW Sets)
	Purple (EW Set)
ASM000206	Red (NNE Set)
	Green and Black (ENE and NE Sets)
	Purple and Blue (EW and WNW Sets)
	Cyan (NW Set)
	Yellow (NNW Set)

The next step in determining sets was to see what fracture sets might be present in the lineament data (Figure 6-6). The lineaments have been classified as either regional or as local major lineaments. The local major lineaments are systematically mapped within the local region, while the regional lineaments intersect the local domain, but extend outside. There may be other regional lineaments that do not intersect the local model domain; as a result, the bias in the regional lineament set makes it inappropriate for the systematic calculations of fracture trace length, but is useful in a qualitative manner for assessing the definition of the lineament trace sets. Figure 6-7 shows the rosette for traces from the local major set of lineaments.

There are two sets present in the regional lineament group, while there are three sets present in the local major lineament group.

One of the interesting differences between the regional and local major sets is the 10°–20° difference in the northeast set. For the regional lineaments, the modal azimuth is between 20° and 30°, while for the local major lineaments, the modal azimuth varies between 40° and 60°. This is not unlike the difference seen in outcrop for the early-formed north-northeast to northeast set.

The relation between the orientations in outcrop and the orientations of the lineaments suggests two possible alternative conceptual models. In the first alternative, three of the outcrop sets are related to the lineament sets, while the rest are not. This alternative conceptual model is consistent with the interpretation of the three dominant local major lineament classes in the local major lineament group rosettes (Figure 6-7).

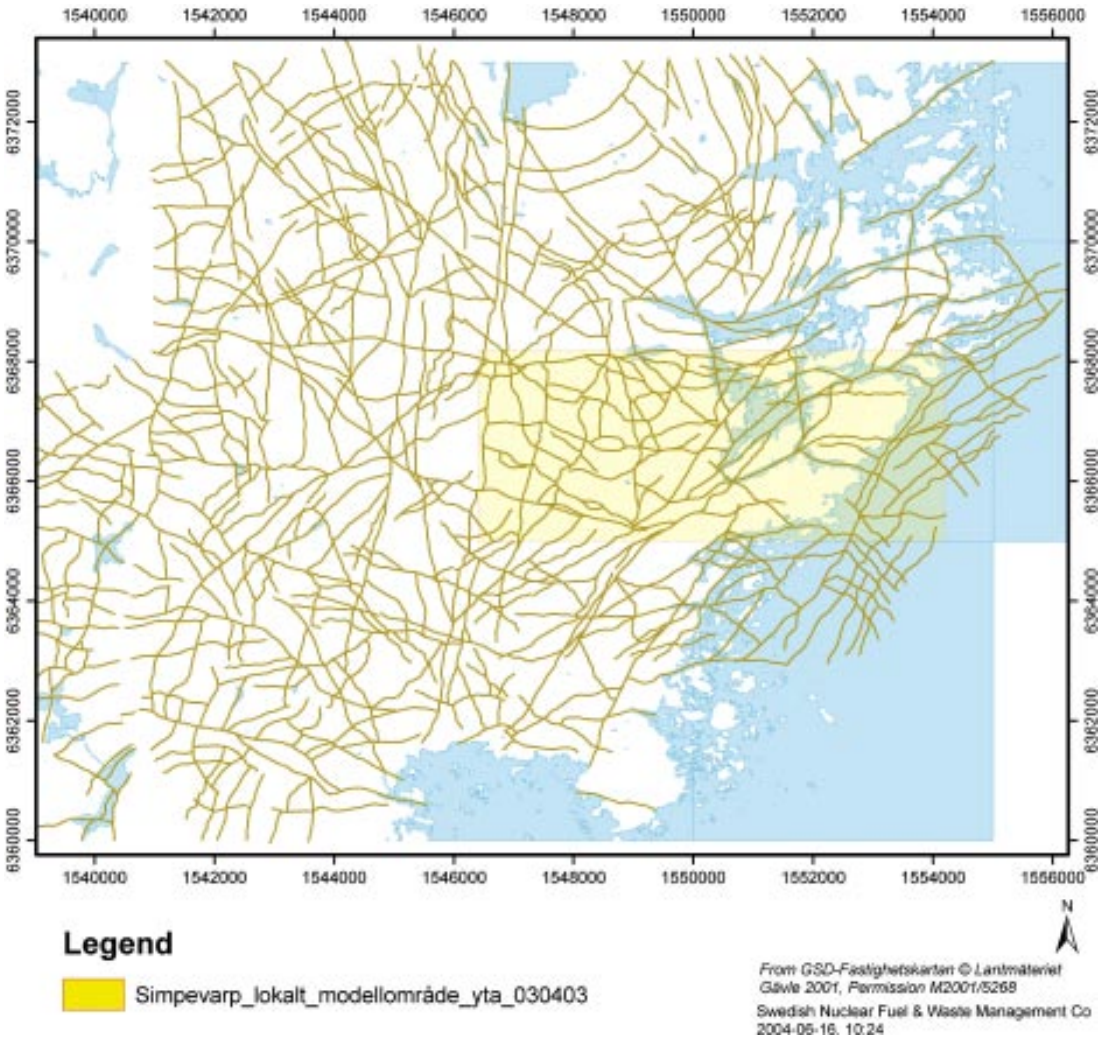

Figure 6-6. *Lineament map for the Simpevarp and Laxemar model region. The local model domain is shown in yellow.*

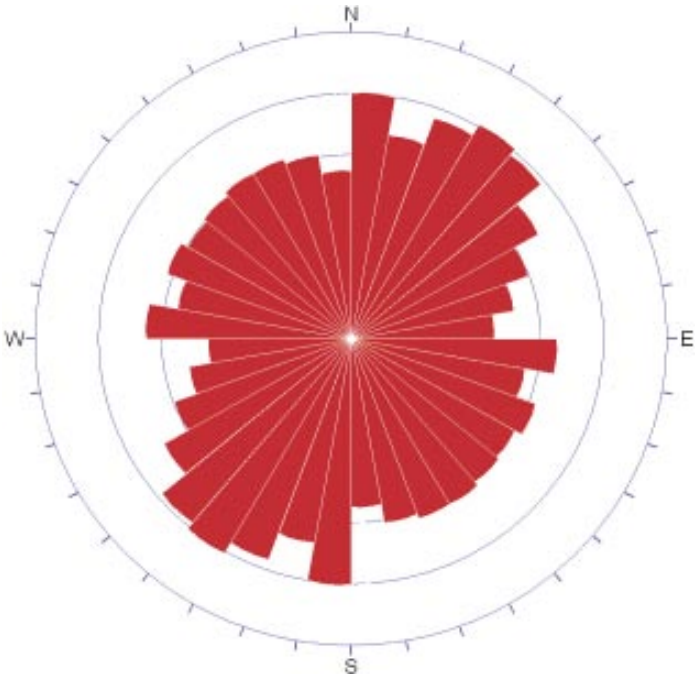

Figure 6-7. *Rosettes for lineaments for the Simpevarp and Laxemar model region.*

Figure 6-8 shows this correspondence more clearly. For example, ASM000025 has a dominant, early north-northeasterly fracture set that is nearly parallel to the adjacent lineament trend. Moreover, this same outcrop shows an early-formed west-northwest set that also parallels an adjacent lineament trend. ASM000206 has a more northeasterly-trending fracture set that is early, but the local lineaments (for example, the lineaments immediately to the northwest of outcrop ASM000206) also show a more northeasterly azimuth rather than a north-northeasterly trend. Dominant sets in ASM000026 are approximately north-northeast and east-west, as are the nearest mapped lineament trends. While these visual similarities are not conclusive, they increase confidence that the early-formed fractures that form a "backbone" or framework for fracturing seen in outcrop are related to the neighboring inferred deformation zone traces. As the trace pattern changes locally across the Simpevarp model area, so does this fracture framework.

The lineament-related fracture sets are termed Group 1 sets.

This conceptual model for the Group 1 fracturing suggests that assigning a single mean fracture orientation to the lineament-related sets would be inaccurate, since the local fracturing at outcrop and lineament scales varies spatially. In terms of developing a regional model, this implies that:

- Some fracture sets identified in outcrop appear to be related to nearby lineaments in terms of orientations.
- Orientations of lineament-related fracture sets, whether at the scale of meters or kilometres, change locally according to the dominant orientations of adjacent lineaments.
- Assignment of a mean orientation for any lineament-related fracture set would be inaccurate. Orientations should be assigned based on adjacent lineament trends, using the dispersion values calculated from the outcrop analyses of the respective sets.

The remaining fracturing not part of the lineament-related sets forms the Group 2 sets.

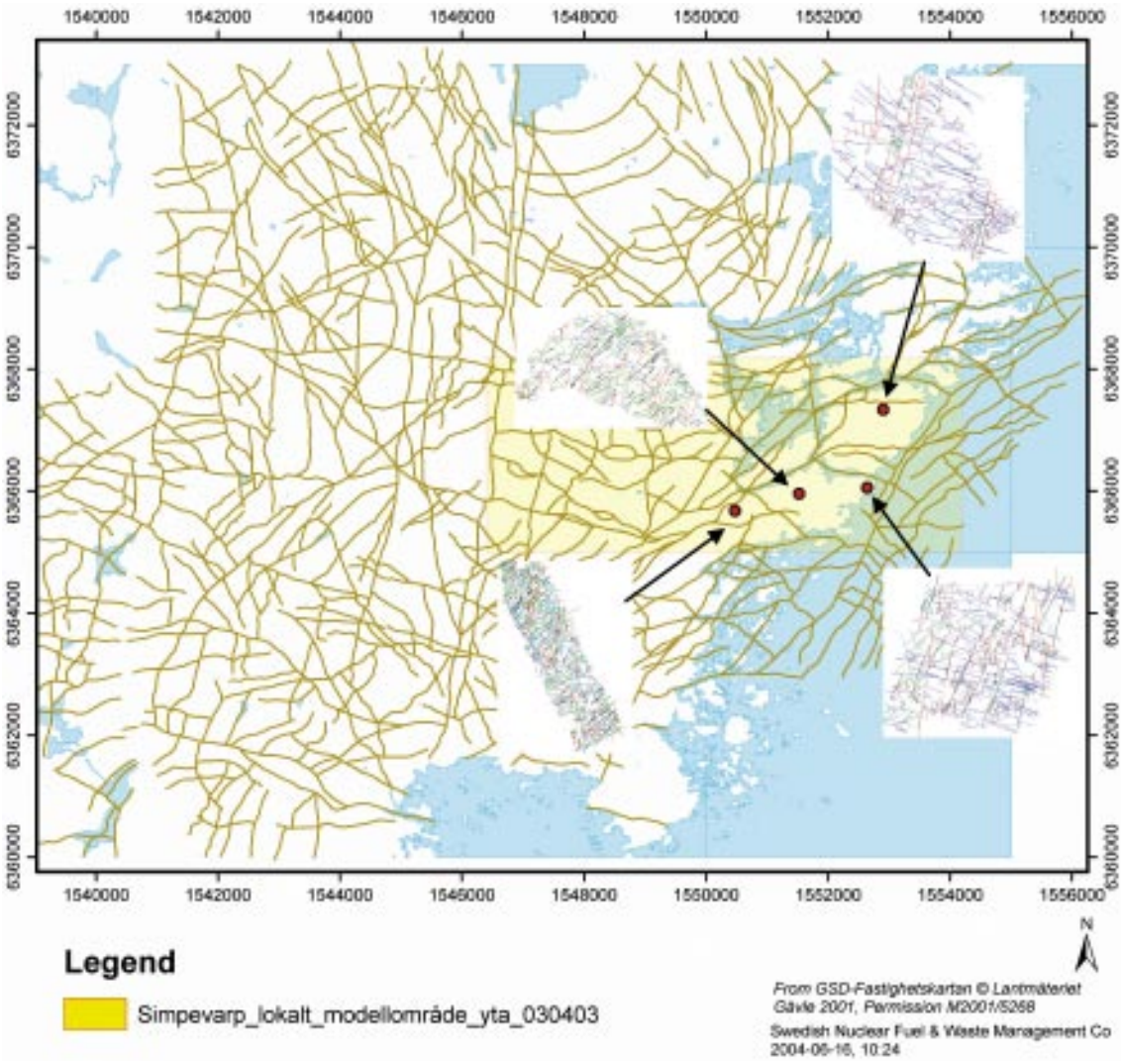

Figure 6-8. *Outcrop trace maps superimposed on lineament map. Note the similarity between adjacent lineament trends and the dominant, older fracture sets in outcrop.*

The outcrop fracture sets that are not part of one of the three lineament sets can be combined to see if they show consistency among outcrops. The resulting equal-area stereoplot is shown in Figure 6-9.

This stereoplot shows that there are two dominant, spatially consistent vertical sets with modal poles orientations at 325/04 and 277/01, as well as possibly one or two sub-horizontal sets oriented 153/75 and 357/69. There are clearly northwesterly striking fractures as well, but their orientations are not well clustered into a distinct set. The northwesterly trending sub-vertical fractures have an approximate mean pole of 038/02.

Figure 6-10 shows the orientations of only the Group 2 fractures designated as open. The two sub-vertical sets have modal poles of 328/03 and 279/03. There is also a sub-horizontal set with a modal pole of 151/76, and abundant, thought poorly clustered, northwesterly-striking sub-vertical fracturing.

Figure 6-11 shows the orientations of only the Group 2 fractures designated as sealed. The two sub-vertical sets have modal poles of 325/05 and 097/01. There is also a sub-horizontal set with a modal pole of 357/70.

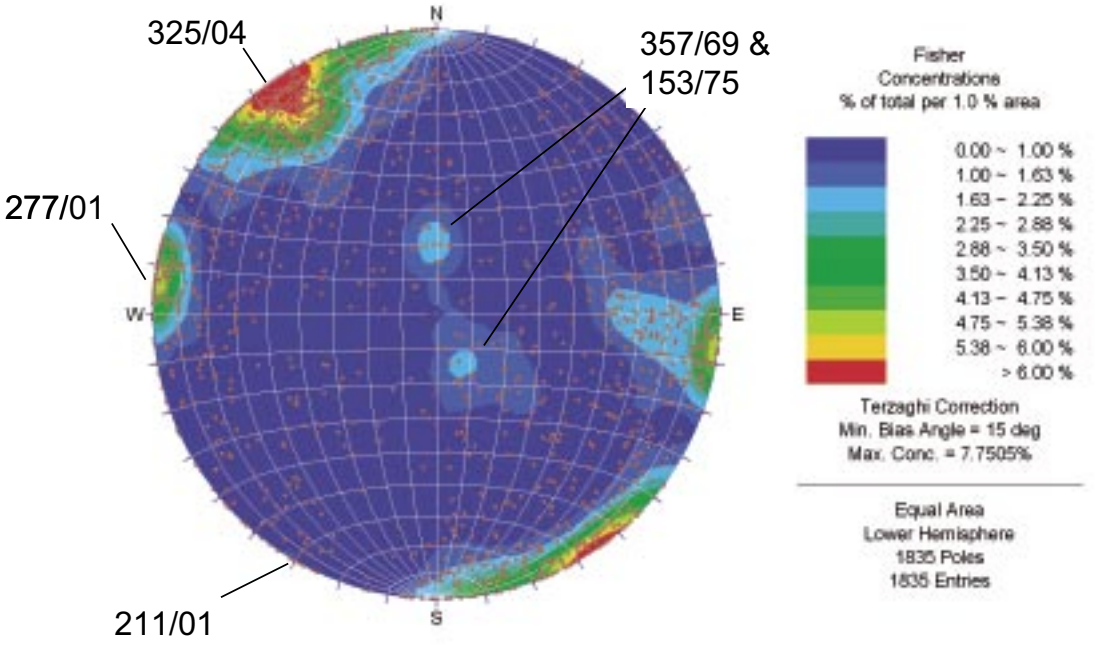

Figure 6-9. *Terzhagi corrected contours of all fracture sets (i.e. open and sealed) not identified as lineament-related in outcrops ASM000025, ASM000026, ASM000205 and ASM000206.*

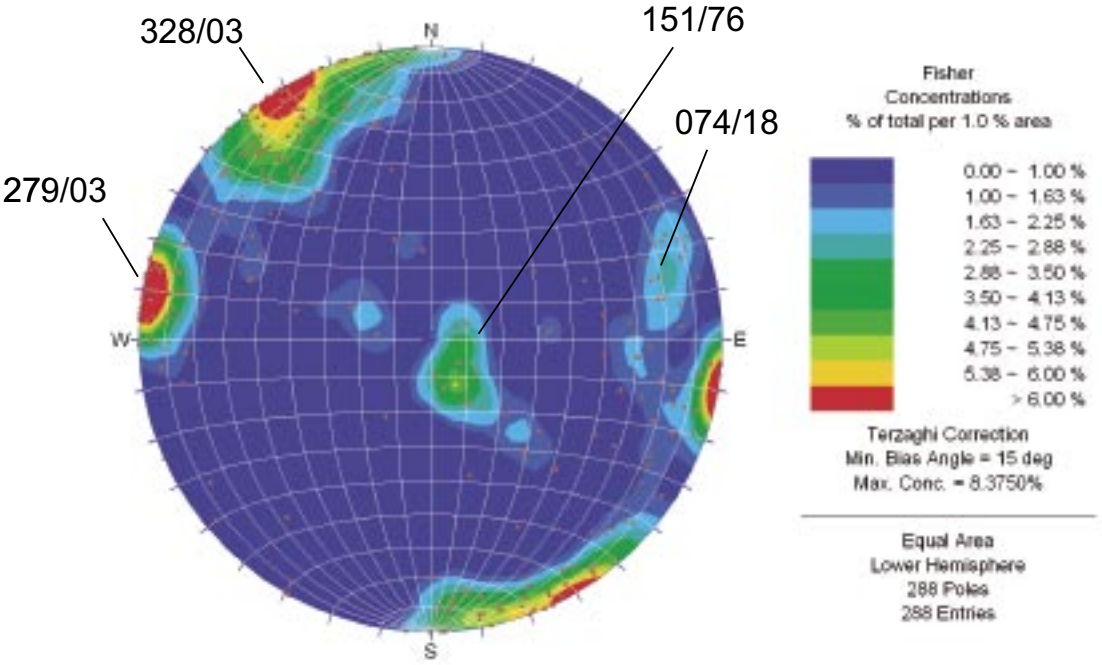

Figure 6-10. *Stereoplot of all Group 2 Open fractures for outcrops ASM000025, ASM000026, ASM000205 and ASM000206.*

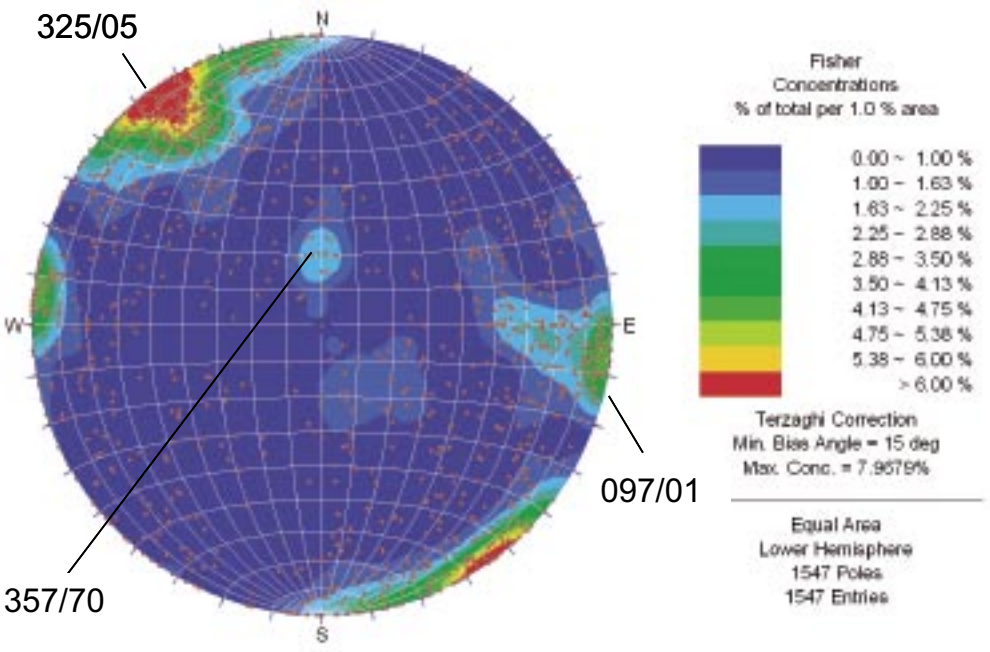

Figure 6-11. *Stereoplot of all Group 2 Sealed fractures for outcrops ASM000025, ASM000026, ASM000205 and ASM000206.*

Table 6-3. Mean dispersion (κ) for lineament-related fracture sets based on averaging outcrop values for each set.

Lineament-related fracture set identifier	Dispersion averaged from outcrop sets
NNE-NE	17.3
EW-WNW	11.2
NW-NNW	13.7

Fractures belonging to the 277/01 group are designated as the “Background – NS” set, or BGNS in the tables and figures. Fractures belonging to the 325/04 group as designated as the “Background – NE” set, or BGNE. The diffuse northwesterly fracturing is designated as the “Background – NW” set, or BGNW. The horizontal fracturing is the “Background – Horizontal” set or SubHz. The orientation parameters determined for the fracture sets in Alternative 1 are summarized in Table 6-4 for sub-vertical sets.

There is an alternative interpretation of the lineament maps that suggests a second conceptual model for fracturing.

The broad range of azimuths of the lineament sets and visual inspection of the lineament trace maps suggests that there might be up to six lineament trace sets as well (Figure 6-12). These six lineament trace sets correspond reasonably well to the six outcrop trace sets.

In the second alternative, all sub-vertical fracture sets have lineament counterparts. The relation between the outcrop data sets and the lineament data sets for Alternative 2 is given in Table 6-5

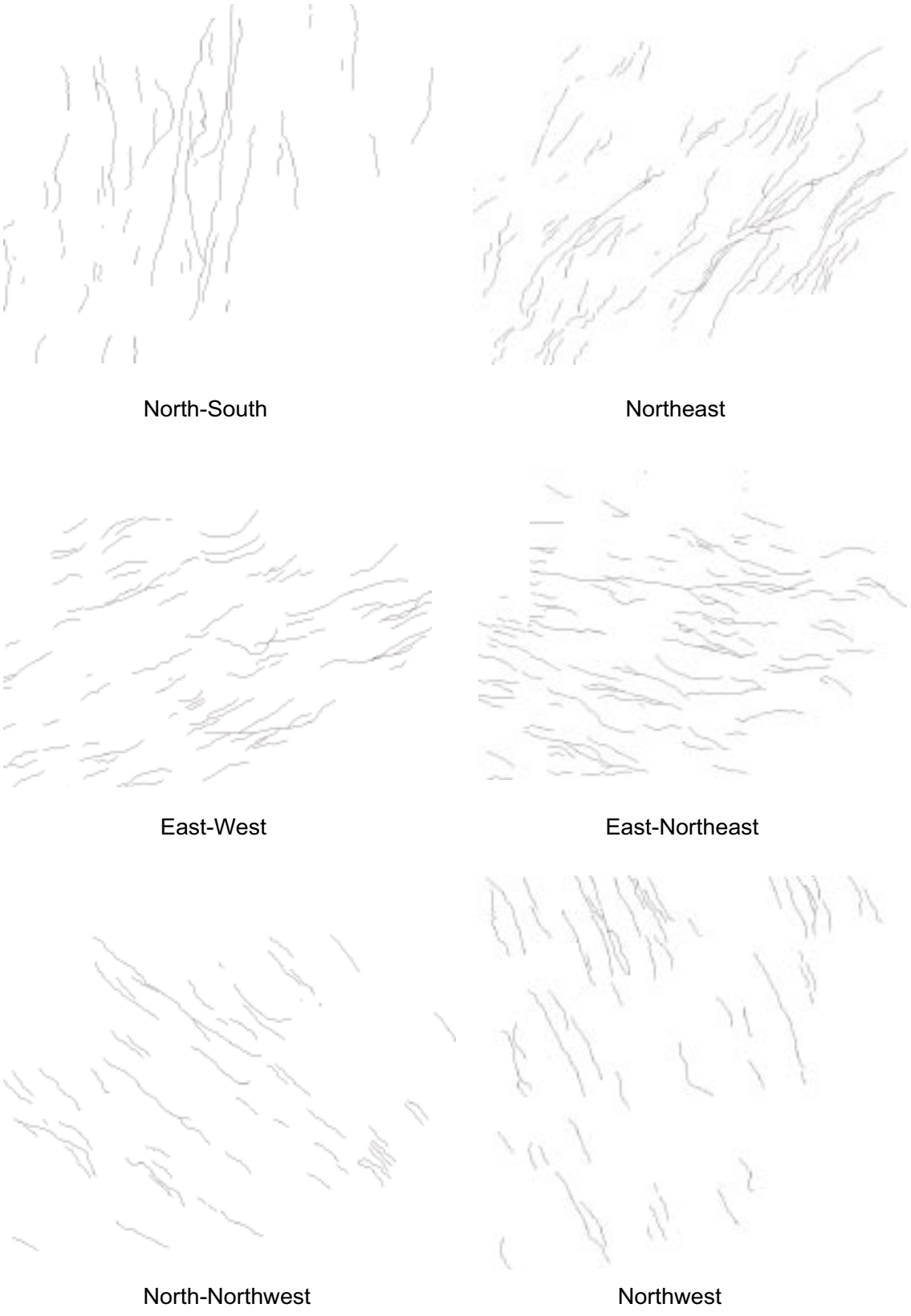

Figure 6-12. *Lineament trace sets (based on lineaments in Figure 6-6) for Alternative 2 conceptual model.*

Table 6-4. Orientation parameters for Alternative 1 sub-vertical fracture sets.

ORIENTATION Set name	Mean pole trend/ plunge/dispersion	Orientation distribution model/ K-S statistic	Relative % of total population of sub-vertical fractures (Terzhaghi corrected)
NNE-NE	118.0/1.9/17.3	Fisher Not significant	18.99%
EW-WNW	17.1/7.3/11.2	Fisher Not significant	17.75%
NW-NNW	73.1/4.7/13.7	Fisher Not significant	22.50%
BGNE	326.3/5.5 K1:17.65 K2:18.14	Bivariate Fisher 0.041/45.4%	18.60%
BGNS	96.8/3.8/20.32	Fisher not significant	15.44%
BGNW	22.1/2.4 K1:5.36 K2: 6.66	Bivariate Fisher 0.051/61.3%	6.71%

Table 6-5. Set names and definitions for Alternative Conceptual Model 2.

Fracture set name	Set name in ASM000025	Set name in ASM000026	Set name in ASM000205	Set name in ASM000206
NS	NNE	NS	NS	NNE
NE	NE	NNE	NE	NE
ENE	ENE	NE	ENE	ENE
EW	WNW	EW	WNW	EW
NW	NW	NW	NW	NW
NNW	NS	NNW	NNW	NNW

Table 6-6. Orientation parameters for Alternative 2 sub-vertical fracture sets.

ORIENTATION Set name	Mean pole trend/ plunge/dispersion	Orientation distribution model/K-S statistic	Relative % of total population of sub-vertical fractures (Terzhaghi corrected)
NS	99.7/6.9/9.63	Fisher Not significant	13.74%
NE	128.4/2.6/8.92	Fisher Not significant	12.32%
ENE	331.7/5.4/10.2	Fisher Not significant	23.72%
EW	6.0/3.1/6.97	Fisher Not significant	15.75%
NW	39.0/0.7/7.78	Fisher Not significant	21.16%
NNW	74.5/9.2/9.17	Fisher Not significant	13.30%

An additional question concerns whether fracture set orientations change with depth.

Figure 6-13 is a plot of fracture strike vs depth. This figure does not indicate that the fracture orientations change systematically with depth, although strike alone does not provide a complete picture.

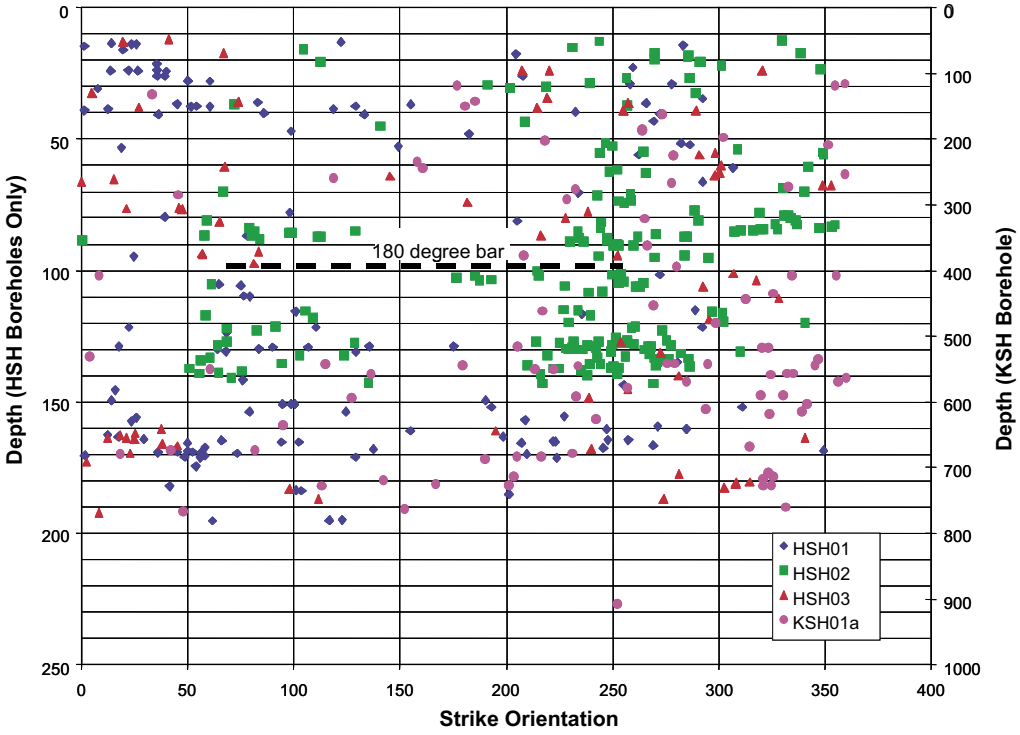

Figure 6-13. *Variation of fracture strike with depth for percussion boreholes and borehole KSH01A. (Schmidt) Equal Area net.*

6.1.2 Sub-horizontal set

Sub-horizontal fractures in outcrops with dips equal or less than 25 degrees constitute about 3% (unweighted) or 9% (Terzaghi corrected) of the sampled population. The mapping of these fractures is difficult in outcrop due to the intersection angle with the horizontal outcrop, weathering and erosion. The sub-sample is also quite small (129 fractures in all four outcrops). Therefore it is considered that borehole data may provide a more comprehensive data source for sub-horizontal fractures.

Borehole data from KSH01A, KSH01B, KSH02, KSH03A, KSH03B, KAV01 and KLX02 as well as HSH01, HSH02 and HSH03 provide around 30,000 fractures with dips less than 25 degrees. A visual analysis of the clustering of all fractures in all orientations in these boreholes indicates that there is no clear set of sub-horizontal fractures. Rather, it is a concentration of sub-horizontal fractures that decreases evenly towards steeper fracture orientations. This pattern prevails even after orientation bias has been corrected. For simplistic reasons, it was decided to capture the slight offset of the sub-horizontal set centre and at the same time provide a set definition that was easy to use for modelling. The sub-horizontal set was defined by all fractures with dips equal to or less than 20 degrees and fractures dipping equal to or less than 25 degrees in the interval N25W to N80E, cf Figure 6-14. Sub-horizontal fractures in this interval constitute about 20% (unweighted) or 12% (Terzaghi corrected) of the borehole fractures. Table 6-7 presents statistics for the sub-horizontal set.

The difference in relative proportion between sub-horizontal and the rest of the fractures in outcrop and borehole is similar once orientation bias is considered (9% in outcrop and 12% in borehole). This similarity gives some confidence that borehole data can be used for estimating orientation characteristics of a sub-horizontal set.

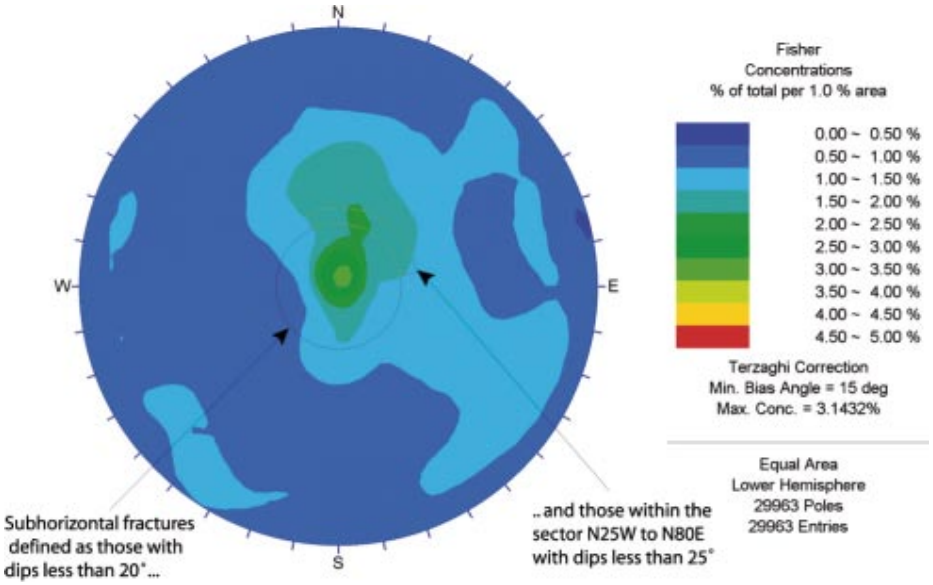

Figure 6-14. *Definition of sub-horizontal fractures from borehole data for the purposes of evaluating intensity variations with depth. The plot shows open and sealed fractures from boreholes KSH01A, B, KSH02, KSH03A, B, KAV01 and KLX02 as well as HSH01, HSH02, and HSH03.*

Table 6-7. Orientation parameters for Alternatives 1 and 2 sub-horizontal fracture sets.

ORIENTATION Set name	Mean pole trend/ plunge/dispersion	Model/K-S	Relative % of total population in boreholes Unweighted (Terzhagi corrected)
SubHZ	33/86/31.3	Fisher	20.1% (12.4%)

6.2 Estimation of fracture sizes

The size distribution parameters were estimated in two different ways, depending upon whether the fracture set was lineament-related (Group 1) or not.

The Group 1 calculations were carried out by first computing the mass dimension of the fracture traces, and then using the mass dimension for determining the appropriate area renormalization scaling. If the mass dimension was close to 2.0, then the scaling is approximately Euclidean and the area re-normalization is accomplished by simply dividing the number of fractures by the outcrop or lineament map area. For Group 2 fractures, the size was determined by carrying out the FracSize approach on the outcrop data alone.

Figure 6-15 through Figure 6-18 show the mass dimension plots for each identified outcrop fracture set. The mass dimension parameters are shown in Table 6-8. The mass dimension analyses for each fracture data set shows that intensity does not scale (except in rare cases) linearly with area. In other words, the scaling behavior is rarely Euclidean. In general, the regression through the locus of the mean for each mass dimension plot indicates that a fractal scaling behavior is a valid model for these fracture sets.

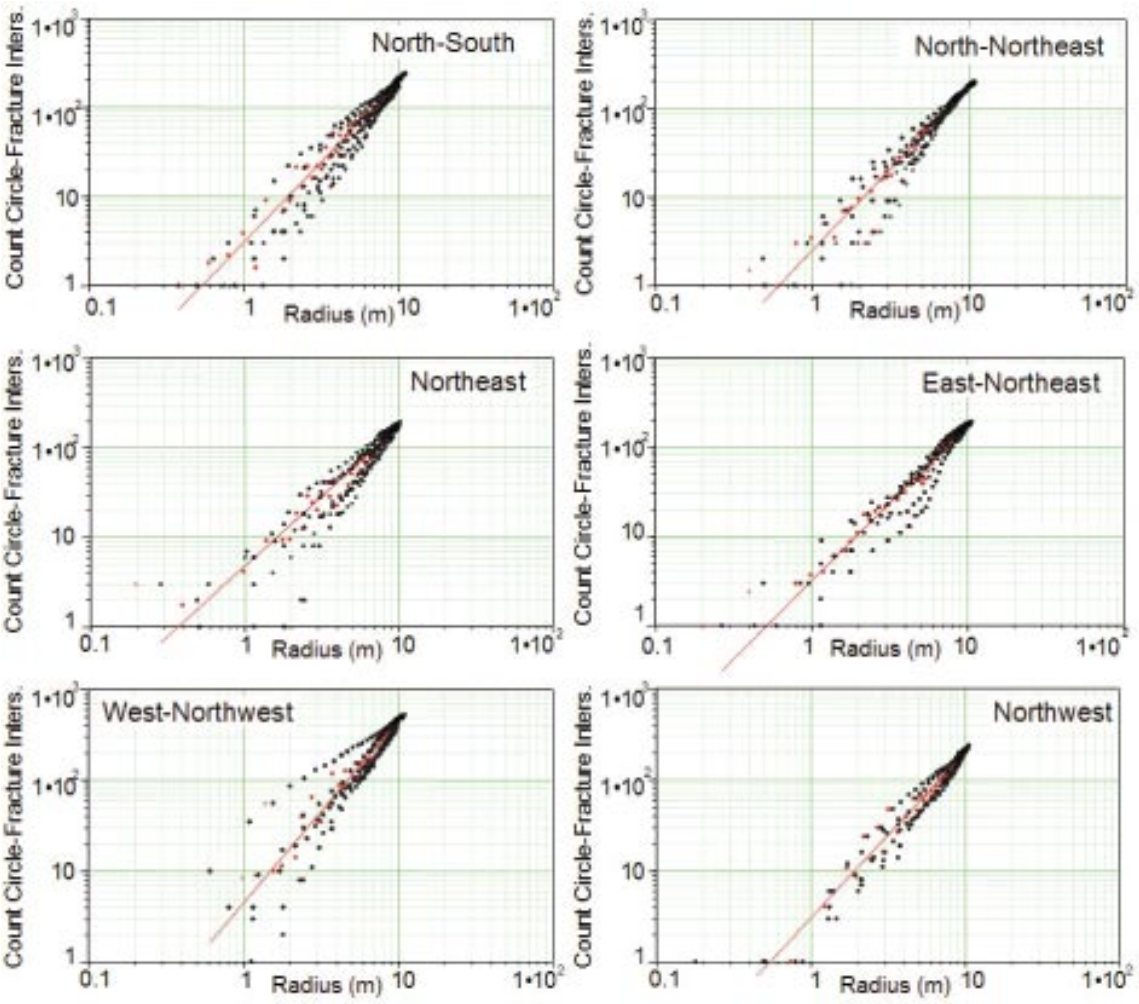

Figure 6-15. *Mass dimension calculations for individual fracture sets identified in outcrop ASM000025.*

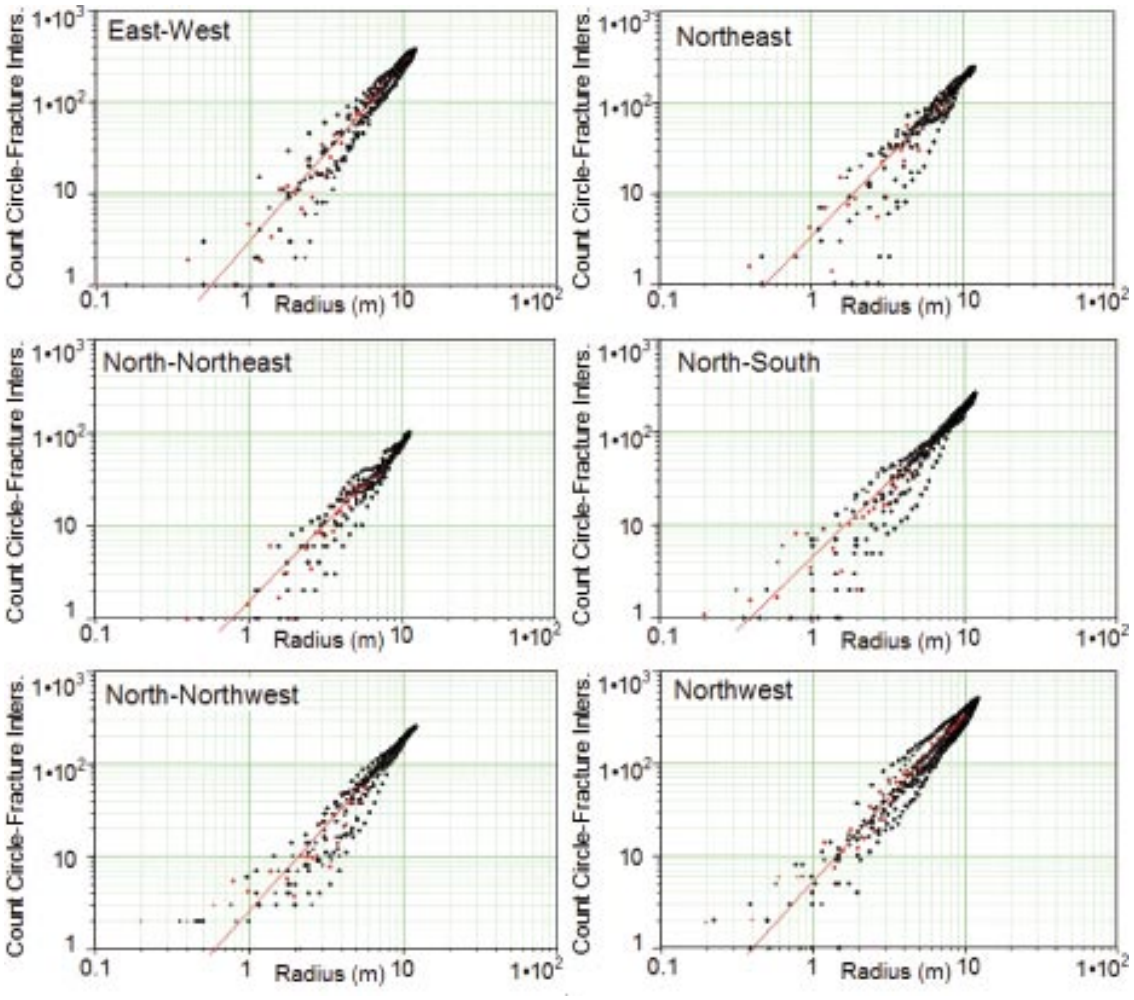

Figure 6-16. *Mass dimension calculations for individual fracture sets identified in outcrop ASM000026.*

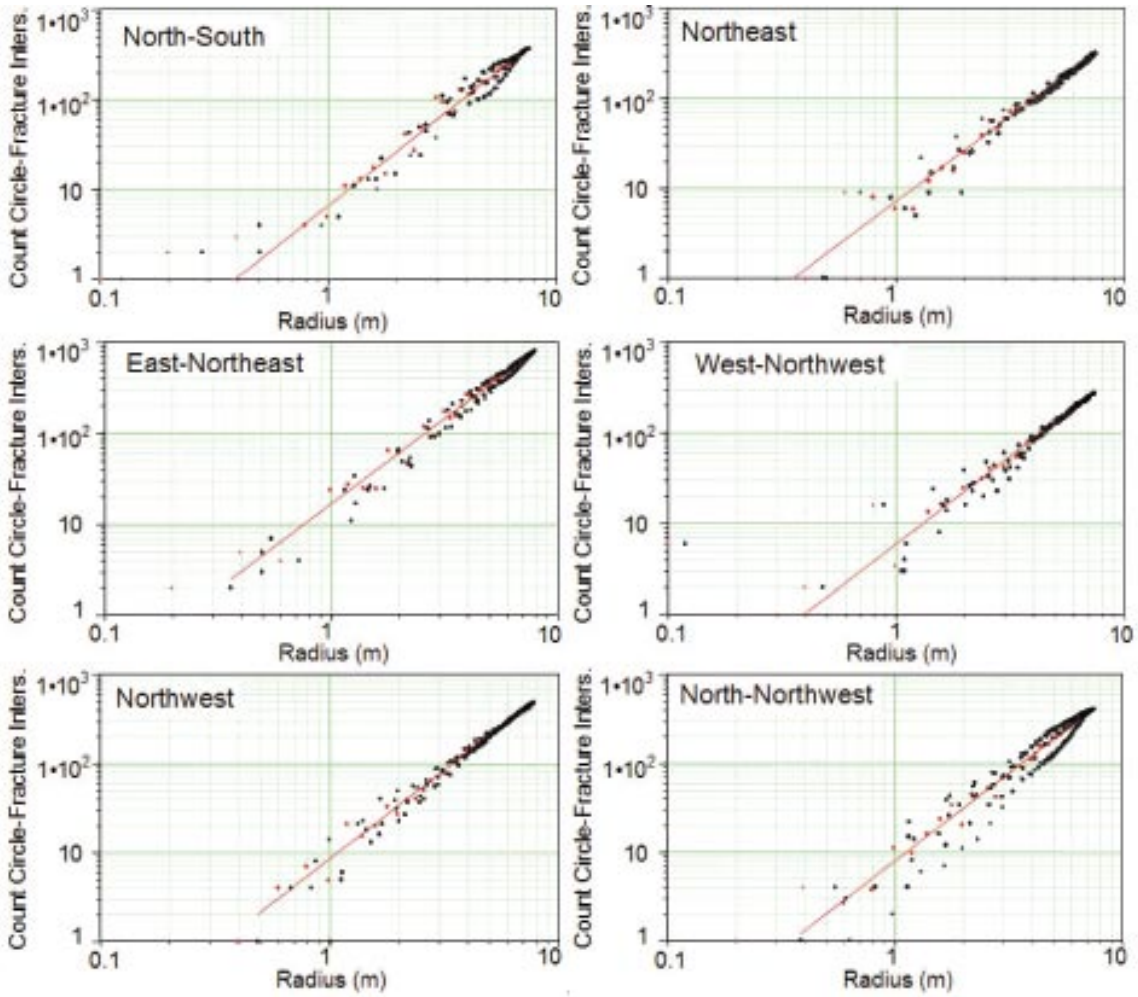

Figure 6-17. *Mass dimension calculations for individual fracture sets identified in outcrop ASM000205.*

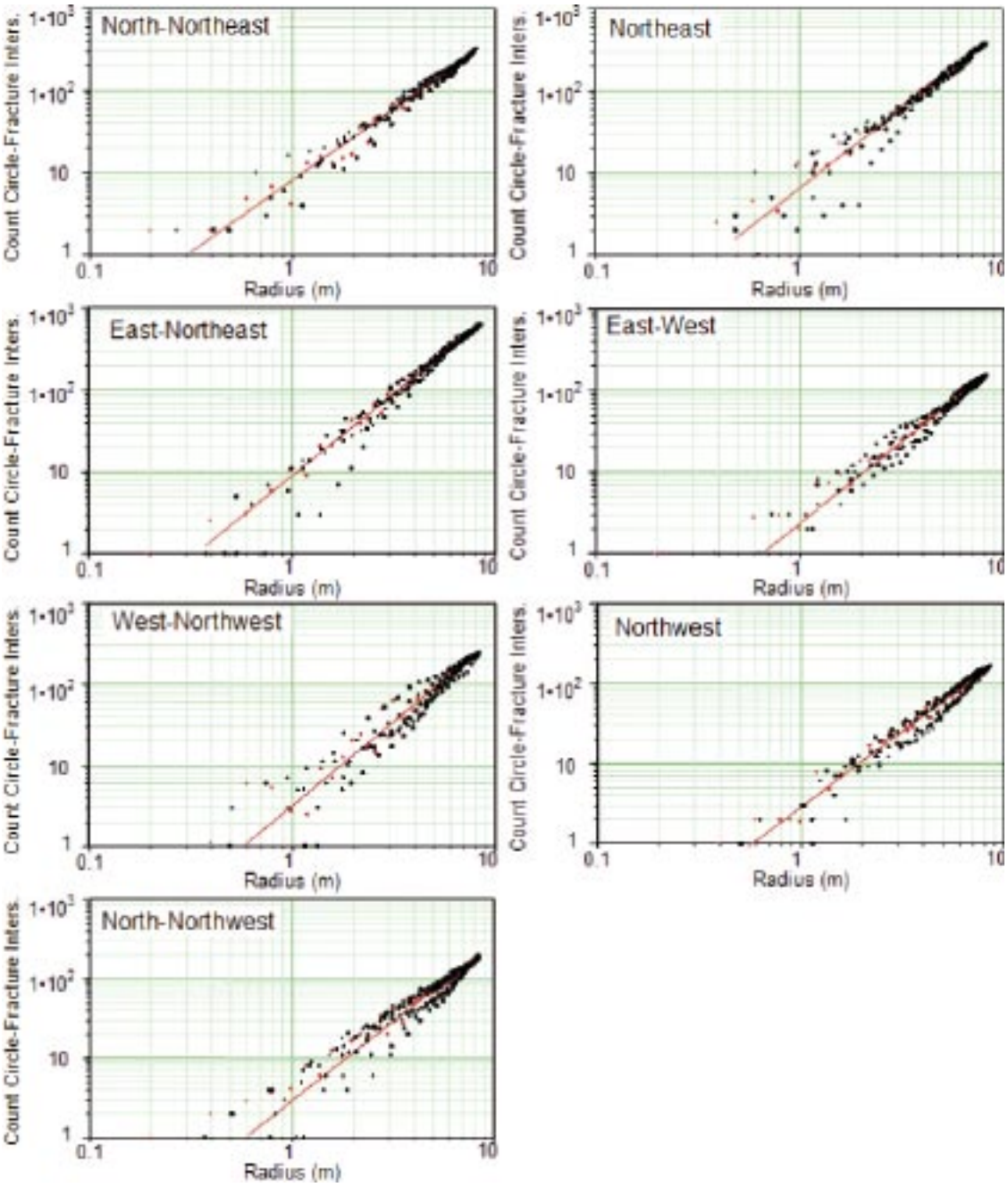

Figure 6-18. *Mass dimension calculations for individual fracture sets identified in outcrop ASM000206.*

Table 6-8. Mass dimension parameters for the outcrop data sets.

Outcrop	Set name	ρ	Dmass	SSQ	St. dev error
ASM000025	NS	3.09	1.80	3,525.25	8.32
ASM000025	NNE	2.50	1.85	941.20	4.34
ASM000025	NE	4.74	1.56	4,218.11	9.68
ASM000025	ENE	3.16	1.74	3,556.90	8.52
ASM000025	WNW	4.45	2.01	16,969.90	19.87
ASM000025	NW	3.06	1.82	3,226.67	9.34
ASM000025	EW	3.05	1.93	8,018.03	11.97
ASM000026	NE	3.30	1.73	6,470.95	10.95
ASM000026	NNE	1.50	1.69	726.16	3.81
ASM000026	NS	4.45	1.60	4,603.93	8.91
ASM000026	NNW	2.55	1.85	2,390.03	6.65
ASM000026	NW	5.24	1.81	7,890.95	11.87
ASM000205	NS	6.60	2.01	12,562.60	20.13
ASM000205	NE	7.06	1.91	835.79	5.28
ASM000205	ENE	16.75	1.87	12,620.30	19.56
ASM000205	WNW	5.94	1.93	1,036.38	6.08
ASM000205	NW	8.49	1.99	1,230.92	5.85
ASM000205	NNW	7.91	1.98	1,885.87	7.68
ASM000206	NNE	8.05	1.74	4,717.42	11.29
ASM000206	NE	6.38	1.95	1,159.26	5.93
ASM000206	ENE	8.99	2.00	8,288.86	14.58
ASM000206	EW	2.35	2.00	566.59	4.42
ASM000206	WNW	3.18	2.07	3,787.26	10.26
ASM000206	NW	2.83	1.90	761.22	4.54
ASM000206	NNW	2.91	2.00	3,693.61	9.99

The trace length scaling plots (Figure 6-19 through Figure 6-24) show the renormalized data and three lines fit visually to the data. The lines labeled as “Upper” and “Lower” represent the upper and lower bounds on the data, and are measures of the uncertainty in the trace length scaling calculations. The median line is the visual best fit to the data. The statistics reported in each plot consist of the slope of the line, labeled as k_t, and the parameter t_0 for the power law distribution. These two trace length parameters are used to calculate the parameters for the parent radius distribution according to Equation 5-6. Trace length scaling plots for the Euclidean scaling assumption are provided as a reference in Figure 6-25 through Figure 6-30 to facilitate comparison with other previous studies in the Simpevarp area.

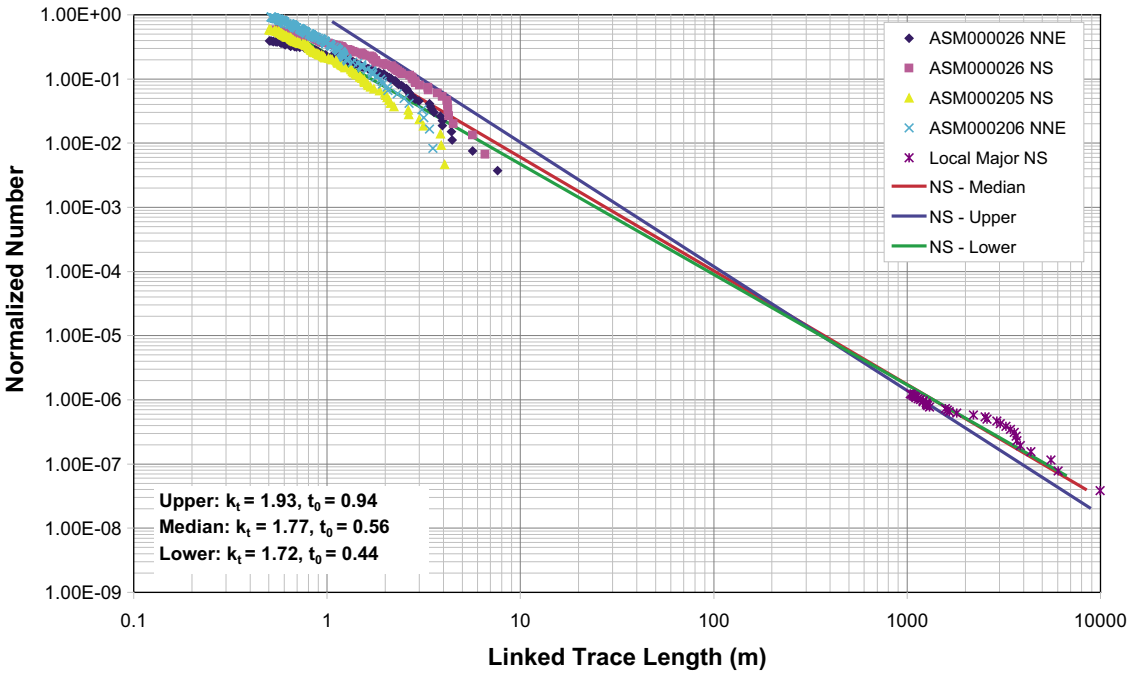

Figure 6-19. *Trace length scaling plot for the NS set (Alternative 2 only).*

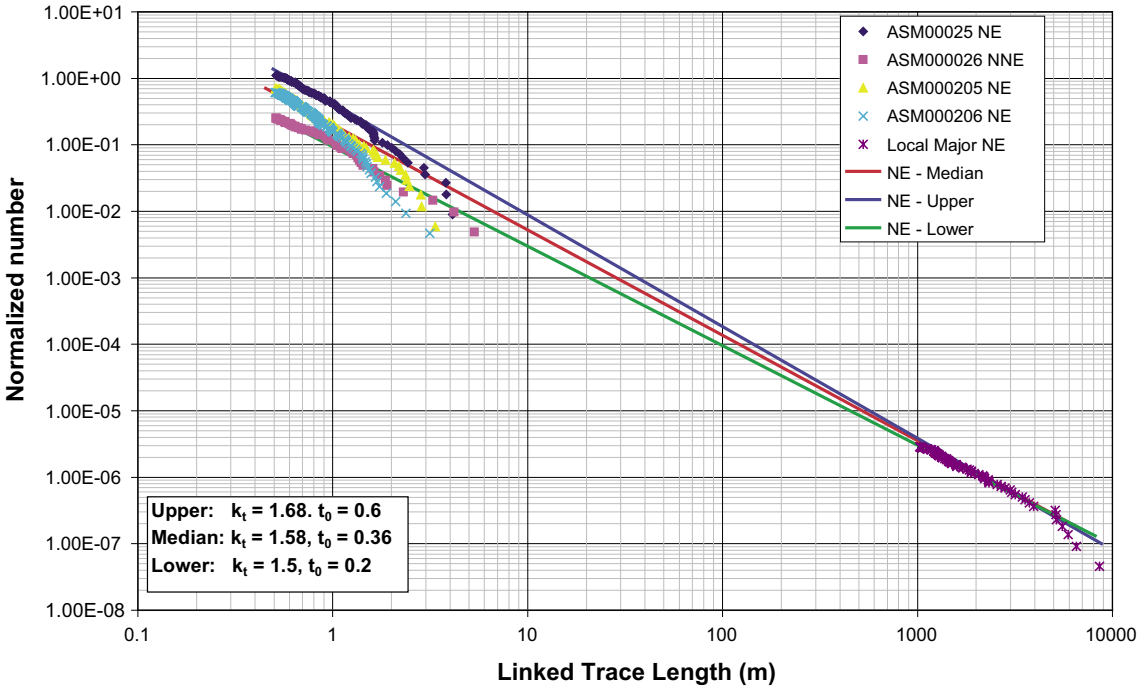

Figure 6-20. *Trace length scaling plot for the NE set (Alternatives 1 and 2).*

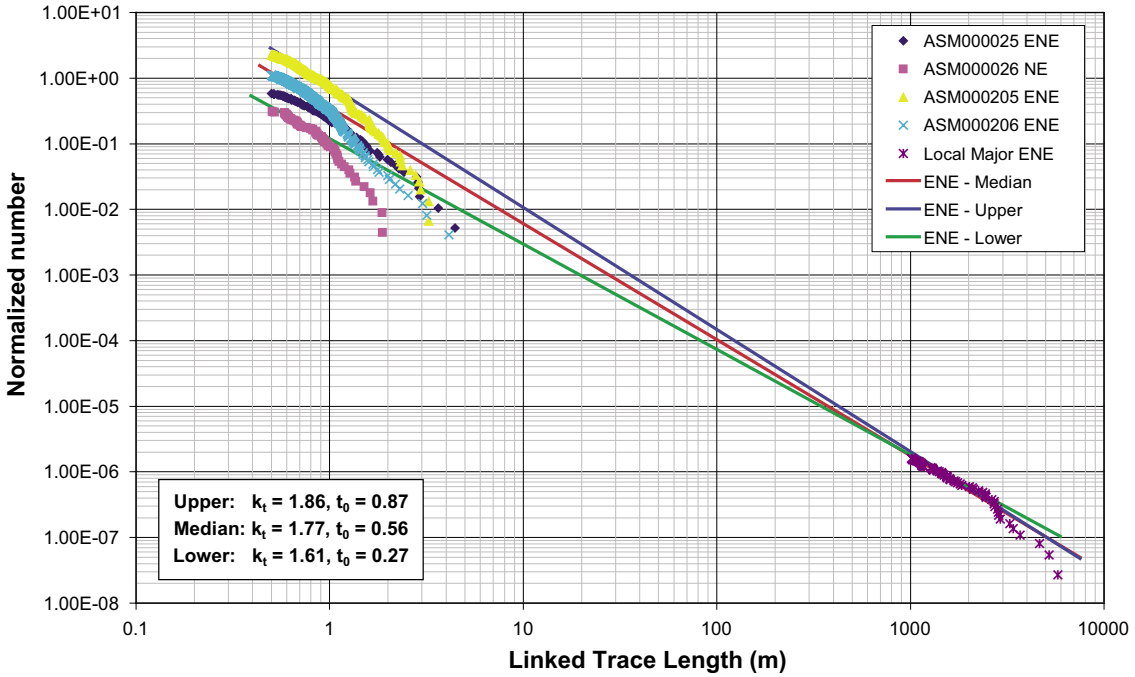

Figure 6-21. *Trace length scaling plot for ENE set (Alternative 2 only).*

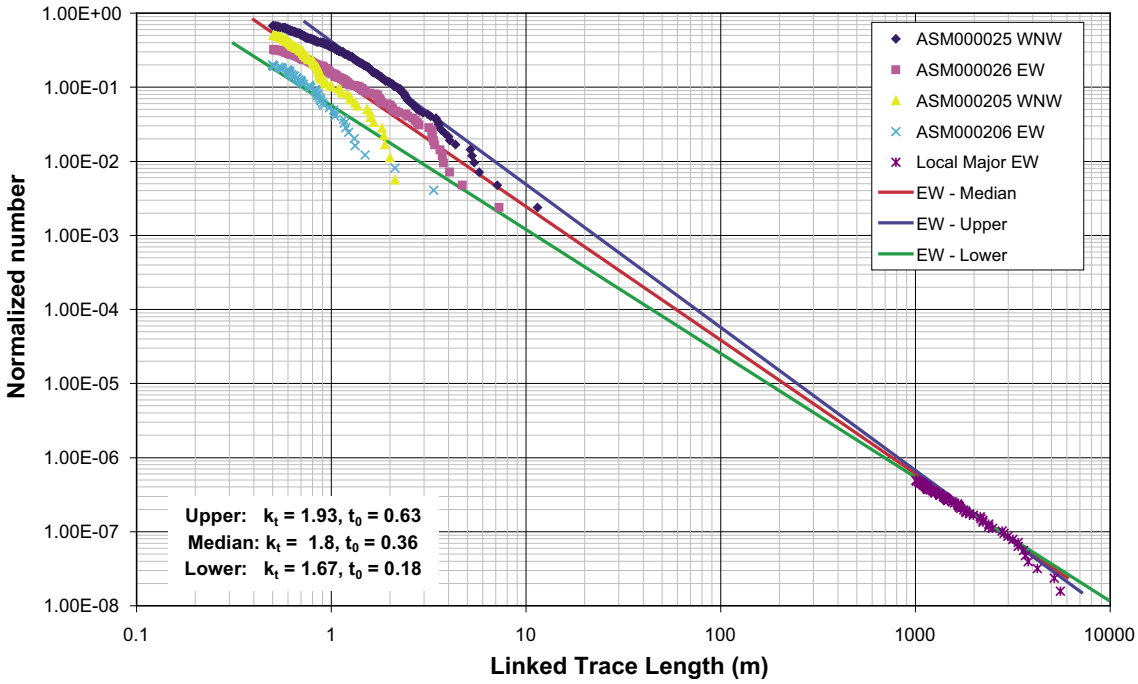

Figure 6-22. *Trace length scaling plot for the EW set (Alternatives 1 and 2).*

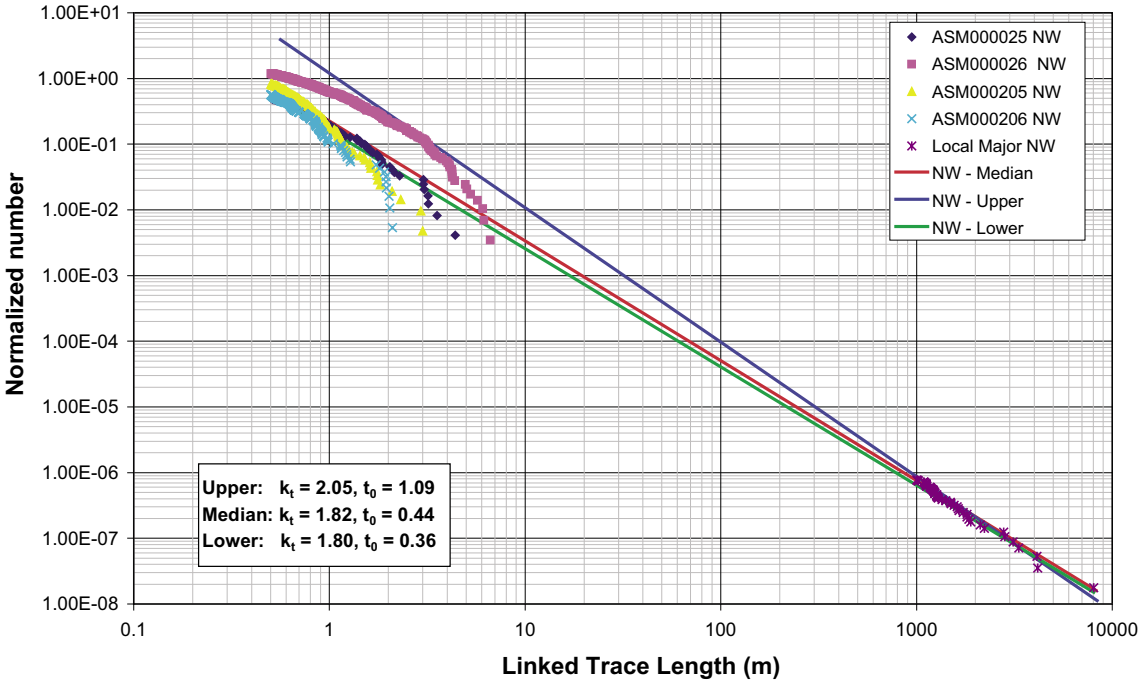

Figure 6-23. *Trace length scaling plot for NW set (Alternative 2 only).*

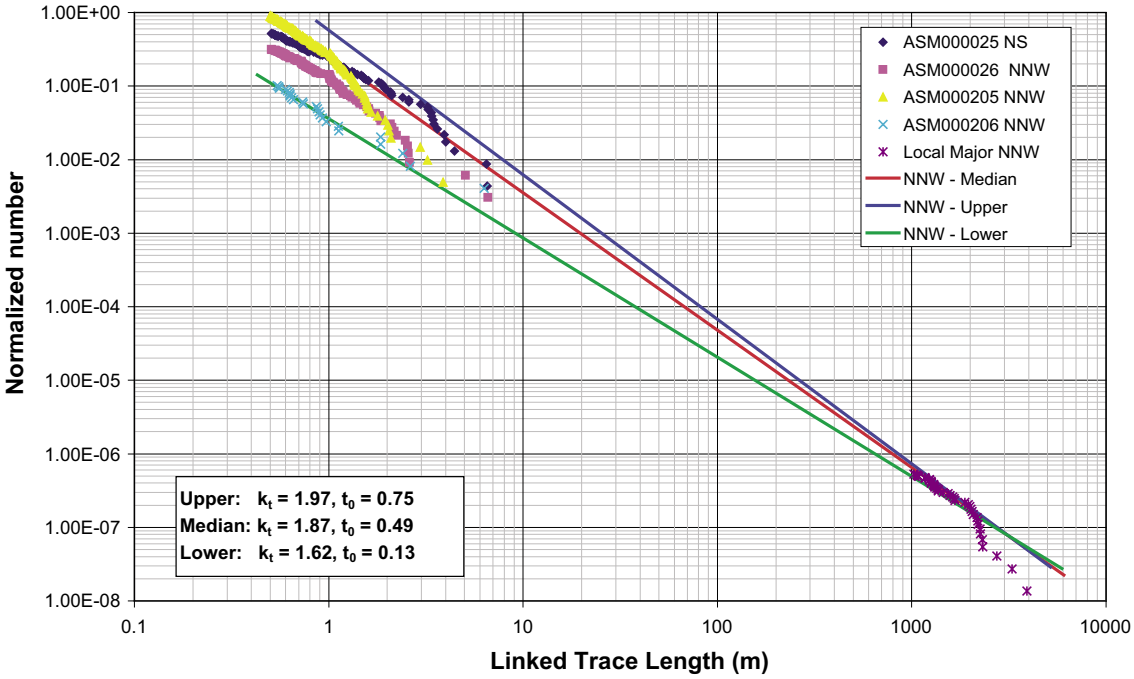

Figure 6-24. *Trace length scaling plot for the NNW set (Alternatives 1 and 2).*

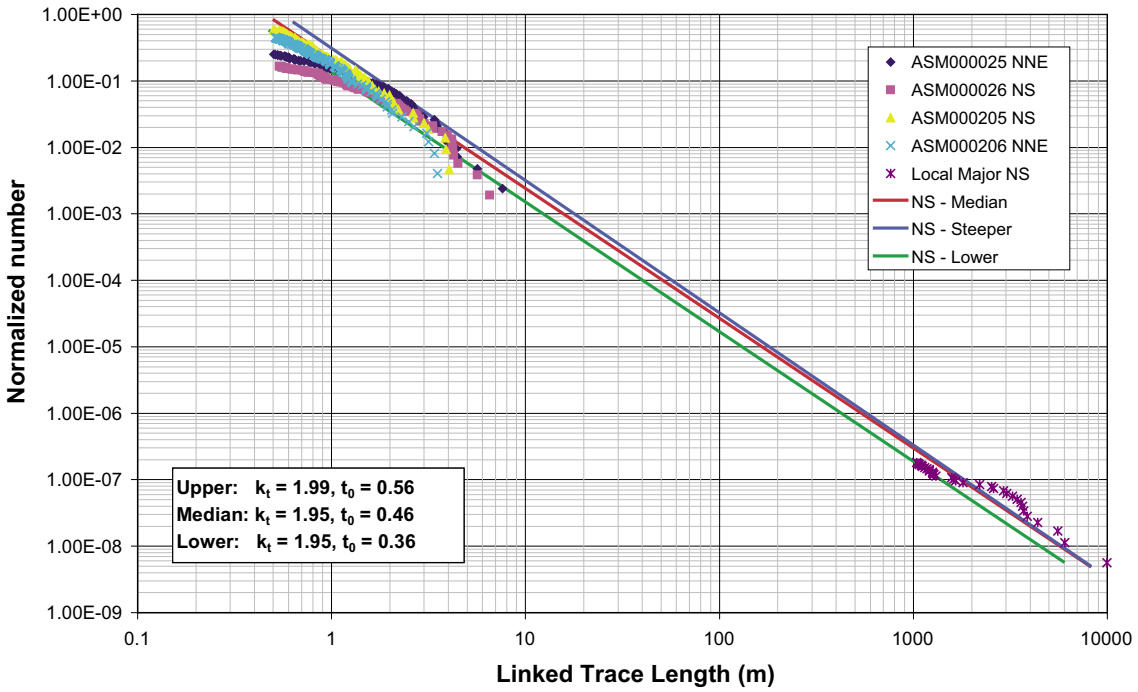

Figure 6-25. *Trace length scaling plot for the NS set (Alternative 2 only).*

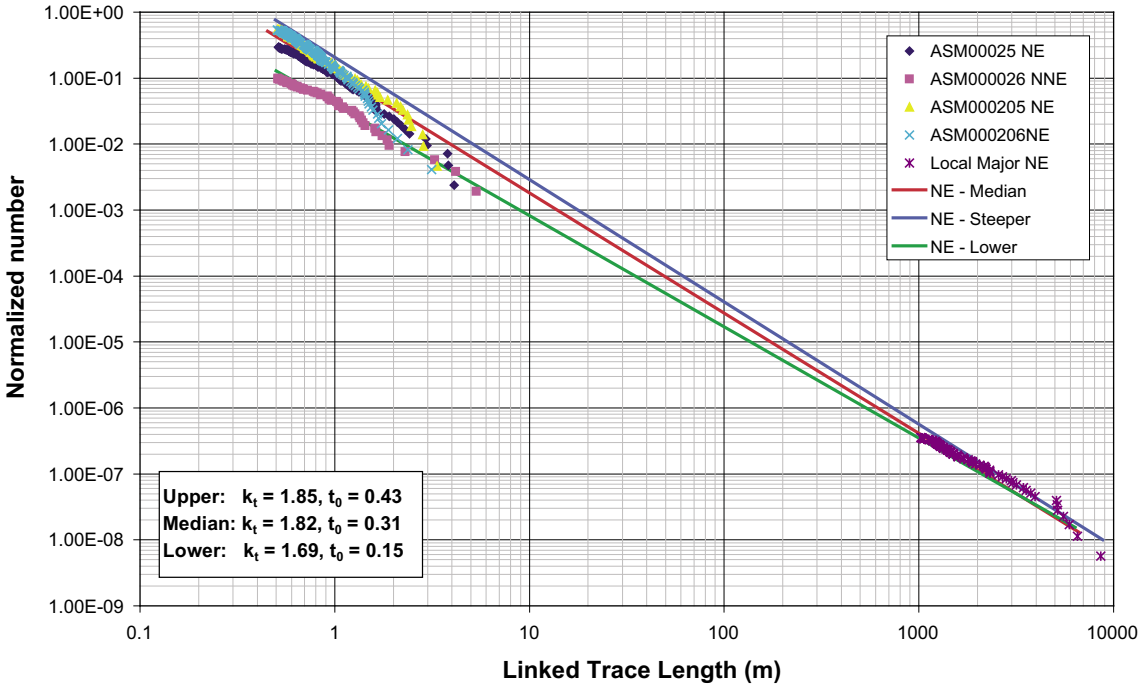

Figure 6-26. *Trace length scaling plot for the NE set (Alternatives 1 and 2).*

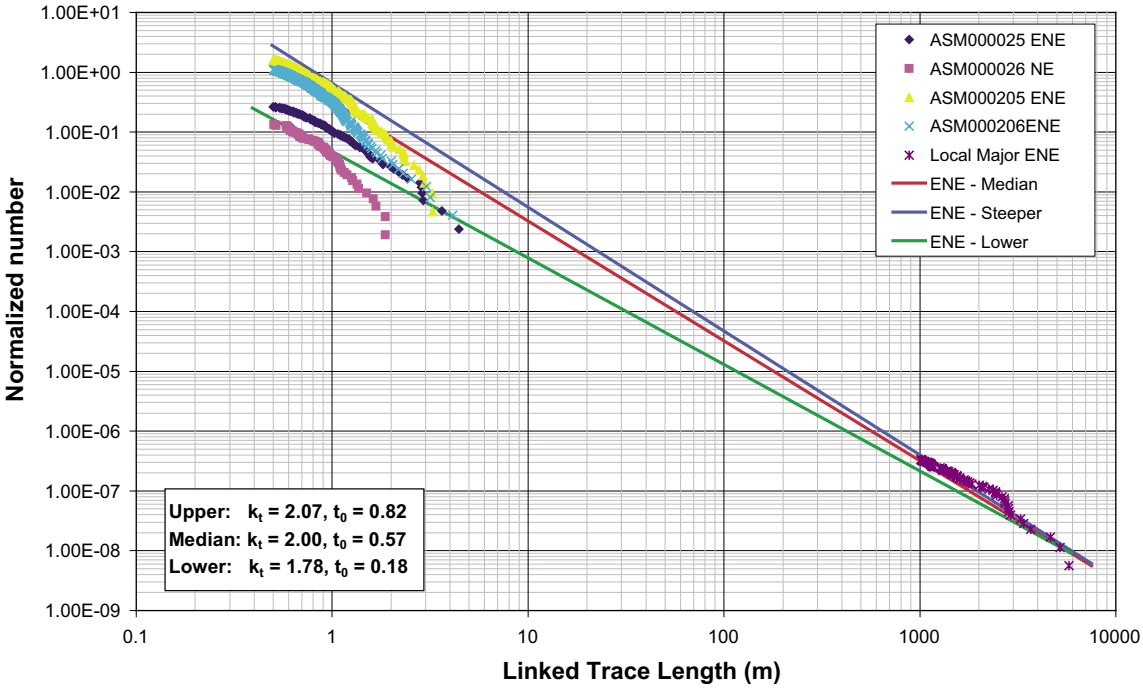

Figure 6-27. *Trace length scaling plot for ENE set (Alternative 2 only).*

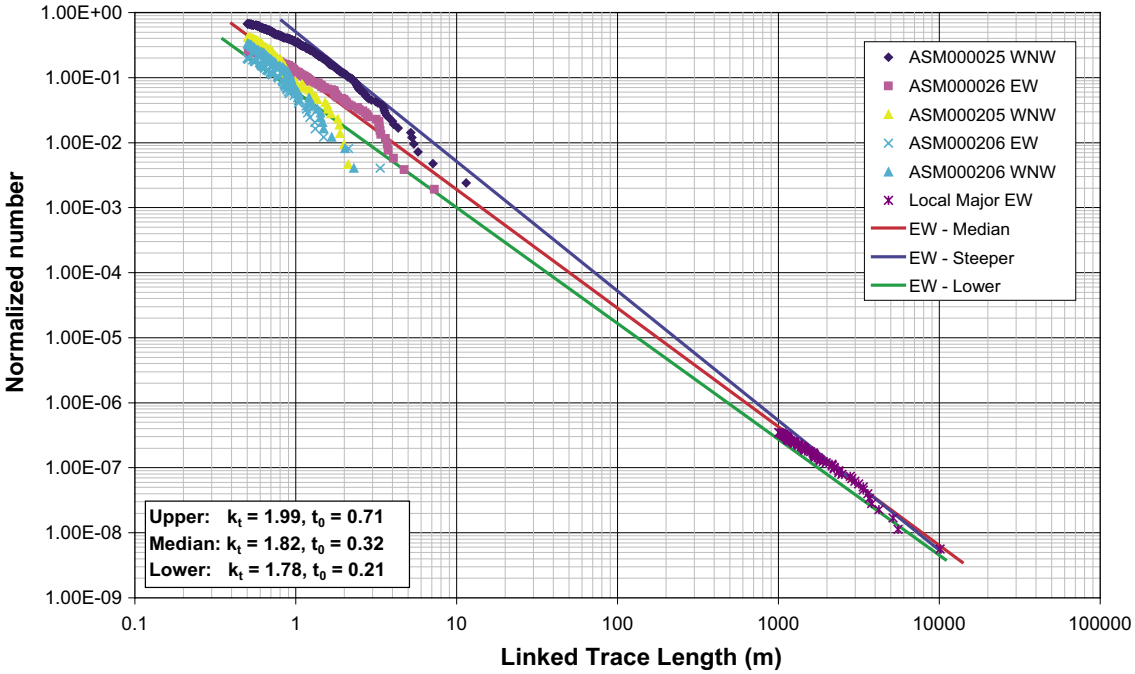

Figure 6-28. *Trace length scaling plot for the EW set (Alternatives 1 and 2).*

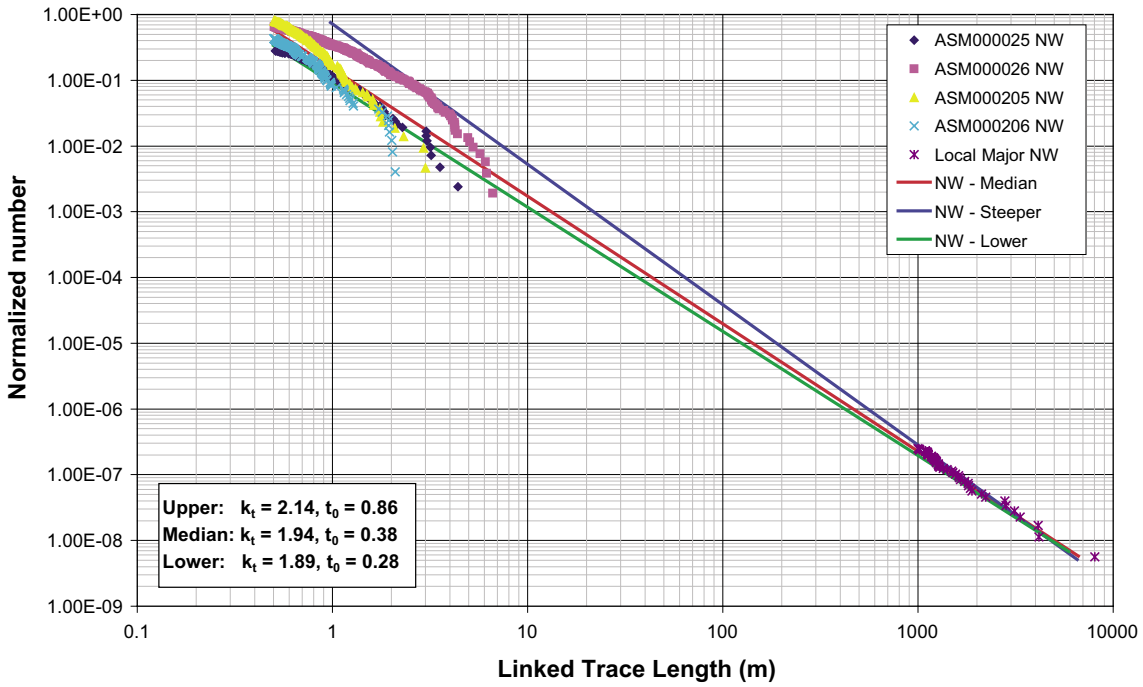

Figure 6-29. *Trace length scaling plot for NW set (Alternative 2 only).*

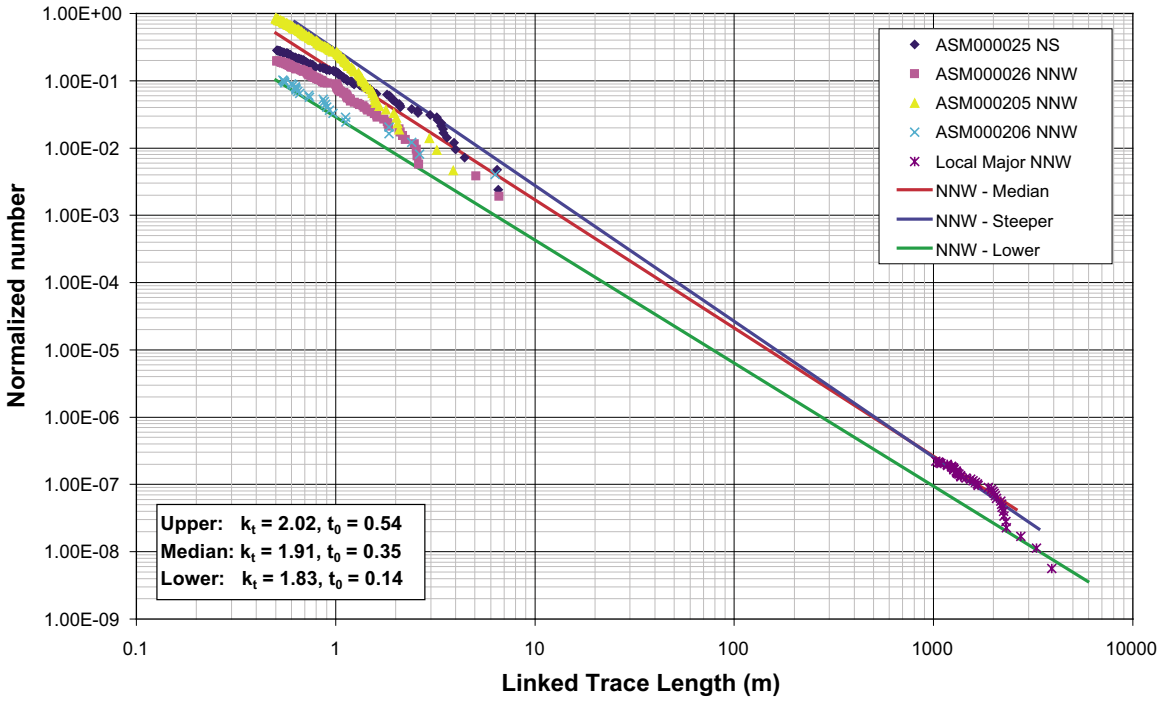

Figure 6-30. *Trace length scaling plot for the NNW set (Alternatives 1 and 2).*

The results for Alternative 1 are given in Table 6-9. The table gives the parameters for the parent fracture radius distribution for the upper, median and lower bound lines. Values are also given for both mass dimension and Euclidean scaling. The values for the Group 1 sets were estimated from the area renormalization plots. Fracture radius values for the background Group 2 sets were estimated according to the FracSize algorithm described in Chapter 5. In all cases for the Group 2 sets, the best fitting distribution was a lognormal distribution. Parameters were also estimated for power law distributions for these Group 2 fracture sets in order to facilitate comparisons with other studies of fracturing that have been carried out in the past in the Simpevarp area. However, the preferred size model for Group 2 fractures is lognormal based upon statistical significance.

The size calculations for Alternative 2 are given in Table 6-10.

Table 6-9. Fracture size parameters for Alternative 1 fracture sets.

Set	Size model preferred, (alternative)	Lognormal (radius distribution)			Powerlaw (radius distribution)		
		Arithmetic space Mean [(1/n) Σx_i] (m)/st. dev.	Log^{10} space Mean [(1/n) $\Sigma \log^{10} x_i$]/st. dev.	LN space Mean [(1/n) $\Sigma \ln x_i$]/st. dev.	Upper $k_r/t_0/r_0$ (mass) (euclidean)	Median $k_r/t_0/r_0$ (mass) (euclidean)	Lower $k_r/t_0/r_0$ (mass) (euclidean)
NNE-NE	Powerlaw				2.68/0.6/0.38 2.85/0.43/0.27	2.58/0.36/0.23 2.82/0.31/0.20	2.50/0.20/0.13 2.69/0.15/0.10
EW-WNW	Powerlaw				2.93/0.63/0.40 2.99/0.71/0.45	2.80/0.36/0.23 2.82/0.32/0.20	2.67/0.18/0.11 2.78/0.21/0.13
NW-NNW	Powerlaw				2.97/0.75/0.48 3.02/0.54/0.35	2.87/0.49/0.31 2.91/0.35/0.22	2.62/0.13/0.08 2.83/0.14/0.10
BGNE	Lognormal (Powerlaw)	0.48/0.55	–0.50/ 0.60	–1.15/ 0.92	2.86/0.87/0.55 3.07/0.82/0.51	2.77/0.56/0.35 3.00/0.57/0.36	2.61/0.27/0.17 2.78/0.18/0.11
BGNS	Lognormal (Powerlaw)	0.67/0.82	–0.37/0.63	–0.86/0.96	2.93/0.94/0.60 2.99/0.56/0.36	2.77/0.56/0.35 2.95/0.46/0.29	2.72/0.44/0.28 2.95/0.36/0.23
BGNW	Lognormal (Powerlaw)	0.45/1.00	–0.73/0.88	–1.69/1.33	3.05/1.09/0.69 3.14/0.86/0.55	2.82/0.44/0.28 2.94/0.38/0.24	2.80/0.36/0.23 2.89/0.28/0.18
SubH	Lognormal	0.57/1.86	–0.78/1.03	–1.79/1.57			

Table 6-10. Fracture size parameters for Alternative 2 fracture sets.

Set	Size model preferred	Powerlaw (radius distribution)		
		Upper k_r/r_0 (mass) (euclidean)	Median k_r/r_0 (mass) (euclidean)	Lower k_r/r_0 (mass) (euclidean)
NE	Powerlaw	2.68/0.38 2.85/0.27	2.58/0.23 2.82/0.20	2.50/0.13 2.69/0.10
EW	Powerlaw	2.93/0.40 2.99/0.45	2.80/0.23 2.82/0.20	2.67/0.11 2.78/0.13
NNW	Powerlaw	2.97/0.48 3.02/0.35	2.87/0.31 2.91/0.22	2.62/0.08 2.83/0.10
NS	Powerlaw	2.93/0.60 2.99/0.36	2.77/0.35 2.95/0.29	2.72/0.28 2.95/0.23
NW	Powerlaw	3.05/0.69 3.14/0.55	2.82/0.28 2.94/0.24	2.8/0.23 2.89/0.18
ENE	Powerlaw	2.86/0.56 3.07/0.52	2.77/0.36 3.00/0.36	2.61/0.17 2.78/0.12
SubH	Lognormal	0.57/1.86	–0.78/1.03	–1.79/1.57

6.3 Intensity

Analysis of fracture intensity as a function of lithology and domain shows that both parameters are potential controls that could be used to stratify the data and reduce model uncertainty.

Figure 6-31 shows the fracture intensity for borehole data from HSH01, HSH02, HSH03, KAV01, KLX02, KSH01A, KSH01B, KSH02, KSH03A, and KSH03B. This data set includes only fractures located outside of brittle and ductile deformation zones. The differences in mean values indicate that there may be differences in fracture intensity by rock type. Although both sealed and open fractures are included in the analysis, examination of fracture intensity with depth for the cored boreholes showed no significant differences between sealed fractures and open fractures in terms of variations with depth. Areas that had high sealed fracture intensity with depth also showed high open fracture intensity, and similarly with zones of lower intensity.

Overall population statistics as a function of lithology and fracture type were calculated to provide initial insight into possible variations. This included the calculation of mean, median, confidence intervals and other statistical parameters as appropriate.

The rigorous statistical testing was carried out using the Kruskal-Wallis non-parametric ANOVA procedure, in which the null hypothesis was that there was no intensity difference among lithological classes. Rejection of the null hypothesis is evidence that intensity does vary by lithologic class. Rejection is quantified by the probability (denoted as a or p) of observing the calculated test statistic given that the null hypothesis is true. Values of a or $p <= 0.10$ are taken as rejection. The results of the Kruskal-Wallis test are shown in Table 6-11.

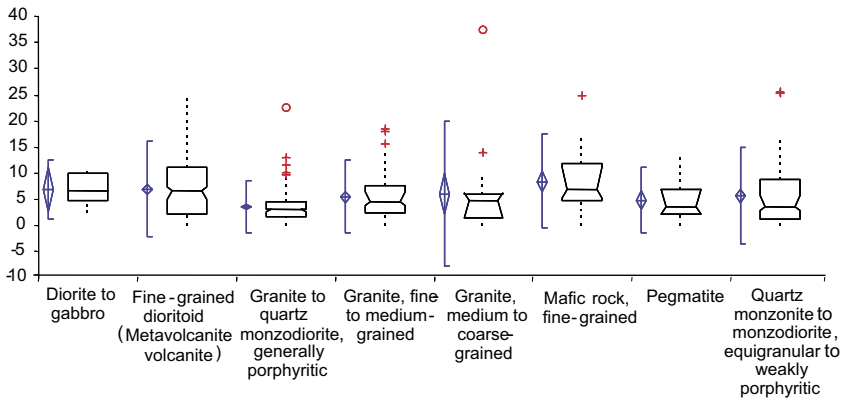

P10 by Lithology	n	Mean	Std. Dev.	Std. Err.	95% CI of Mean	Median	IQR	95% CI of Median
Mafic rock, fine grained	30	8.488	5.5456	1.0125	6.418 to 10.559	6.932	7.195	5.310 to 11.314
Fine-grained dioritoid (Metavolcanite, volcanite)	128	7.053	5.6	0.495	6.073 to 8.032	6.675	9.305	5.044 to 7.558
Diorite to Gabbro	5	6.890	3.5194	1.5739	2.520 to 11.260	6.78	5.172	
Granite, medium to coarse grained	19	6.045	8.457	1.9402	1.969 to 10.121	4.783	4.664	1.205 to 6.250
Quartz monzonite to monzodiorite, equigranular to weakly porphyritic	88	5.706	5.6975	0.6074	4.499 to 6.914	3.761	7.911	2.692 to 5.749
Granite, fine to medium grained	69	5.542	4.337	0.5221	4.500 to 6.584	4.526	5.274	3.953 to 6.517
Pegmatite	19	4.850	3.8814	0.8904	2.979 to 6.720	3.62	4.959	2.000 to 7.080
Granite to quartz monzodiorite, generally porphyritic	123	3.585	3.1192	0.2812	3.028 to 4.142	3.022	3.139	2.488 to 3.284

Figure 6-31. *Values of P_{10} fracture intensity by classified by lithology for open and sealed fractures. Note that "n" refers to the number of continuous intervals of a particular lithology, not to the number of fractures*

Table 6-11. Results of Kruskal-Walis test on possible differences in fracture intensity as a function of lithology. Note that "n" refers to the number of continuous intervals of a particular lithology.

Comparison:	P_{10} by Lithology
Performed by:	Paul Lapointe
Date:	18-Jun-04
n (total):	481

P_{10} by Lithology	**n**	**Rank sum**	**Mean rank**
Diorite to Gabbro	5	1,510.5	302.10
Fine-grained dioritoid (Metavolcanite, volcanite)	128	35,282.5	275.64
Granite to quartz monzodiorite, generally porphyritic	123	23,249.0	189.02
Granite, fine to medium grained	69	17,076.5	247.49
Granite, medium to coarse grained	19	4,292.0	225.89
Mafic rock, fine grained	30	9,642.5	321.42
Pegmatite	19	4,339.5	228.39
Quartz monzonite to monzodiorite, equigranular to weakly porphyritic	88	20,528.5	233.28
Kruskal-Wallis statistic	36.98		
p	< 0.0001	chisqr approximation, corrected for ties	

The Kruskal-Wallis test value, p, is considerably below a value of 0.10. The null hypothesis is strongly rejected and it is concluded that intensity varies by lithological group. In general, fine-grained mafic rock has a higher intensity than coarse-grained granitic rock. There might be some potential for grouping fine-grained dioritoid, diorite to gabbro and fine-grained mafic; the remaining groups (with the exception of the granite to quartz monzonite, generally porphyritic lithology); and the remaining granite to quartz monzonite, generally porphyritic lithology.

Next, rock domain controls are examined in order to determine if fracture intensity values should be specified differently for different rock domains (A, B, C, and D) whether some domains can be grouped, or whether domains are of no use in reducing model uncertainty.

The analyses are based on borehole data from HSH01, HSH02, HSH03, KAV01, KLX02, KSH01A, KSH01B, KSH02, KSH03A, and KSH03B. Fractures in brittle or ductile deformation zones have been treated separately from fractures outside of deformation zones. The upper and lower bound of interpreted deformation zones has been taken from single hole interpretations by /Mattson et al. 2004ab/. All identified deformation zones have been divided into a) brittle zones and b) ductile zones according to the interpretation given by /Mattson et al. 2004ab/. Brittle and ductile zones have only been treated as groups, i.e. no individual breakdown into single zone analysis has been performed. Fractures were further separated into Open, Partly Open and Sealed and analyzed, as well as combining all fracture types. P_{10} values were corrected for borehole orientation before analysis.

Table 6-12 shows mean values of Terzaghi-corrected P_{10} as a function of Rock Domain, fracture type and whether the fracture is inside a brittle deformation zone or entirely outside of ductile and brittle deformation zones. Domain B is consistently higher intensity, both inside and outside of deformation zones. Domain A typically has the lowest intensity.

Results for Partly Open fractures are based on far fewer fractures, resulting in greater uncertainty about intensity.

Table 6-13 shows the standard deviation for values of Terzaghi-corrected P_{10} as a function of rock domain, fracture type and whether the fracture is in side a brittle deformation zone or entirely outside of ductile and brittle deformation zones.

Table 6-12. Mean P_{10} intensity for fractures as a function of rock domain and fracture type.

Outside Domain	All Uncorrected P10	Corrected P10	Open Uncorrected P10	Corrected P10	Partly Open Uncorrected P10	Corrected P10	Sealed Uncorrected P10	Corrected P10
A	4.36	4.67	2.30	2.42	0.05	0.05	2.01	2.21
B	11.47	11.68	3.11	3.15	0.07	0.07	8.29	8.45
C	8.23	8.88	1.83	1.97	0.11	0.12	6.29	6.79
Brittle DZ Domain	**All Uncorrected P10**	**Corrected P10**	**Open Uncorrected P10**	**Corrected P10**	**Partly Open Uncorrected P10**	**Corrected P10**	**Sealed Uncorrected P10**	**Corrected P10**
A	10.45	10.46	6.25	6.26	0.00	0.00	4.19	4.20
B	14.25	14.48	6.65	6.75	0.12	0.12	7.48	7.61
C	10.45	11.39	5.27	5.73	0.30	0.31	4.89	5.37

Table 6-13. Standard deviation of P_{10} intensity for fractures as a function of rock domain and fracture type.

Outside Domain	All Uncorrected P10	Corrected P10	Open Uncorrected P10	Corrected P10	Partly Open Uncorrected P10	Corrected P10	Sealed Uncorrected P10	Corrected P10
A	0.47	0.80	0.60	0.42	0.07	0.07	0.92	1.21
B	4.63	4.82	0.80	0.77	0.11	0.11	5.33	5.53
C	2.86	3.53	0.58	0.72	0.15	0.16	2.59	3.09
Brittle DZ Domain	**All Uncorrected P10**	**Corrected P10**	**Open Uncorrected P10**	**Corrected P10**	**Partly Open Uncorrected P10**	**Corrected P10**	**Sealed Uncorrected P10**	**Corrected P10**
A	ND	ND	ND	ND	ND	ND	ND	ND
B	1.70	1.81	3.03	3.07	0.20	0.21	4.92	5.03
C	3.38	4.62	1.77	2.22	0.30	0.32	3.03	3.65

Table 6-14. Results of statistical testing for fracture intensity variation by domain.

p / a Values	All	Open	Partly open	Sealed
Outside DZ and DUC	0.09	0.11	0.33	0.08
Brittle DZ	0.3	0.87	0.35	0.87

The results of the Kruskal-Walis tests are shown in Table 6-14. The values shown in the table above are the p or a values for the test of the null hypothesis that intensity does not vary by domain. The results show that this hypothesis would be rejected at the a = 0.10 level for All and Sealed fractures outside of deformation zones, and nearly rejected for open fractures outside deformation zones. The hypothesis would not be rejected for fractures within brittle deformation zones. These results suggest that fracture intensity, especially for all fractures and for sealed fractures, is statistically different among the three rock domains for which there was data (note: no data was available for Domain D). However, fracture intensity within brittle fracture zones does not appear to be a function of rock domain.

These results suggest that the rock domain property can be used to reduce model uncertainty, as the variability of intensity between domains is greater than the variability within domains. In order to make use of this conclusion, it is necessary to calculate the intensity of fractures both as a function of domain and by set. The data for calculating the intensity by rock domain for the vertical sets is derived from the outcrops, as they provide the most reliable data for the sub-vertical sets. Likewise, the calculation of sub-horizontal fracture intensity relies upon the borehole data. The results are shown in Table 6-15 and Table 6-16 provide an estimate of the mean fracture intensity by rock domain for each group (vertical and horizontal) of fracture sets. In order to determine the appropriate P_{32} for an individual sub-vertical fracture set for a specified rock domain, all that needs to be done is to multiply the rock domain P_{32} value shown in the table by the set's proportion as given in Table 6-1 for Alternative 1 and in

Table 6-6 for Alternative 2 for sub-vertical fractures and in Table 6-7 for sub-horizontal fractures.

Table 6-15. Intensity (P_{32}) for sub-vertical sets.

Rock domain	P_{32} Sub-vertical (All)	P_{32} Sub-vertical (Open fractures)	Comments
A	2.10	0.47	Outcrop ASM000026
B	4.86	0.69	Outcrop ASM000205
C	2.92 – 3.27	0.65 – 0.93	Two outcrops, ASM000025 and ASM000206, both close to boundary of C domain
D	No data	No data	No data

Table 6-16. Intensity (P_{32}) for horizontal set. The * mark represent intensities where the lower 95% confidence limit, based on the assumption of normality, is below 0.0. It has been set to 0.0 as negative intensities are not physically possible.

Fractures by domain	P_{32} Mean	SD	SE	95% CI of mean
All by Domain – A	0.924	0.1611	0.0930	0.524 to 1.324
All by Domain – B	2.798	0.1318	0.0932	1.614 to 3.982
All by Domain – C	2.008	0.9178	0.4105	0.868 to 3.147
All by Domain – D	No Data			
Open by Domain – A	0.491	0.1498	0.0865	0.118 to 0.863
Open by Domain – B	0.726	0.4690	0.3316	0.000* to 4.940
Open by Domain – C	0.429	0.2510	0.1122	0.117 to 0.741
Open by Domain – D	No Data			
Partly Open by Domain – A	0.008	0.0144	0.0083	0.000* to 0.044
Partly Open by Domain – B	0.000	–	–	– to –
Partly Open by Domain – C	0.006	0.0093	0.0041	0.000* to 0.017
Partly Open by Domain – D	No Data			
Sealed by Domain – A	0.425	0.2968	0.1714	0.000* to 1.163
Sealed by Domain – B	2.072	0.6008	0.4248	0.000* to 7.470
Sealed by Domain – C	1.573	0.6836	0.3057	0.724 to 2.422
Sealed by Domain – D	No Data			

6.4 Spatial model

The spatial model is closely related to the intensity model, as described in Section 5.5. The results of the mass dimension calculation suggest that the spatial pattern at the outcrop level is Euclidean to mildly fractal (Table 6-8). Though there are a few values below 1.75, which indicate a departure from Euclidean scaling, there are still a large number of mass dimensions equal to or close to 2.0. This suggests that a Poisson Point process, which has a mass dimension of 2.0, is a reasonable fit to much of the mass dimension data. Until further results suggest otherwise, it appears that the Poisson model at least at the outcrop scale, is a reasonable mode given the existing trace length data.

Another issue concerns how fracture intensity may vary with depth. One of the key issues is whether fractures seen in outcrop or near the surface are representative of fractures at repository depths hundreds of meters below the surface. If surficial stress relief has produced increased fracturing near the surface, then this fracturing should have certain characteristics, such as increased horizontal fracture intensity and also characteristics like low temperature mineral fillings or relatively unaltered walls relative to fracturing at depth. To test these hypothesises, fractures from boreholes KAV01, KSH01A, HSH01, HSH02 and HSH03 were evaluated in several different ways:

- Variation of intensity with depth as a function of “open” or “sealed”.
- Variation of intensity with depth as a function of dip for open fractures.
- Variation of intensity with depth as a function of mineral fillings for open fractures.

The three percussion boreholes and KAV01 provide data coverage in the depth range over the first hundred meters, which is where depth-related surface stress-relief effects may be most prominent. KAV01 also extends to a depth of several hundred meters. KSH01A and KLX02 do not begin until about 100 m below the surface, but extend down over 1,000 m, and contains what may be more reliable fracture data than the percussion boreholes.

The relationship between depth and fracture intensity is explored through the use of cumulative fracture intensity (CFI) plots; see Figure 5-9 for more details. The results of this analysis are shown in Figure 6-32 through Figure 6-38.

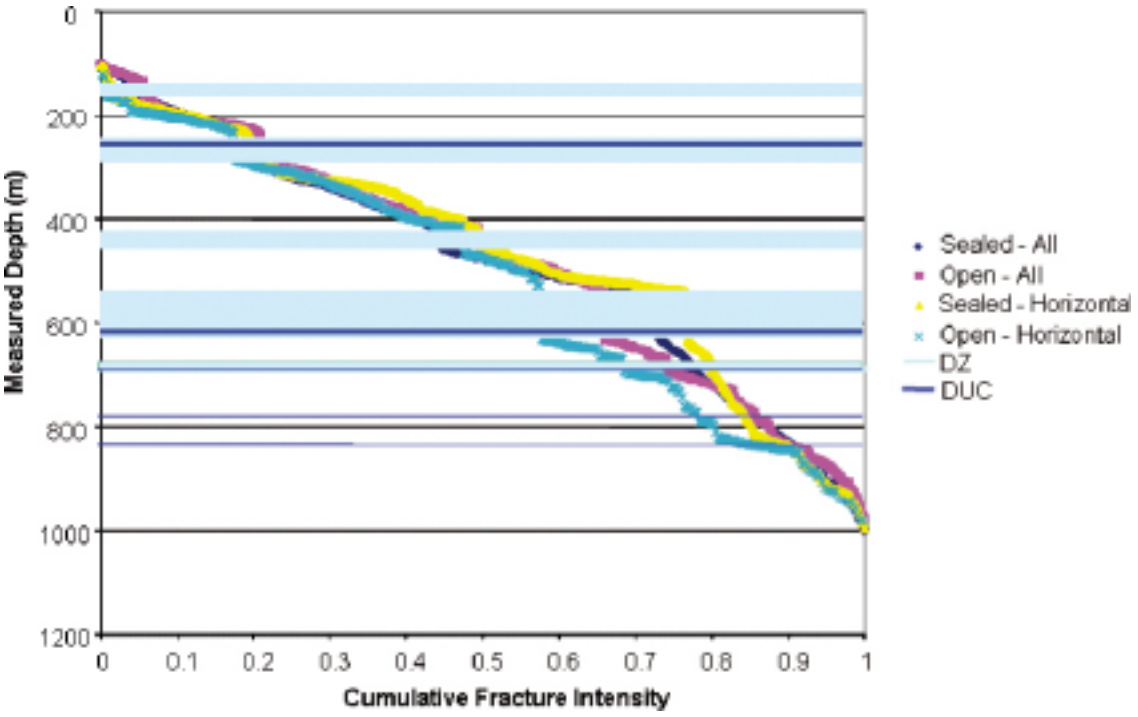

Figure 6-32. *CFI plot for borehole KSH01A.*

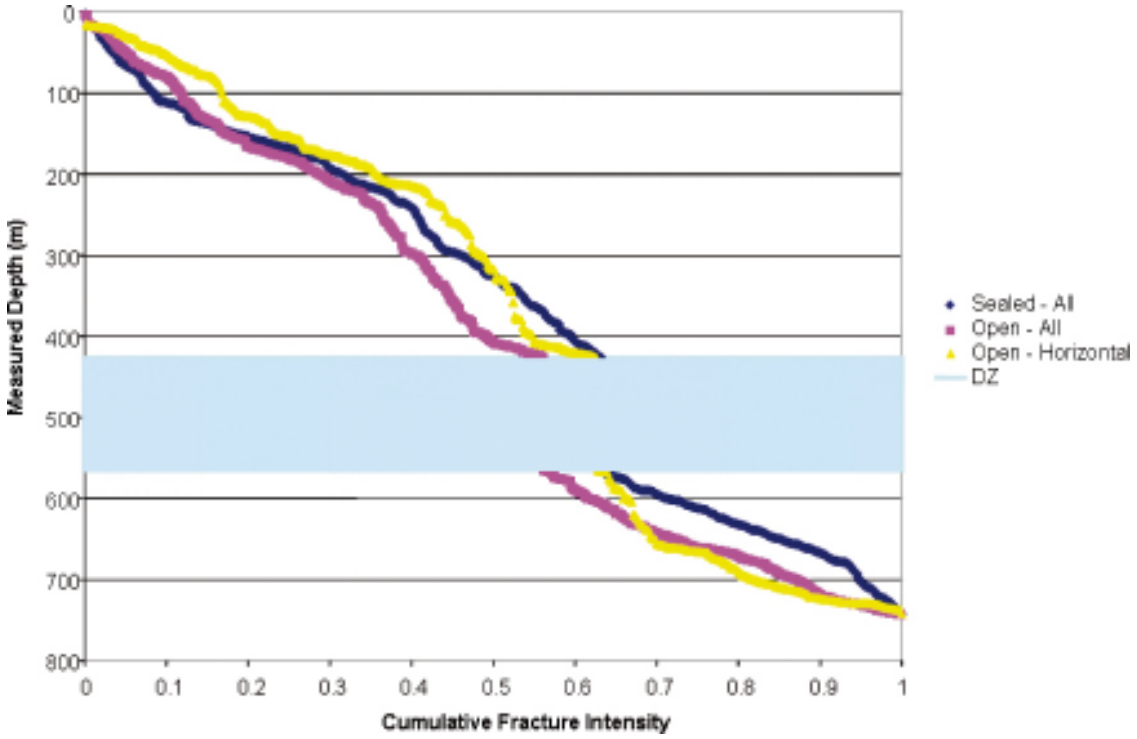

Figure 6-33. *CFI plot for borehole KAV01.*

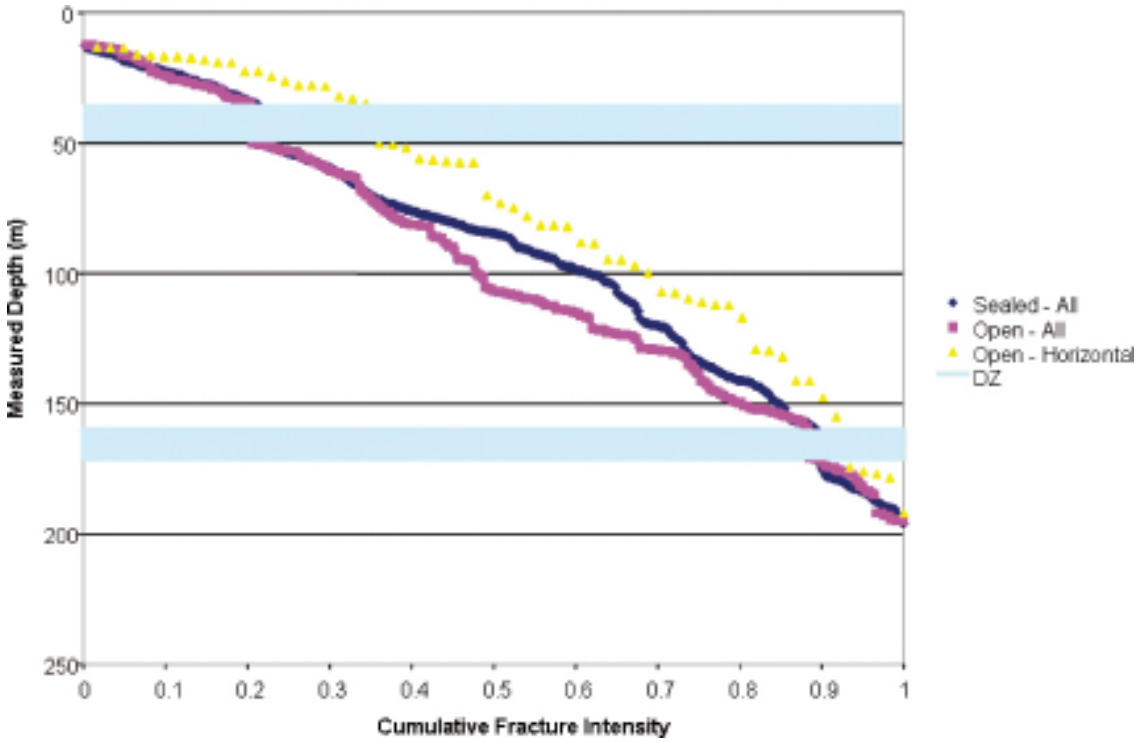

Figure 6-34. *CFI plot for borehole HSH01.*

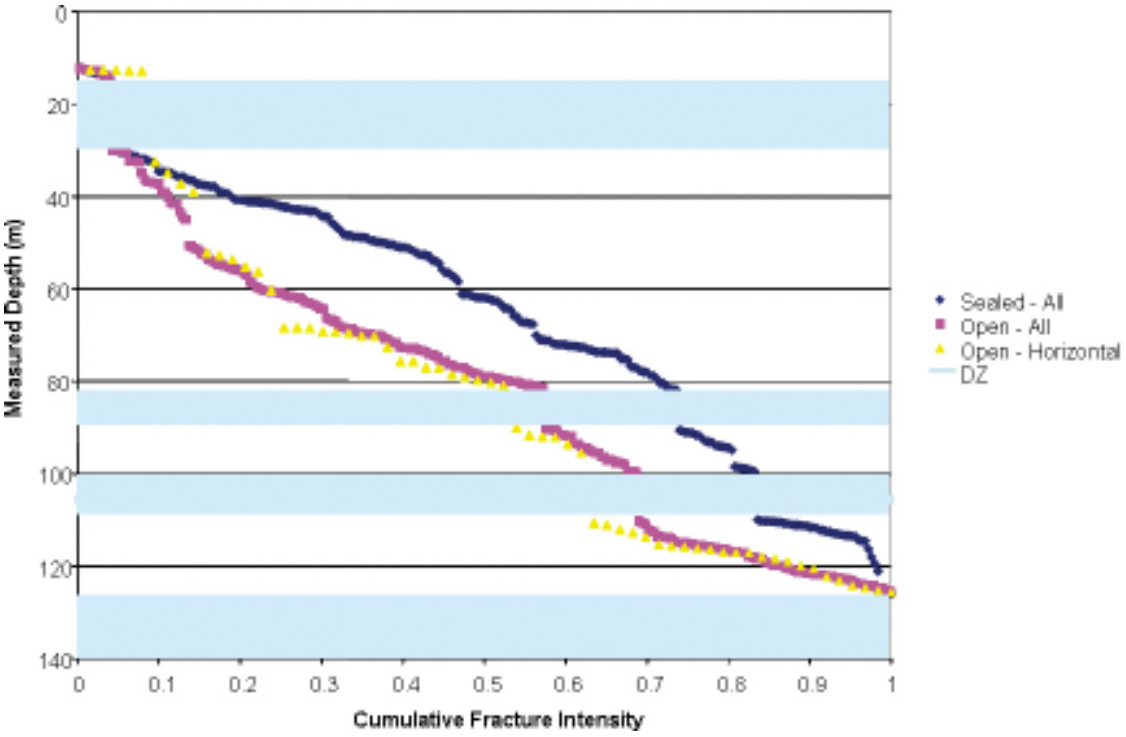

Figure 6-35. *CFI plot for HSH02.*

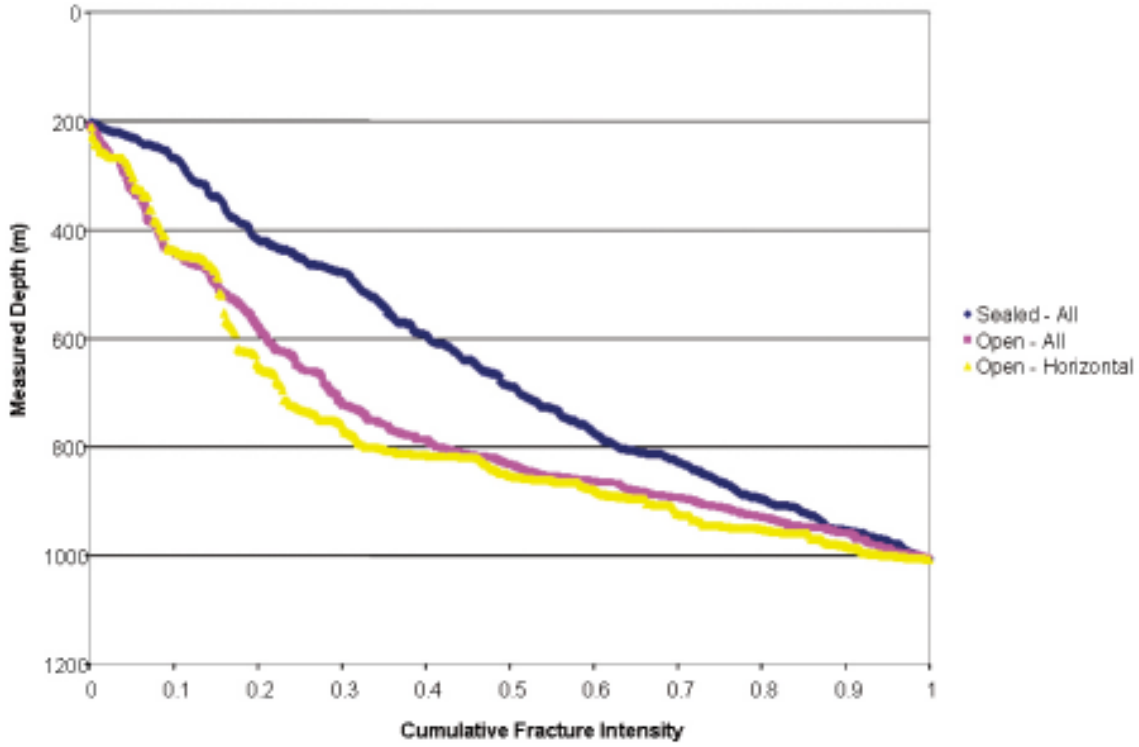

Figure 6-36. *CFI plot for HSH03.*

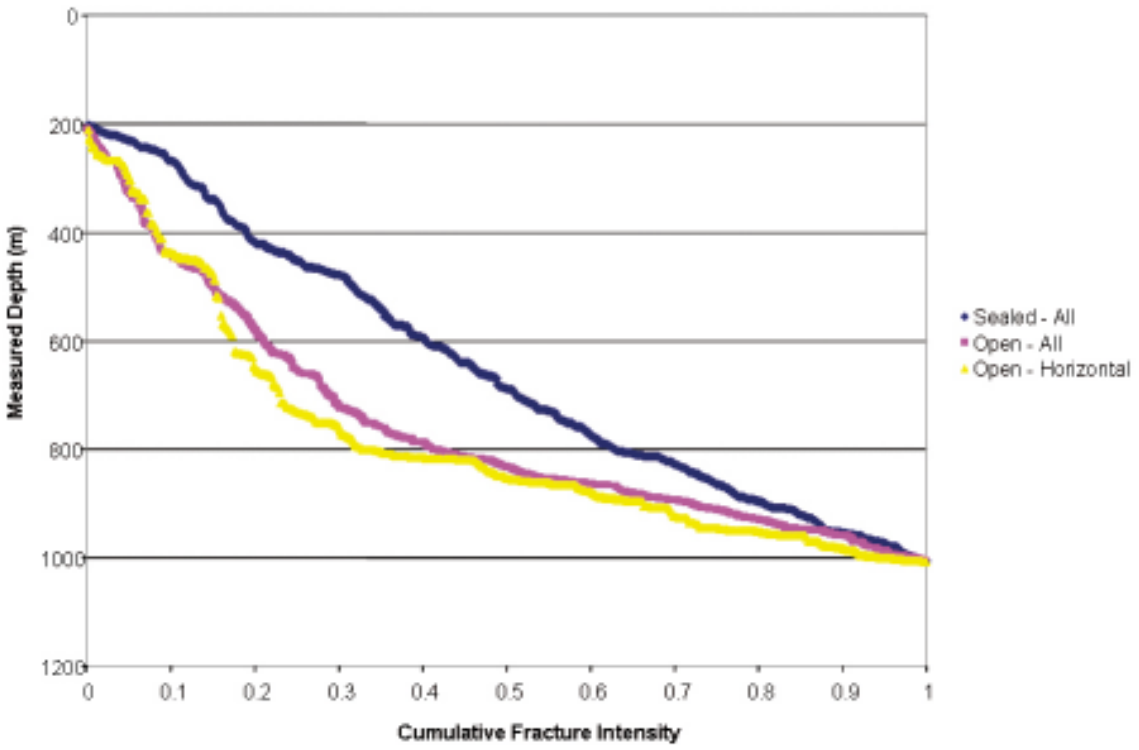

Figure 6-37. *CFI plot for borehole KLX02. Note that this borehole was analyzed without access to a single-hole interpretation and consequently no deformation zones where considered.*

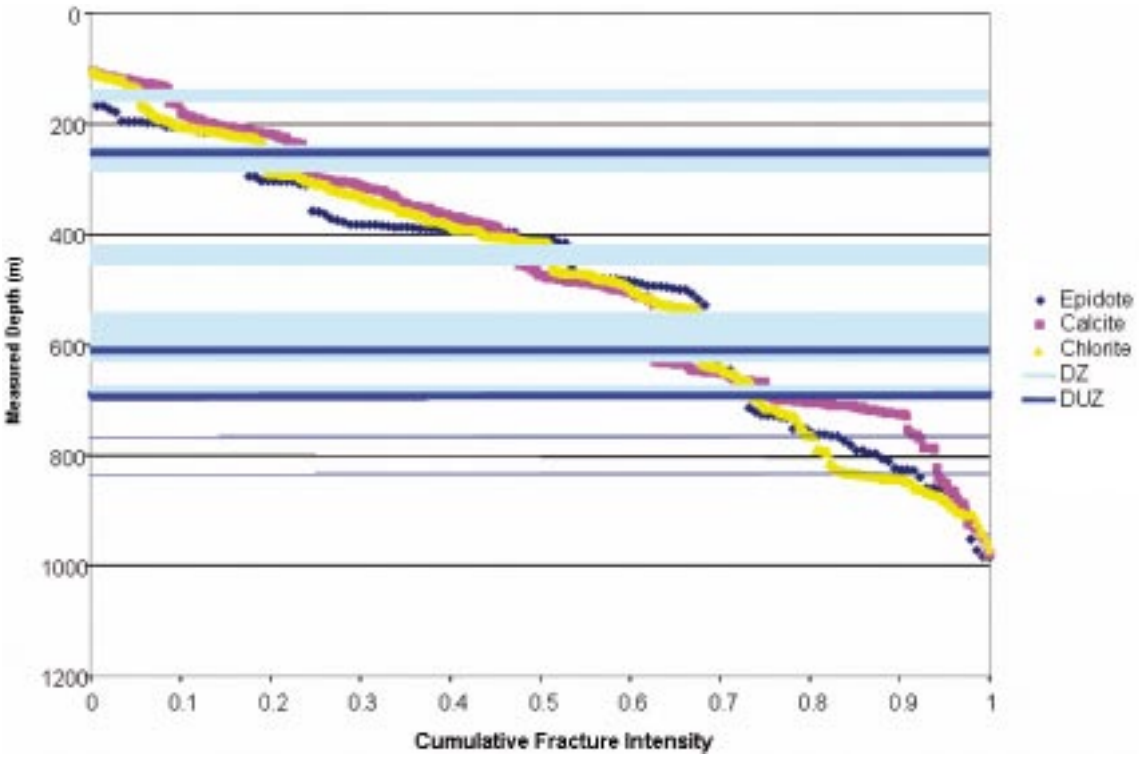

Figure 6-38. *CFI plot for mineral fillings for borehole KSH01A.*

All of the plots show little evidence of enhanced fracture intensity near the surface. KAV01 shows lower intensity in the upper 100 m compared to the interval from about 125 m to 250 m measured depth. The intensity plots for the three percussion boreholes (HSH01, HSH02 and HSH03) show little intensity variation with depth. In addition, the intensities of open and sealed fractures generally are very close to one another, as are open horizontal and all open fractures. Plots for the deeper-penetrating boreholes (KSH01A, KAV01 and KLX02) have their zones of highest intensity at the deeper intervals.

The plots for mineral fillings (Figure 6-38) also suggests that the fracturing is very old, as the open, epidote-filled fractures show the same intensity patterns as calcite and chlorite filled fractures. This mineral filling is probably not related to any recent stress relief or glacial event. If the patterns of intensity for epidote filled fractures are mirrored by other fractures with low temperature fillings, then this is consistent with all of the fractures being much older and not formed due to recent causes like stress relief. This figure shows no obvious evidence that epidote-filled fractures have different intensity patterns than other fractures.

The consequence of these CFI plots is that there is no evidence that fracture intensity is higher near the surface due to stress relief or crustal rebound following the recent de-glaciation. Fractures, in fact, appear to have been formed very early when epidote and other high temperature mineral fillings were present.

7 Evaluation of uncertainties

7.1 Quantification and propagation of uncertainty

Uncertainty in the Simpevarp 1.2 model is derived from several sources, including the uncertainty inherent in the data variability among the various outcrops and boreholes (parameter uncertainty), as well as in the conceptual model in which the data is used to construct (conceptual uncertainty).

The parameter uncertainty in fracture orientation has been quantified in two different ways: the conceptual model uncertainty has been addressed by evaluating two alternative models for fracture sets; the uncertainty in orientations within each set has been quantified by calculating the orientation dispersion for each set at each of the four outcrops. Since there are many alternative ways to aggregate the data at each outcrop, for example, by weighting by area or by fracture intensity, it is left to the users of the results to decide the best way to propagate the uncertainty for their own purposes.

The parameter uncertainty in size is quantified in two different ways. For local fracture sets, the size model for the parent fracture radius distributions are based on aggregating all of the outcrop data for that set, and estimating a model for the distribution of fracture radii. For the lineament-related sets, three values are given: two bounding cases and a ‘best-guess‘ case. Because of the artifacts related to censoring of trace length data from outcrop maps, the trace length model fit to the normalized data is done visually rather than through non-linear regression. The ‘best-guess’ case is the best visual fit through all of the outcrop and lineament data. The two bounding cases are visually-fit slopes that approximate the shallowest and steepest lines that could be fit through the data. These represent the span of possible size variation given the existing data. As in the case of orientations, it is up to the user of this data to decide which parameter values to select. It may be worthwhile to further evaluate the fractures mapped in outcrop to determine what evidence for re-activation exists, and perhaps to construct an alternative size model based only on outcrop fractures than have clear evidence for re-activation or shear movement.

The intensity of fracturing is specified, where data allows, as a function of the geological factors in terms of the mean and standard deviation of P_{32}. However, for the vertical sets, only one outcrop in each rock domain exists, except in one case, the C domain, where there are two outcrops. The user of this information should decide whether a mean value suffices, or whether something more complex, such as a Monte Carlo sample from the distribution, is appropriate for the intended usage.

7.2 Validation of the Simpevarp 1.2 DFN model

7.2.1 Objectives

The goal of the DFN model validation analyses is to build confidence in the Simpevarp 1.2 model’s usefulness in predicting fracture intensity and orientation throughout the rock mass. It is not a complete validation of the entire DFN model, but rather an attempt to assess how useful it is in predicting variations in fracture intensity and orientation, which are two parameters that are important for both the fluid flow and mechanical models that use the DFN model.

Two validation approaches have been performed:

1. Validation of conceptual model Alternative 1 using outcrop data and borehole data from rock domain A. This approach was made with a thorough re-examination of fracture intensity on outcrop ASM000026 and in borehole KLX02 and was focused on open, sub-vertical fracturing.
2. Validation of conceptual model Alternative 2 using the estimated model parameters for sub-vertical and sub-horizontal fractures in Alternative 2. This approach made use of the presented tables for orientation, size and intensity.

7.2.2 Strategy

The available data limits the ways in which the DFN model can be validated. The Simpevarp 1.2 DFN model consists of six vertical fracture sets and one horizontal fracture set. Available fracture data comes from five outcrops and a series of percussion and cored boreholes. Statistical analyses of the fracture data indicates that rock domain can be used to stratify the fracture intensity data. In other words, the variability within each fracture domain is less than the variability among fracture domains.

The DFN model has been derived to simulate fracturing within the local model volume. The orientation and size models are global, which means that these components of the fracture sets reflect the observed fracturing in the whole local model volume with no differentiation between different rock domains. However, the intensity model does reflect the variability between rock domains.

The presence of alteration zones also appears to play a significant role, one that is not entirely separate from rock domain. For example, Domain B in the boreholes is often associated with the presence of alteration zones, so it is difficult to determine whether the higher fracture intensity associated with Domain B is a result of lithology or the greater preponderance of alteration zones. In addition, there are ductile and brittle deformation zones in many of the boreholes, which may have occurred somewhat independent of lithology.

The strategy for the Simpevarp 1.2 DFN model validation was to pick a subset of data that might be least affected by multiple geological factors. The borehole data covers Domains A, B and C. There is currently no data for Domain D. Of the three domains for which there is borehole data, Domain A has very few mapped alteration zones, unlike Domains B and C. For this reason, Domain A was chosen for the validation.

Only one outcrop is in Domain A: ASM000026. Of the boreholes that contain lithologies belonging to Rock Domain A, borehole KLX02 is the most straightforward. This is because;

1. The entire borehole is in Domain A.
2. There are only one mapped deformation zone in KLX02, in section 770 m to 960 m.
3. The borehole has been cored, so that the type of fracture data that has been obtained is probably of the highest confidence.
4. The intensity of fracturing can be divided into three zones of approximately constant intensity (Figure 7-1), where section 3 indicates the highest frequency of fracturing in the deformation zone in section 770 m to 960 m.

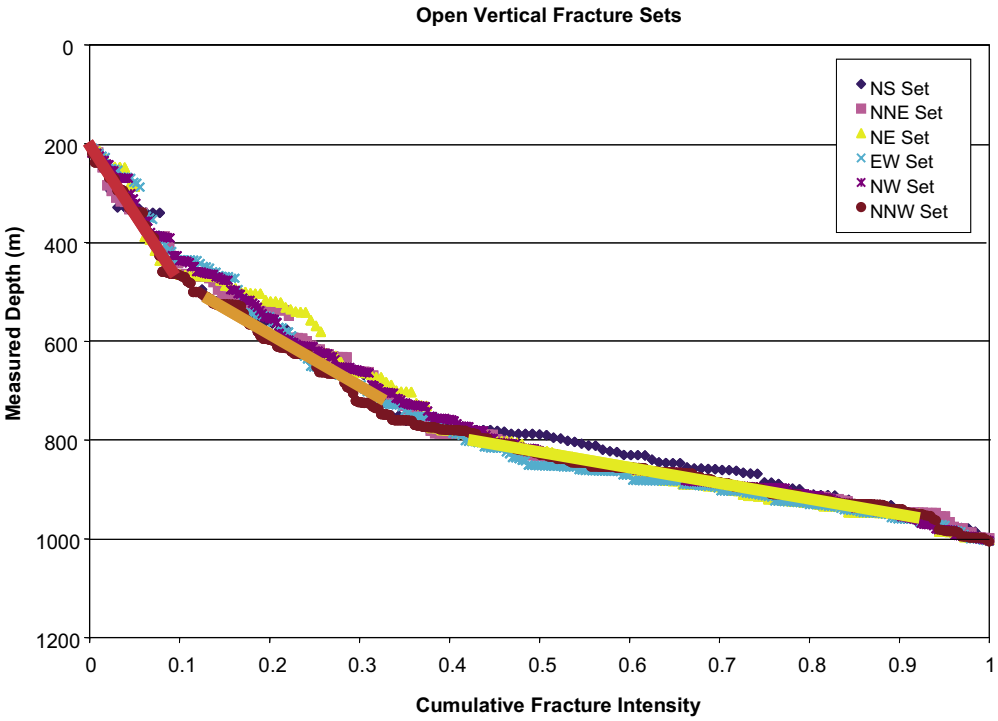

Figure 7-1. *Cumulative fracture intensity plot for open fractures in borehole KLX02. The bold red, orange and yellow demarcate the approximate measured depth intervals over which fracture intensity is constant. Note that the intensity pattern with depth differs little by set. Section 1 is the red section; Section 2 is the orange section; Section 3 is the yellow section, and is identified as deformation zone in the single hole interpretation.*

7.2.3 Validation of the conceptual model Alternative 1

The validation exercise consisted of predicting the P_{32} intensity for open fractures for each vertical set based on the P_{21} values for each vertical set in outcrop ASM000026. These values of P_{32} are then used to create a series of realizations of the fracture model, which are sampled by a borehole with the same orientation as KLX02. The calculated values of P_{10} in the simulation are then compared to the measured values. This means that the validation is made explicitly from one outcrop (ASM000026) in one rock domain (A) instead of using the more general conceptual Alternative 1 model for the whole local model volume (given in Table 6-4, Table 6-9, and Table 6-14), as this model doe not have sufficient spatial resolution for predicting the behavior of one single borehole in one specific rock domain.

Open fractures were selected for this validation as these are the most important subset for fluid flow and transport. Only the vertical sets were incorporated; the horizontal set was not incorporated because its intensity in the outcrop data is highly sensitive to outcrop orientation, so that intensity values for this set in outcrop are much more uncertain than the vertical sets.

The calculation of the P_{32} for each vertical set was carried out in a two-stage process. First, 25 realizations of each set were generated according to the orientation distribution in Table 6-4.

Outcrop ASM000026 have been used to specify the relative proportion of intensity between the sub-vertical sets (Table 7-1). These proportions of intensity of the sub-vertical sets differ from what was originally proposed in conceptual model Alternative 1. However, in order to test Rock Domain A data as thoroughly as possible, these proportions was used in this validation example.

Table 7-1. Relative proportion of intensity of sub-vertical sets in outcrop ASM000026. These proportions differs from what was originally proposed in conceptual model, Alternative 1, and is used here to test only domain A data.

ASM000026 set	Relative P21 %
NNE-NE	0.91%
EW-WNW	24.26%
NW-NNW	12.11%
BGNS	14.76%
BGNE	3.67%
BGNW	44.29%

An arbitrary value of P_{32} was selected for each set. The value was typically of the order of 0.05 1/m; this value was necessary in order to generate enough fractures so that the coefficient of variation was less than 0.5. The fractures were generated in a 200 m by 200 m by 200 m cube.

For each realization for each set, a horizontal surface extending 100 m by 100 m was placed into center of the DFN model, and the P_{21} for fracture traces on this surface were tabulated. The total trace length on this plane was divided by the area of the plane (10,000 m^2) to calculate the simulated P_{21} for each realization. The mean value of all 25 realizations was then calculated.

This mean value of the simulations was compared to the measured value. The ratio between the measured value and the simulation mean was then used to adjust the P_{32}. A second set of 25 confirmatory realizations for the new P_{32} were then carried out, and if still needed because the estimated P_{32} was unstable, a third round of realizations was performed to provide the final estimate of P_{32}.

Once the final P_{32} values were determined for each set, a series of 25 Monte Carlo realizations of the DFN were carried out using this final value. A borehole with the same trajectory as KLX02 was placed into each realization, and then the number of fractures intersected was recorded. This number was then divided by the borehole length. The borehole used was 100 m in total length, so the number of fractures was divided by 100 m to calculate P_{10} in the simulations. This value was then compared to the measured P_{10} for open fractures in KLX02.

7.2.4 Results of the validation for conceptual model Alternative 1

The results for the first set of simulations, involving the calculation of P_{32} from P_{21}, are shown in Table 7-2.

The next step was to calculate the P_{10} for a borehole in the same orientation as the KLX02 borehole. The results for the preliminary round of realizations and the confirmatory round are given in Table 7-3. A comparison is shown in Table 7-4.

Table 7-2. Results from 25 realizations for each vertical fracture set. Note that the 25th realization in the second confirmatory set of realizations for the NW set failed, and is not included. The mean was based on the 24 successful realizations for this set.

Simulation	NNE-NE		EW-WNW		NW-NNW		BGNS		BGNE		BGNW	
	0.011	0.003	0.045	0.112	0.038	0.058	0.034	0.068	0.047	0.014	0.184	0.217
	0.014	0.007	0.048	0.104	0.047	0.078	0.046	0.056	0.037	0.017	0.192	0.235
	0.007	0.002	0.037	0.128	0.051	0.060	0.051	0.062	0.054	0.016	0.213	0.205
	0.011	0.011	0.051	0.106	0.069	0.046	0.073	0.067	0.047	0.023	0.191	0.238
	0.004	0.003	0.047	0.127	0.052	0.043	0.048	0.064	0.028	0.021	0.204	0.201
	0.007	0.005	0.040	0.104	0.041	0.052	0.041	0.077	0.042	0.009	0.204	0.177
	0.012	0.004	0.046	0.097	0.048	0.046	0.051	0.064	0.061	0.030	0.160	0.194
	0.011	0.006	0.042	0.107	0.033	0.044	0.035	0.070	0.047	0.018	0.161	0.215
	0.008	0.005	0.050	0.121	0.041	0.047	0.052	0.055	0.053	0.016	0.191	0.178
	0.009	0.007	0.064	0.112	0.055	0.045	0.050	0.072	0.045	0.017	0.182	0.215
	0.009	0.002	0.052	0.133	0.044	0.060	0.046	0.083	0.036	0.009	0.177	0.199
	0.011	0.006	0.040	0.126	0.044	0.061	0.049	0.083	0.052	0.015	0.164	0.207
	0.004	0.000	0.038	0.117	0.042	0.052	0.048	0.074	0.044	0.014	0.199	0.195
	0.007	0.008	0.049	0.125	0.042	0.040	0.040	0.090	0.046	0.023	0.190	0.193
	0.011	0.007	0.049	0.128	0.041	0.069	0.037	0.070	0.040	0.023	0.189	0.220
	0.009	0.004	0.066	0.106	0.051	0.060	0.054	0.088	0.068	0.015	0.155	0.210
	0.010	0.003	0.034	0.113	0.046	0.064	0.045	0.058	0.047	0.017	0.211	0.196
	0.011	0.003	0.040	0.122	0.049	0.058	0.050	0.071	0.041	0.015	0.176	0.197
	0.012	0.006	0.042	0.103	0.043	0.047	0.041	0.069	0.053	0.017	0.187	0.214
	0.004	0.009	0.040	0.108	0.061	0.066	0.057	0.078	0.053	0.015	0.197	0.194
	0.013	0.003	0.045	0.124	0.047	0.048	0.047	0.066	0.056	0.020	0.157	0.170
	0.014	0.004	0.040	0.118	0.040	0.059	0.045	0.074	0.049	0.011	0.162	0.192
	0.007	0.004	0.035	0.094	0.053	0.053	0.050	0.066	0.052	0.019	0.192	0.184
	0.004	0.006	0.051	0.102	0.041	0.061	0.044	0.074	0.049	0.018	0.161	0.201
	0.007		0.059	0.107	0.033	0.061	0.039	0.097	0.049	0.026	0.184	0.196
CV	0.341	0.507	CV 0.180	0.096	CV 0.176	0.170	CV 0.171	0.146	CV 0.172	0.282	CV 0.095	0.081
Sim Ave P21	0.009	0.005	Sim Ave P21 0.046	0.114	Sim Ave P21 0.046	0.055	Sim Ave P21 0.047	0.072	Sim Ave P21 0.048	0.017	Sim Ave P21 0.183	0.202
Target P21	0.004	0.004	Target P21 0.110	0.115	Target P21 0.060	0.057	Target P21 0.070	0.070	Target P21 0.017	0.017	Target P21 0.210	0.210
Sim P32	0.010	0.004	Sim P32 0.050	0.120	Sim P32 0.050	0.060	Sim P32 0.050	0.072	Sim P32 0.050	0.018	Sim P32 0.200	0.220
Target P32	0.004	0.004	Target P32 0.120	0.121	Target P32 0.065	0.062	Target P32 0.075	0.070	Target P32 0.018	0.018	Target P32 0.229	0.229

Table 7-3. Results from P10 calculations from simulations based on outcrop P21.

Set	Average number	P_{10} predicted	Proportion P_{10} predicted
NNE-NE	0.21	0.0021	1.43%
EW-WNW	3.48	0.0348	23.89%
NW-NNW	1.32	0.0132	9.06%
BGNS	0.56	0.0056	3.84%
BGNNE	0.96	0.0096	6.59%
BGNW	8.04	0.0804	55.19%

Table 7-4. Comparison of measured and simulated P10 values.

Set	P_{10} Section 1	P_{10} Section 2	P_{10} Section 3 (DZ)	Proportion P_{10} Section 1	Proportion P_{10} Section 2	Proportion P_{10} Section 3 (DZ)	Proportion P_{10} Predicted
NNE-NE	0.065	0.138	0.550	10.56%	11.04%	12.61%	1.43%
EW-WNW	0.150	0.225	0.844	24.22%	18.06%	19.34%	23.89%
NW-NNW	0.100	0.275	0.975	16.15%	22.07%	22.35%	9.06%
BGNS	0.050	0.108	0.325	8.07%	8.70%	7.45%	3.84%
BGNNE	0.077	0.179	0.625	12.42%	14.38%	14.33%	6.59%
BGNW	0.177	0.321	1.044	28.57%	25.75%	23.93%	55.19%

7.2.5 Discussion of results of conceptual model Alternative 1

The predicted fracture intensity is about an order of magnitude lower than the observed P_{10} intensity. This could be due to the 0.5 m cutoff in the outcrop data; the severity and sensitivity of the Terzaghi correction; and the fact that intensity varies vertically in KLX02 (sections 1 to 3).

A quick estimate using the size parameters for the various sets indicates that if trace lengths were measured down to 7 cm, there would be an increase of P_{21} (and thus P_{32}) by at least an order of magnitude. Also, it could well be that the intensity calculated from outcrops is more appropriate for some other part of section A. In fact, there are "A" portions in other wells that have a much lower intensity than that seen in KLX02.

The relative intensity patterns forecast are fairly consistent with the borehole data. The NW set is clearly dominant, as is the EW set. The NS set is clearly minor. The other sets are in the middle.

It should also be pointed out that the derivation of orientation sets in Table 6-4 is a mean value of all outcrops together, regardless of rock domain. There are clearly differences between the relative intensity among sets in different outcrops. The DFN model, however, is more general and does not include these differences. This becomes evident when an attempt is made to try and simulate the fractures in a single borehole in one rock domain.

This also shows that to do a better validation, one need to account for the mapping protocol that eliminated all traces less than 0.5 m, and also the borehole data should be from a deviated borehole rather than a nearly vertical one. It also shows that the vertical variations in fracture intensity are due to additional factors beyond the rock domain scale, and have not yet been analyzed.

7.2.6 Validation of the conceptual model Alternative 2

This validation consists of predicting the absolute and relative P_{10} for all and open fractures by sampling a DFN model with a simulated borehole identical in orientation to KLX02. The validation is performed on each set described in conceptual model Alternative 2

Input data to the DFN model is the parameter values given for all and open fractures in conceptual model Alternative 2 as summarized in Table 7-5.

Table 7-5. Input parameters to the validation test for conceptual model Alternative 2.

Parameter	Value	Reference
Orientation sub-vertical fractures	See Reference	Table 6-6
Orientation sub-horizontal fractures	See Reference	Table 6-7
Fracture Size (radius)	See Reference	Table 6-10
Intensity sub-vertical fractures, Domain A, all	See Reference	Table 6-15
Intensity sub-vertical fractures, Domain A, open	See Reference	Table 6-15
Intensity sub-horizontal fractures, Domain A, all	See Reference	Table 6-16
Intensity sub-horizontal fractures, Domain A, open	See Reference	Table 6-16
Spatial model	Poissonian	
Model size	200 m x 200 m x 200 m	
Simulated borehole, length	50 m	
Simulated borehole, orientation (trend, plunge)	189/75	
Number of realizations	5 for each set (35 total)	

The validation consisted of generating a series of realizations of the fracture model based on orientation, size and the P_{32} intensity for all and open fractures, respectively, using Rock Domain A fracture intensity data. The simulation includes all seven fracture sets. The model is then sampled by a borehole with the same orientation as KLX02. The calculated values of P_{10} in the simulation are then compared to the observed P_{10} values in KLX02, excluding the deformation zone section between 770 m and 960 m (section 3). The relative intensity between the simulated fracture sets was also compared with the observations in KLX02.

7.2.7 Results of the validation of the conceptual model Alternative 2

The observed fracture intensity in KLX02, sections 1 and 2 are presented in Table 7-6. The observed data has been divided into sets according to the definition of the orientation model in conceptual model Alternative 2. The total intensity for steeply dipping fractures is about two times higher in section 2, except for the ENE and the sub-horizontal sets, which do not appear to change. Looking only at open fractures, a similar but even stronger increase in intensity is seen, and is very prominent for the steeply dipping sets.

Simulation results are shown in Table 7-7. The simulated total fracture frequency for all fractures is in the same order of magnitude as the observed data. However, looking only at the sub-vertical fracture sets, observed P_{10} are about 1.2 to 1.5 times higher than simulated P_{10}s, except for the ENE set. The simulated sub-horizontal set intensity is almost twice as high as KLX02 data.

The simulated total fracture frequency for open fractures is in the same order of magnitude as the observed intensity in section 1. However, simulated sub-vertical fracture sets are of about one order of magnitude lower intensity. The simulated sub-horizontal set intensity is 1.8 (section 1) to 1.3 (section 2) times higher than KLX02 data.

The simulated relative intensities also shows that the sub-horizontal set is over-estimated compared to observations in KLX02. This is especially true when comparing with observed open fractures. Most sub-vertical sets show similar behavior as the observed data from KLX02 both for all fractures and for the open fractures.

Table 7-6. Fracture frequency (P10) for all and open fractures in KLX02, sections 1 and 2 and relative intensity between different sets.

Set	KLX02 P_{10} Sect 1 All	KLX02 P_{10} Sect 1 All Terzhagi	KLX02 P_{10} Sect 1 Open	KLX02 Rel % P_{10} Sect 1 Open Terzhagi	KLX02 P_{10} Sect 2 All	KLX02 Rel % P_{10} Sect 2 All Terzhagi	KLX02 P_{10} Sect 2 Open	KLX02 Rel % P_{10} Sect 2 Open Terzhagi
NS	0.16	13%	0.07	11%	0.24	13%	0.13	11%
NE	0.20	14%	0.10	15%	0.41	16%	0.25	16%
ENE	0.12	12%	0.05	9%	0.14	8%	0.08	8%
EW	0.29	20%	0.16	22%	0.56	22%	0.36	22%
NW	0.28	16%	0.16	18%	0.53	18%	0.31	17%
NNW	0.13	11%	0.06	11%	0.24	12%	0.16	14%
HZ	0.56	15%	0.27	15%	0.56	10%	0.35	11%
Total	1.73		0.88		2.67		1.65	

Table 7-7. Simulation results for conceptual model, Alternative 2.

Set	Simulated P_{10} All	Proportion of simulated P_{10} All Terzhagi	Simulated P_{10} Open	Proportion of simulated P_{10} Open Terzhagi
NS	0.09	10%	0.01	5%
NE	0.10	9%	0.02	7%
ENE	0.14	17%	0.02	9%
EW	0.12	14%	0.02	8%
NW	0.08	9%	0.03	10%
NNW	0.06	7%	0.03	12%
HZ	0.99	34%	0.48	51%
Total	1.58		0.62	

7.2.8 Discussion of results of conceptual model Alternative 2

The validation of conceptual model Alternative 2 shows that;

1. predicted total intensity is in the same order of magnitude as observations in KLX02, however,
2. most sub-vertical sets have about an order of magnitude lower intensity than observed,
3. the sub-horizontal set intensity is about twice as high as observed,
4. most of the relative proportion of the sub-vertical set intensity show similar behavior as KLX02, except for the sub-horizontal sets that are considerably stronger than observed.

The main differences with the DFN model and observations in KLX02 are the intensity for the sub-horizontal set. The difference in intensity may be coupled to the way fractures are mapped in outcrop and boreholes which is identical to the results of conceptual model Alternative 1. Relatively small samples of sub-horizontal traces from outcrop have been used for estimating size, and these traces are considered to be highly uncertain due to the low angle of intersection with the outcrops.

The intensity of sub-horizontal fractures in the validation simulations is about twice as high as in KLX02, which also may be due to the fact that fracture intensity for Rock Domain A is based on all boreholes with Rock Domain A intervals. Data from KAV01 show that there is about 20% higher overall fracture intensity than in KLX02. However, a computational error that may also add to this effect is the fact that the definition of the sub-horizontal set is based on a hard sector definition, cf Figure 6-14. This definition has then been estimated assuming a Fisher spherical probability distribution with a dispersion coefficient value of 31.3. The Fisher distribution gives a smoother, wider set than the hard sector definition. When the Fisher distribution is used in the DFN model, this might give rise to a larger population of simulated fractures belonging to the sub-horizontal set, than using the hard sector approach.

8 Summary

The geological data available in core and percussion boreholes, outcrops and lineament maps has been used to calculate geometrical parameters for geological DFN models within the local model domain. Major conceptual and data uncertainties have been quantified with the exception of uncertainties in how fracture intensity and size might vary by rock domain.

The fracturing, both open and sealed, outside of deformation zones, can be characterized as consisting of six sub-vertical sets and one horizontal set. There are two possible conceptual models concerning the vertical sets. Alternative Conceptual Model 1 relates three of these sets to three lineament sets, while the other three are unrelated to lineament sets. In Alternative Conceptual Model 2, all six vertical sets are related to lineament sets.

The differences the two conceptual models are in how orientations and size are specified for the DFN model. In Alternative 1, the three lineament-related sets have mean strikes equal to the local trend of the lineaments, while the three unrelated sets have mean orientations that are fixed throughout the model region. The sizes of the sets unrelated to the lineaments are based only on matching outcrop trace lengths, and as such, have a very much smaller size than the lineament-related sets. On the other hand, the orientations for all six sets in Alternative 2 have mean orientations related to the trends of nearby lineaments, and do not have constant mean orientations throughout the model region. In addition, the sizes of the three previously unrelated sets, as they are now lineament related, have a much greater size range.

The mass dimensions of the facture traces suggests that fracture intensity does scale, at least for some sets, with area. This implies that a simple Poissonian spatial model may not be appropriate for extrapolating fracture intensities measured in outcrop or borehole to models at the kilometer scale. It also suggests that the trace length distributions derived from the mass dimension renormalization, rather than the Euclidean renormalization, more accurately quantify the size distribution of most of the fracture sets.

The orientations of the sub-vertical fractures appear to be relatively constant with depth.

There are distinct zones of higher and lower fracture intensity in the borehole fracture data logs. These zones are of varying length, and can range from a few meters to hundreds of meters. These zones are preferentially associated with certain rock types, rock domains and alteration zones. This implies that the fracture intensity of the DFN model can be stratified by rock domain or lithology, both to reduce uncertainty and to more accurately reproduce the measured data.

Validation tests of the DFN model described above suggest that, in its current form, the intensity of sub-vertical fracture sets is under-estimated by an order of magnitude. The reasons for this are likely to be differences in mapping techniques on outcrop and in boreholes together with uncertainties added to the analysis by orientation bias corrections. Outcrop data is mapped with a trace length truncation of 0.5 m, which seems to miss a rather large component of the fractures that are found in boreholes. Estimates based on the assumption of a power law size distribution suggest that, if traces down to less than 10 cm were to be included in the surface mappings, simulated intensity of sub-vertical fractures would increase by an order of magnitude.

Validation tests of the DFN model described above suggest that, in its current form, the intensity of sub-horizontal fracture sets is over-estimated by 1.3 to 2 times compared to observations in borehole KLX02. This may be due to the fact that the fracture intensity for Rock Domain A is based on all boreholes containing Rock Domain A lithologies. Data from borehole KAV01 show an approximately 20% higher overall fracture intensity than in KLX02. The large uncertainties of the estimation of the fracture size distribution for the sub-horizontal set may also enhance this uncertainty. Finally, a computational error may also add to this effect as set membership

for the sub-horizontal set is based on a visually-assigned hard sector definition. However, when simulated in the validation cases, a Fisher distribution is used to model sub-horizontal set orientations, resulting in a 'smoother' pattern of fracturing on stereoplots. The reasons for the poor estimates of the sub-horizontal set needs to be further analyzed.

There is no evidence for, and much evidence against, the hypothesis that there is an increased fracture intensity within a few tens of meters of the surface due to causes such as glacial unloading, surficial stress relief or other mechanism. Rather, all evidence to date from the boreholes suggests that zones of high and low fracture intensity do exist, but may have formed at a much older time, probably prior to 1.7 bypb.

Future work directed at better quantifying the orientation, size and intensity of the horizontal fracture set, and the fracture characteristics of unsampled rock domains, would probably be the most useful in reducing model uncertainty. Likewise, further analyses to distinguish which of the two alternative conceptual models for vertical fracturing is more likely would be useful, as the fracture connectivity of Alternative 2 is likely to be much greater than that of Alternative 1.

8.1.1 Summary tables for Alternative models 1 and 2

This section lists the estimated parameters for the two conceptual model alternatives. The presented models shows the result of DFN parameter estimations based on available data and has not been specifically conditioned to boreholes or specific hydrological or rock mechanical parameters.

Sub-vertical sets are estimated only from surface observations. Validation tests show that estimates of simulated intensity for sub-vertical sets are about 50% (all fractures) to an order of magnitude (open fractures) smaller than observed in boreholes. The major reason for this may be due to the different resolution in mapping of fractures in outcrop and boreholes. If the intended use of the DFN model is to estimate sub-vertical intensity in boreholes, it is suggested that the minimum radius of the power law size distributions are lowered to 5–10 cm when simulating open fractures. Complete conditioning of all sets has not been performed due to time constraints.

Sub-horizontal fractures are estimated partly on surface data (size) and partly on borehole data (orientation and intensity). Validation tests show that sub-horizontal fractures are currently over estimated about two times compared to observations in boreholes. The main reason for this may be the poor definition of sub-horizontal fracture orientation and the size estimation. Relatively small samples of sub-horizontal traces from outcrop have been used for estimating size, and these traces are considered to be highly uncertain due to the low angle of intersection with the outcrops. The orientation of the sub-horizontal set is estimated by hard sector definition, which is converted to a Fisher distribution in the model. When simulating fractures this approach may produce a higher intensity than what was intended. If the intended use of the DFN model is to estimate open and sealed sub-horizontal fracture intensity in boreholes, it is currently suggested to lower the estimated P_{32} for sub-horizontal fractures by 50%. Complete conditioning of the sub-horizontal set has not been performed due to time constraints.

To better define the sub-vertical sets, but specifically the sub-horizontal set in future DFN models, orientation, size and intensity needs to be conditioned to boreholes through simulations and more data is needed from inclined boreholes close to outcrops.

Table 8-1. Summary table for conceptual model Alternative 1.

Orientation Set name	Mean pole Trend	Plunge	Distribution	Dispersion K (K1/K2)	% of fracture population
NNE-NE	118	1.9	Fisher	17.3	16.64%
EW-WNW	17.1	7.3	Fisher	11.2	15.55%
NW-NNW	73.1	4.7	Fisher	13.7	19.71%
BGNE	326.3	5.5	Bivariate Fisher	17.65/18.14	16.29%
BGNS	96.8	3.8	Fisher	20.32	13.53%
BGNW	22.1	2.4	Bivariate Fisher	5.36/6.66	5.88%
SubH**	33	86	Fisher	31.3	12.40%
Size	**Probability distribution**	**Distribution parameters Mean radius**	**St deviation**	**k_r**	**r_0**
NNE-NE	Power Law	N/A	N/A	2.58	0.23
EW-WNW	Power Law	N/A	N/A	2.8	0.23
NW-NNW	Power Law	N/A	N/A	2.87	0.31
BGNE	Lognormal	0.48	0.55	N/A	N/A
BGNS	Lognormal	0.67	0.82	N/A	N/A
BGNW	Lognormal	0.45	1	N/A	N/A
SubH**	Lognormal	0.57	1.86	N/A	N/A
Intensity	**P_{32}, All fractures**		**P_{32}, Open fractures**		
	A	**B**	**A**	**B**	**C**
NNE-NE	0.4	0.92	0.09	0.13	0.15
EW-WNW	0.37	0.86	0.08	0.12	0.15
NW-NNW	0.47	1.09	0.11	0.16	0.18
BGNE	0.39	0.9	0.09	0.13	0.15
BGNS	0.32	0.75	0.07	0.11	0.12
BGNW	0.14	0.33	0.03	0.05	0.05
SubH**	0.92	2.8	0.49	0.73	0.43

Table 8-2. Summary table for conceptual model, Alternative 2.

Orientation Set Name	Mean Pole Trend	Plunge	Distribution	Dispersion K	% of fracture population
NS	99.7	6.9	Fisher	9.63	12.04%
NE	128.4	2.6	Fisher	8.92	10.79%
ENE	331.7	5.4	Fisher	10.2	20.78%
EW	6	3.1	Fisher	6.97	13.80%
NW	39	0.7	Fisher	7.78	18.45%
NNW	74.5	9.2	Fisher	9.17	11.65%
SubH	33	86	Fisher	31.3	12.40%

Size	Probability distribution	Distribution parameters Mean radius	St deviation	k_r	r_0
NS	Power Law	N/A	N/A	2.77	0.35
NE	Power Law	N/A	N/A	2.58	0.23
ENE	Power Law	N/A	N/A	2.77	0.36
EW	Power Law	N/A	N/A	2.8	0.23
NW	Power Law	N/A	N/A	2.82	0.28
NNW	Power Law	N/A	N/A	2.87	0.31
SubH	Lognormal	0.57	1.86	N/A	N/A

Intensity	P_{32}, All fractures A	B	C	P_{32}, Open fractures A	B	C
NS	0.29	0.67	0.43	0.06	0.09	0.11
NE	0.26	0.6	0.38	0.06	0.09	0.1
ENE	0.5	1.15	0.73	0.11	0.16	0.19
EW	0.33	0.77	0.49	0.07	0.11	0.12
NW	0.44	1.03	0.65	0.1	0.15	0.17
NNW	0.28	0.65	0.41	0.06	0.09	0.11
SubH	0.92	2.8	2.01	0.49	0.73	0.43

9 References

Dershowitz W S, Busse R, Geier J, Uchida M, 1996. A stochastic approach for fracture set definition. In Proceedings of the 2nd North Smerican Rock Mechanics Symposium (NARMS' 96), Rock Mechanics Tools and Techniques, M. Aubertin, F. Hassani and H. Mitri, Eds., A. A. Balkema, Rotterdam. ISBN 90 5410 838 X, pp 1809–1813.

Golder, 2004. Selection of borehole data from SICADA delivery 04_95 /SICADA, 2004a/ assembled in file fract_core_FOR_DFN_V1.2_COMPLETE_040617.xls, dated 2004-06-17.

La Pointe P R, 1995. Estimation of undiscovered hydrocarbon potential through fractal geometry. Chapter 3, Fractals in Petroleum Geology and Earth Processes, C. C. Barton and P. R. La Pointe, Eds., Plenum Press, New York. pp 35–57.

La Pointe P R, 2001. Scaling analysis of natural fracture systems in support of fluid modeling and seismic risk assessment [abstr.]. Annual Meeting, American Geophysical Union, December 14, 2001, San Francisco, CA.

La Pointe P R, 2002. Derivation of parent fracture population statistics from trace length measurements for fractal fracture populations. International Journal of Rock Mechanics and Mining Sciences, Vol. 39, 381–388.

Mattsson H, Stanfors R, Wahlgren C-H, Stenberg L, 2004a. Oskarshamn site investigation. Geological single-hole interpretation of KSH01A, KSH01B, HSH01, HSH02 and HSH03. SKB P-04-32. Svensk Kärnbränslehantering AB.

Mattsson H, Stanfors R, Wahlgren C-H, Carlsten S, Hultgren P, 2004b. Oskarshamn site investigation. Geological single-hole interpretation of KSH02 and KAV01. SKB P-04-133. Svensk Kärnbränslehantering AB.

Munier R, 1989. Brittle tectonics on Äspö, SE Sweden. SKB PR 25-89-15. Svensk Kärnbränslehantering AB.

SDE, 2004a. XSM_Linked_lineament_line.shp (2004-03-30).

SDE, 2004b. Extended_merged_d.shp (ArcMap format).

SDE, 2004c. Extended_merged_d.dxf (AutoCad format).

SDE, 2004d. GIS files SDEADM.GOL_OH_GEO_1915 (ASM000205), SDEADM. GOL_OH_GEO_1924 (ASM000206), SDEADM.GOL_OH_GEO_1921 (ASM000025), SDEADM.GOL_OH_GEO_1918 (ASM000026). SDE GIS archive, SKB.

SICADA, 2004. SICADA delivery file 04_95.

SKB, 2005. Preliminary site description. Simpevarp subarea – version 1.2. SKB R-05-08. Svensk Kärnbränslehantering AB.

SKB, 2006. Preliminary site description. Laxemar subarea – version 1.2. SKB R-06-10. Svensk Kärnbränslehantering AB.

Triumf C-A, 2004. Oskarshamn site investigation. Joint interpretation of lineaments. SKB P-04-49. Svensk Kärnbränslehantering AB.